



P-124

IN-39718

(NASA-TM-86789) NASA ROTOR SYSTEMS RESEARCH  
AIRCRAFT: FIXED-WING CONFIGURATION  
FLIGHT-TEST RESULTS (NASA) 124 p CSCL 01C

N87-12557

Unclas  
G3/05 44615

---

# NASA Rotor Systems Research Aircraft: Fixed-Wing Configuration Flight-Test Results

---

R.E. Erickson, J.L. Cross, R.M. Kufeld,  
C.W. Acree, Jr., D. Nguyen, and R.W. Hodge

---

February 1986



National Aeronautics and  
Space Administration

---

# **NASA Rotor Systems Research Aircraft: Fixed-Wing Configuration Flight-Test Results**

---

R. E. Erickson,  
J. L. Cross,  
R. M. Kufeld,  
C. W. Acree, Jr.,  
D. Nguyen, Ames Research Center, Moffett Field, California  
and  
R. W. Hodge, Sikorsky Aircraft Company, Stratford, Connecticut

February 1986



National Aeronautics and  
Space Administration

**Ames Research Center**  
Moffett Field, California 94035

# NASA ROTOR SYSTEMS RESEARCH AIRCRAFT: FIXED-WING CONFIGURATION FLIGHT-TEST RESULTS

R. E. Erickson, J. L. Cross, R. M. Kufeld, C. W. Acree, Jr., D. Nguyen,

and R. W. Hodge\*

Ames Research Center

## SUMMARY

This report documents the fixed-wing, airplane configuration flight-test results of the Rotor Systems Research Aircraft (RSRA), NASA 740, at Ames/Dryden Flight Research Center. Fourteen taxi and flight tests were performed from December 1983 to October 1984. This was the first time the RSRA was flown with the main rotor removed; the tail rotor was installed. These tests confirmed that the RSRA is operable as a fixed-wing aircraft. Data were obtained for various takeoff and landing distances, control sensitivity, trim and dynamics stability characteristics, performance, rotor-hub drag, and acoustics signature. Stability data were obtained with the rotor hub both installed and removed. The speed envelope was developed to 261 knots true airspeed (KTAS), 226 knots calibrated airspeed (KCAS) at 10,000 ft density altitude. The airplane was configured at 5° wing incidence with 5° wing flaps as a "normal" configuration. Level-flight data were acquired at 167 KCAS for wing incidence from 0° to 10°. Step inputs and doublet inputs of various magnitudes were utilized to acquire dynamic stability and control sensitivity data. Sine-wave inputs of constantly increasing frequency were used to generate parameter identification data. The maximum load factor attained was 2.34 g at 206 KCAS.

---

\*Flight Test Engineer, Sikorsky Aircraft Company, Stratford, Connecticut.

## 1. INTRODUCTION AND BACKGROUND

This report presents a summary of the flight-test results obtained from the Rotor Systems Research Aircraft (RSRA, NASA 740) flight development program for the fixed-wing configuration.

The report covers the maintenance check flight of the RSRA on December 14, 1983; the compound-configuration ferry flight of the aircraft from Moffett Field, California, to the Dryden Flight Research Facility, Edwards AFB, California, on December 19, 1983; and the ensuing period until its return ferry flight to Moffett Field, as a fixed-wing aircraft, on October 3, 1984. Sixteen flights were completed--taxi tests, test flights, and ferry flights. More than 11 hours of flight time were accumulated in the fixed-wing configuration. A log of the flights is given in table 1 (sec. 3).

The RSRA is designed to fly as a helicopter, as a compound helicopter, and as a fixed-wing aircraft. NASA 740 is one of two RSRA manufactured by Sikorsky Aircraft in the mid-1970s for Army and NASA rotor research programs. Following initial tests by Sikorsky Aircraft, these aircraft were transferred in late 1979 to NASA Ames Research Center, Moffett Field, California. The other RSRA, NASA 741, was subsequently sent back to Sikorsky Aircraft for modifications for the NASA/DARPA X-wing project. In 1983 the NASA/DARPA X-wing project requested that the NASA 740 aircraft be utilized to support the X-wing project by demonstrating its airplane capability and by providing airplane control sensitivity data. This report documents that demonstration and provides additional data acquired for loads, stress, vibration, trim, takeoff and landing distance, performance, acoustics, and aeroelastics.

A description of the RSRA, with tabulated dimensions and general data, is presented in appendix A.

There were five test objectives:

1. Demonstrate the RSRA as a fixed-wing aircraft
2. Obtain fixed-wing control sensitivity and stability data in support of the NASA/DARPA RSRA/W-wing program
3. Develop the flight envelope to 250 knots
4. Obtain baseline main-rotor-off acoustics data
5. Obtain rotor-hub drag data

The plan was to attain these objectives with and without the main-rotor hub installed. The design envelope for the RSRA with tail rotor installed is shown in figure 1.

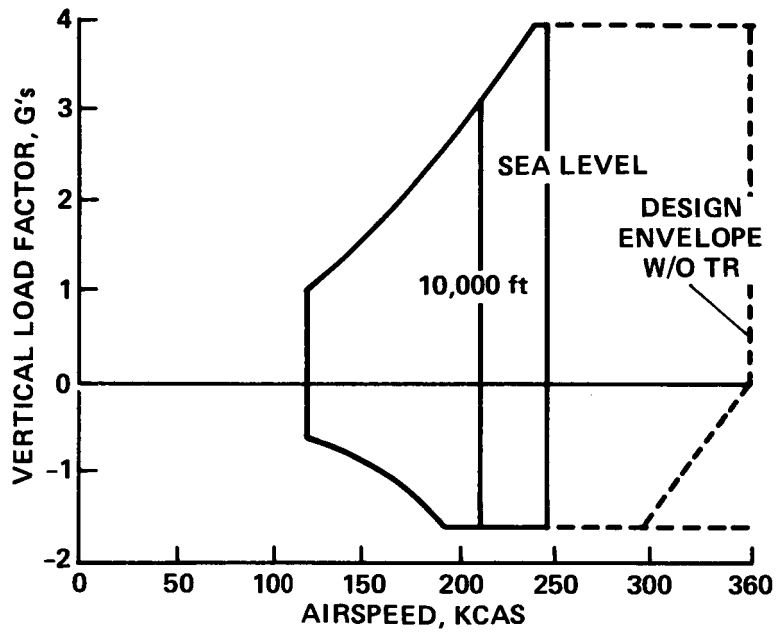


Figure 1.- RSRA planned fixed-wing envelope development.

## 2. TEST PREPARATION

When the requirement to demonstrate the RSRA fixed-wing configuration was confirmed, it was first necessary to define the tasks that would prepare the aircraft and its operating personnel for a safe flight program. The most important tasks were as follows:

1. Reanalysis of aerodynamic predictions
2. Aeroelastic analysis
3. Tail-rotor pitch adjustment
4. Piloted moving-base simulation
5. In-flight fixed-wing simulation
6. TF-34 engine thrust-control redesign
7. Emergency escape system redesign and fabrication, qualification, and installation
8. Landing-gear reanalysis
9. Landing-gear door analysis and modification
10. Low-speed stall and spin analysis
11. Test site
12. Aircraft instrumentation
13. Administrative planning

Each of these items is discussed in the following paragraphs.

Aerodynamic predictions- It was presumed that original analytical predictions by Sikorsky, made in the mid-1970s, were dated and that the model used probably did not incorporate the results of the latest wind-tunnel tests. The new predictions made for this program with the latest mathematical models supported the previous ones, however, and further enhanced our confidence in anticipated stall speeds and aircraft control and stability characteristics. These predictions were made using the Sikorsky General Helicopter Simulation Program (GENHEL) for the RSRA modified to remove the main rotor (ref. 1).

Aeroelastic analysis- The original fixed-wing aeroelastic analysis was reviewed and found adequate. The tail rotor was reanalyzed because of structural and aeroelastic considerations. This opened the analyzed envelope for the tail rotor to 250 knots true airspeed (KTAS) from 200 knots, sea level standard. Three conditions were made requisite: that the tail-rotor pitch remain at 0° at speeds above

200 knots, that the tip Mach number not exceed unity, and that sideslip be limited to less than  $\pm 7^\circ$ .

Tail-rotor pitch adjustment- To comply with the conditions resulting from the tail-rotor structural and aeroelastic analysis and to achieve full-authority tail-rotor thrust in each direction, the tail-rotor pitch was adjusted to provide equal control in each direction, and the yaw-control phasing unit (CPU) was modified to provide zero pitch when the yaw CPU lever was placed in the zero rotary-control-gradient position. Figure 2 shows the function of the yaw CPU control with respect to tail-rotor pitch.

Piloted Moving-base simulation- A simulation of the RSRA was performed on the six-degree-of-freedom Flight Simulator for Advanced Aircraft (FSAA) at Ames Research Center. A static validation of the simulation was accomplished by comparing data for the compound configuration of the RSRA with FSAA output for the same configuration. The rotor module was then removed from the FSAA program, and the pilots were trained on the simulator for nearly a month. This simulation was quite useful in establishing technique and wing incidence and flap configurations for takeoff and landings, as well as the other flight regimes. Previous recommendations had specified a  $10^\circ$  wing incidence ( $I_w$ ) as optimum, but the piloted simulation showed that an  $I_w$  of  $5^\circ$  was preferred. Later flight experience substantiated the fidelity of this simulation from a quantitative and a qualitative standpoint. This simulation is documented in reference 2.

In-flight fixed-wing simulation- Several flights were made with the compound RSRA to investigate flying characteristics of the RSRA at minimal rotor lift. The purpose of this test was to load the wing with the full weight of the aircraft and investigate stall speeds and characteristics. This was accomplished by lowering the collective to full low position. In some high-speed cases, rotor lift was reduced to 2,000 lb, but at lower speeds it was in the 4,000-8,000-lb range.

Stall speed was determined (approximately) in the 100-110-knot range with full flaps. Stall approach roughness, if any, tended to be masked by vibration of the main rotor. Stall occurred without sudden yaw departure, corroborating the moving-base simulation. The primary characteristic of the stall was the sudden and rapid increase of main-rotor speed as the main rotor tried to pick up the load.

During level flight to 150 knots the fuselage provided about 2,000 lb of lift. This lift decreased as wing incidence was increased to  $10^\circ$ . Figure 3 shows the effect of flap position on wing lift and drag. These data are derived from load-cell measurements at the wing attachment fittings.

TF-34 engine thrust-control redesign- The original RSRA auxiliary engine thrust-control system (throttle control) had poor fidelity relative to pilot inputs and was unacceptable for fixed-wing flight. This was redesigned, using F-18 throttle control components which included a boost device operated by engine bleed air pressure. The redesigned system characteristics were very satisfactory.

Emergency escape system- The RSRA was equipped originally with an emergency escape system that featured a blade-severance subsystem and a crew-extraction subsystem. A Stanley Yankee extraction seat was used. As installed, the operation of this extraction seat was validated to 200 knots only. To obtain improved speed capability for the fixed-wing program, a Martin-Baker MK US 10 LT ejection seat was used. This modification provides an emergency escape envelope from zero-altitude/zero-speed through the entire design speed range of the RSRA airplane configuration (360 knots).

Landing-gear reanalysis- The landing gear of the RSRA, as delivered, was rated to 120 knots only. A reanalysis was performed, and this rating was extended to 192 knots at a sink rate of 8 ft/sec for a 28,500-lb vehicle. This extension was required to accommodate the fixed-wing configuration, for which normal touchdown speeds of 130 knots were planned. Consideration of flaps-up emergency landings and high-density altitudes raised the possible touchdown speeds to the 160-knot range.

Landing-gear door analysis and modification- On the last flight of the RSRA in the compound configuration of the fixed-wing simulation program, the left main landing-gear door was blown from the aircraft. Analysis, redesign, and fabrication of a strengthened door were accomplished. The new door, although analytically validated to 200 knots, was limited to 170 knots maximum in the extended position to reduce the possibility of another failure.

Low-speed stall and spin analysis- Stall speeds were recalculated using the latest version of the RSRA GENHEL model (ref. 1) to determine stall speeds. A stall of 110 knots with  $I_w = 5^\circ$  and full flaps at 28,500 lb gross weight was calculated. This result also was supported by the low-speed, low-collective tests of the compound configuration.

Spin-departure tendencies were analyzed by calculating  $C_{n\beta}$  dynamic from simulation data and previous wind-tunnel data. This calculation obtained  $C_{n\beta}$  dynamic for a range 0.001 to 0.0037 which, according to reference 3, should provide acceptable stall behavior with no yaw-departure tendency if stall is not prolonged. This result was also supported by the FSAA moving-base simulator. Figure 4 presents the descriptive phraseology for specific  $C_{n\beta}$  dynamic values.

The stall and spin characteristics were predicted to be acceptable. However, since no specific aerodynamic model testing was performed, it was decided to avoid stall in the test program and to limit wing angle of attack to a maximum of  $15^\circ$ .

Test site- The RSRA is usually based at Ames Research Center (Moffett Field, Calif). Since the fixed-wing testing would require high-speed taxi tests before first flight and since braking distances were estimated to be too long to avoid overheating, the RSRA was moved to the Ames Dryden Flight Research Facility (ADFRF), Edwards AFB, California, where a 15,000-ft runway and a 12,000-ft overrun are available. This was accomplished by a compound-configuration ferry flight in two legs, with a refueling stop at Vandenberg AFB. The ferry flight took place in December 1983. Upon arrival at ADFRF, the main rotor and hub were removed.

Aircraft instrumentation- A major restructuring of the recorded measured parameters was necessary for the fixed-wing test. In addition, numerous new parameters were added, particularly in the area of the landing gear. The final measured parameter list for this test is tabulated in appendix B.

Test administrative planning- Preparations for the test required the development of an RSRA fixed-wing operations plan, which was written to establish the necessary cooperative procedures for Ames Moffett to operate with Ames Dryden. As usual, a detailed flight-test plan was also developed. In addition, a data-processing requirements plan was written which detailed the telemetry and data-processing responsibilities at both Ames Moffett and Ames Dryden. This plan also specified the RSRA data-measurement system requirements and layout.

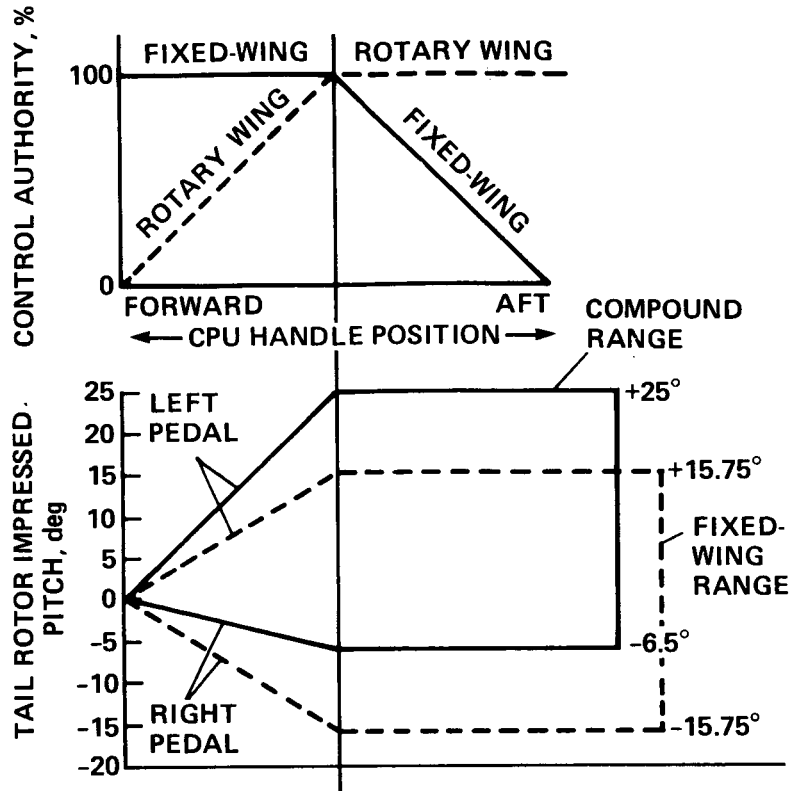


Figure 2.- Tail-rotor control phasing unit.

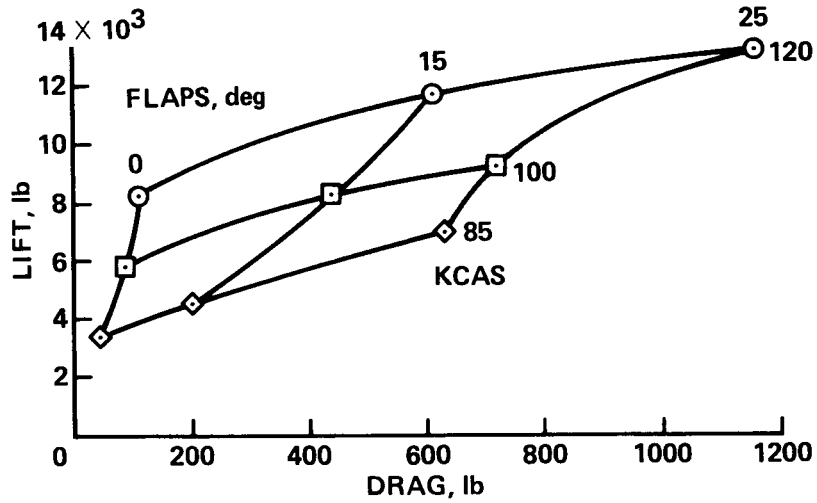


Figure 3.- Wing lift vs wing drag: 10° wing incidence, 40% collective pitch.

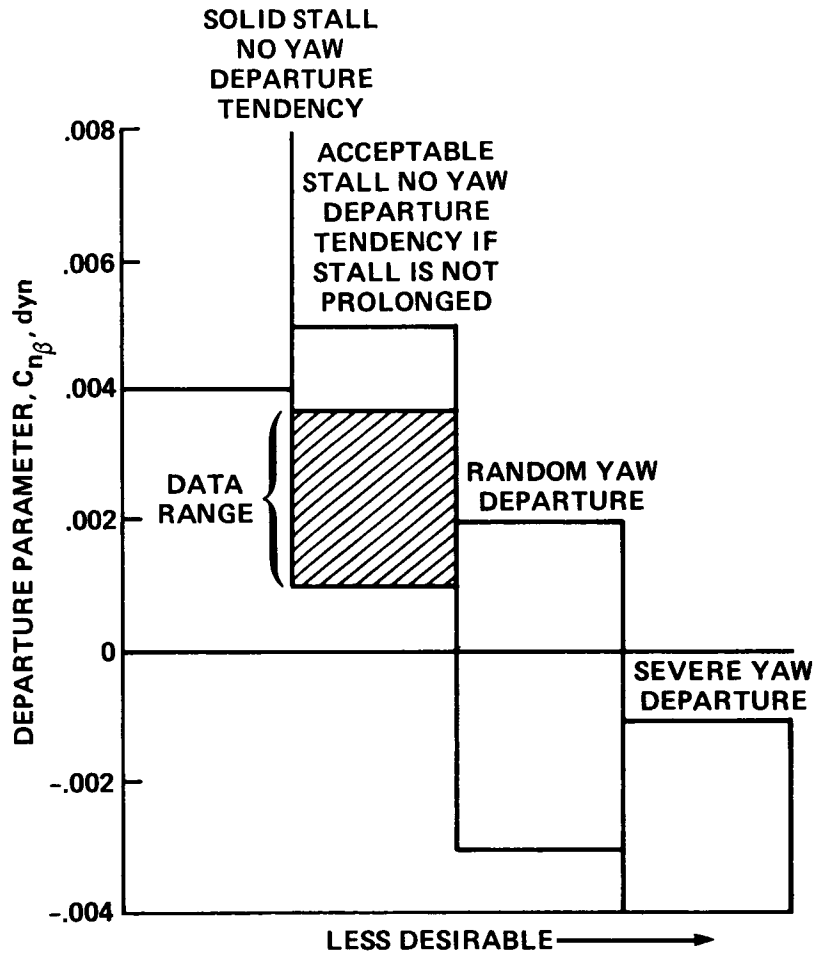


Figure 4.- Expected stall behavior as a function of  $C_{n\beta}$ , dynamic.

### 3. TEST SUMMARY

A summary log of flight tests flown under Flight Test Plan 5A is provided in table 1. The first two flights of this plan were flown with the RSRA in the compound configuration for maintenance checkout and ferry purposes. All remaining flights were airplane(fixed-wing) configuration.

#### Taxi Tests

Familiarization with the ground-handling characteristics and insight into the takeoff flight characteristics of the RSRA were accomplished by three taxi tests. These taxi tests were conducted without the main-rotor hub, which lowered the gross weight to 26,000 lb and lowered the vertical c.g. to WL 219. This represents a vertical c.g. decrease of 6 in. from that of the full compound configuration. Full instrumentation, telemetry, and radar tracking were used in all taxi tests. The radar tracking used a C-band transponder to give aircraft position.

The taxi tests confirmed the selection of  $I_w = 5^\circ$  and half flaps for takeoff. Higher wing incidence caused an uncomfortable nose-down attitude while holding the aircraft on the ground at speeds above the stall speed of 110 knots. Since the at-rest ground attitude for the RSRA is only  $2^\circ$  nose-up, the probability existed that the tail wheel might be on the ground for takeoff at low wing incidence. On the second taxi test ( $I_w = 5^\circ$ ), the aircraft lifted from the ground at 135 knots without touching the tail wheel.

Directional control of the aircraft was adequate at all times. This aircraft has a tail rotor, and for that reason yaw-control power is such that no minimum yaw-control speed exists. Heading was maintained using  $\pm 15\%$  of the control available. Acceleration to 135 knots required slightly less than 3,000 ft. This gave the pilot time to observe the near-takeoff characteristics of the aircraft and then to decelerate to a stop with minimal use of the brakes. Concern about overheating the brakes was dispelled when the pilot found he could aerodynamically decelerate to less than 90 knots, then use the brakes sparingly, and easily stop before using all of the 15,000-ft paved portion of the runway. Brake temperatures rose to only a little more than half of the permissible, even on the repeated runs. Brake stack temperatures were recorded by telemetry and also were displayed to the pilots. Rim temperatures were monitored by surface probes at the end of each run; fans were used to cool the brakes after each run. Stack and rim temperatures were required to show a decline and to be low enough to absorb the temperature rise of a full stop from 120 knots. For brief periods during the second and third taxi tests the aircraft flew and was then immediately landed. In one instance, the radar recorded a 50-ft altitude. All taxi tests were conducted with flight as an option to escape from a hazardous situation. Figure 5 shows the Dryden Aerodynamic Test Range radar data for a taxi run with a lift-off of a few feet. Note that the runway has a slight descent. Figure 6 is a time-history of control motions during the taxi run. A confirmation of the airspeed calibration was obtained from radar ground speed in low

wind conditions and also from static pressure changes at the boom. The previous calibration initially was confirmed to be

$$\text{KIAS} + 10 = \text{KCAS}$$

where KIAS and KCAS are knots indicated and knots calibrated airspeed, respectively. Later, during envelope expansion tests, this finding was refuted by data from the calibrated chase aircraft. The final calibration for fixed-wing flight was

$$\text{KIAS} (1.033) + 8.8 = \text{KCAS for the telemetry system}$$

$$\text{KIAS} (1.033) + 10.2 = \text{KCAS for the pilot's system}$$

#### First Flight: Flight 6

The first flight was made on May 8, 1984, at 0630. Figure 7 shows takeoff data. The aircraft quickly attained 10,000-ft test density altitude ( $H_D$ ). During climb-out, a vibration was noted from the tail area, both by the pilots and telemetry. A brief investigation showed that even the smallest amount of flaps eliminated the vibration. Subsequent flights were conducted with 5° flap settings. Since the flaps were effective, it is believed that turbulence from the inboard wing root streams aft to the lower horizontal stabilator. This turbulence excites the 10-Hz antisymmetric mode of the stabilator. To avoid any aeroelastic envelope expansion, flight speeds were limited to that previously explored by the compound configuration. The remainder of the flight was directed to low-speed landing simulation at altitude to establish the landing technique and flap and wing configuration. The procedure, selected before flight, was to use  $I_w = 5^\circ$ , full flaps, an approach speed of 140 KCAS, and slowing to 125 KCAS for landing. This procedure was acceptable. Main-wheels-first landings were anticipated. Several low-pass practice approaches were made before the final landing, which was slightly tail-wheel first at near 125 KCAS, but otherwise was uneventful. The flight lasted 1 hr. Figure 8 shows approach and landing data. Pilot qualitative impressions of the RSRA handling were that it was comparable to that of a C-130 Hercules.

#### Envelope Expansion: Flights 7 and 9

The speed envelope was expanded to 261 KTAS (226 KCAS at 10,000 ft  $H_D$ ) in two flights. Fixed surface damping was a minimum of 3% for the wing edgewise mode; tail-rotor damping was a minimum of 0.5% in the edgewise mode (0.5% edgewise damping is typical for the S-61 tail rotor). None of the damping ratio trends was decreasing at 261 KTAS. Tail-rotor speed was decreased to 94% (648 ft/sec rotating tip speed) and was in flat pitch above 200 KTAS. This gave a tip Mach number below 1.0. As a convenience, the tail rotor was configured at 94% rotor speed and at flat pitch for all flight speeds once at test altitude. Documentation of the aeroelastic flight envelope is included as appendix C.

The rotor hub was removed for envelope expansion. To obtain comparative vertical c.g. and hub-drag data, the hub and weights used to simulate the complete rotor were reinstalled. Except to monitor effects of turbulence on the tail rotor, no aeroelastic envelope expansion was necessary for the hub-weight configuration. However, this turbulence was of such frequency and magnitude that only two flights were conducted in the hub-on configuration. This phenomenon is discussed in more detail in the vibrations section.

#### Control Sensitivity and Dynamic Stability: Flights 7, 9, 11, 13-15

Experimental data were acquired by step and reversal inputs at 160 and 205 KCAS. Stability data for analysis by systems identification methods were obtained by testing sine-shape control inputs while continuously increasing the frequency in each axis. Flight 13 acquired main-rotor-hub-on data (flight 12 data were unacceptable because of turbulence).

#### Level-Flight Trim and Hub Drag: Flights 13 and 15

Trim data were acquired throughout the test speed range (150 to 226 KCAS) for purposes of determining control trim trends and performance and rotor-hub drag measurements. Hub-drag measurement capability is described in reference 4. Flight 13 was with main-rotor hub on.

#### Acoustics: Flights 14 and 15

Flyover acoustics signature data with the main-rotor hub off were acquired for the 160 to 215 KCAS speed range during flybys at 492 ft above ground level (AGL) and in 3° glide-slope approaches.

Separate reports will be forthcoming to document (1) control sensitivity and stability at two vertical c.g.'s and performance with and without rotor hub; (2) rotor-hub drag comparison with the hub removed and the hub installed; (3) systems identification analysis of aircraft stability; and (4) the acoustics of RSRA with tail rotor only.

TABLE 1.- FLIGHT-TEST LOG: RSRA 740, FLIGHT TEST PLAN, 5A COMPOUND AND FIXED-WING CONFIGURATIONS

Flt No.	Date	Time per flt	Accum time, total	Accum time, fixed wing	Long c.g.	Vert c.g.	Gross wt, lb	Test objective
Compound								
1	12/14/83	:45	81:45	0	302	--	28,000	Maintenance flight
2	12/19/83	2:10	83:55	0	302	--	28,238	Ferry to DFRF <sup>a</sup>
Fixed wing								
3	2/15/84	0	83:55	0	302	219	24,206	Low-speed taxi
4	2/23/84	0	83:55	0	302	219	25,700	High-speed taxi
5	2/28/84	:05	84:00	:05	302	219	25,132	High-speed taxi
6	5/8/84	1:00	85:00	1:05	302	219	25,757	First flight
7	5/22/84	1:00	86:00	2:05	301.5	219	25,332	Envel expan <sup>b</sup>
8	5/22/84	1:05	87:05	3:10	301.2	219	25,702	2nd pilot fam, envel expan <sup>c</sup>
9	6/20/84	1:00	88:05	4:10	301.7	219	25,811	Complete envel expan <sup>d</sup>
10	6/20/84	1:00	89:05	5:10	302	219	25,811	Control power and dyn stab <sup>e</sup>
11	6/28/84	1:00	90:05	6:10	301.3	219	25,908	Control power and dyn stab <sup>f</sup>
12	8/9/84	:30	90:35	6:40	302.4	226	28,022	First flight with MR hub, trim and dyn stab data <sup>g</sup>
13	9/6/84	1:00	91:35	7:40	302.4	226	27,800	Control power, dyn stab, trim and hub drag data <sup>h</sup>
14	9/19/84	1:00	92:35	8:40	302.3	219	25,856	Control power, dyn stab and acoustics data <sup>i</sup>
15	9/19/84	1:10	93:45	9:50	302.3	219	25,712	Dyn stab, trim, acoustics and hub drag data <sup>j</sup>
16	10/3/84	1:30	95:15	11:20	302	219	25,800	Ferry to Ames/Moffett <sup>k</sup>

<sup>a</sup>Refuel stop at Vandenberg AFB.

<sup>b</sup>Steps, ldg gear down @ 182 KCAS.

<sup>c</sup>195 KCAS, drag brake out.

<sup>d</sup>225 KCAS, steps.

<sup>e</sup>Steps.

<sup>f</sup>226 KCAS, steps and sine wave.

<sup>g</sup>Poor data, fairing failed.

<sup>h</sup>With MR hub, 209 KCAS, steps, wing change.

<sup>i</sup>Level flight to 225 KCAS.

<sup>j</sup>Sine waves, acoustics, wing change.

<sup>k</sup>Refuel at NAS Lemoore.

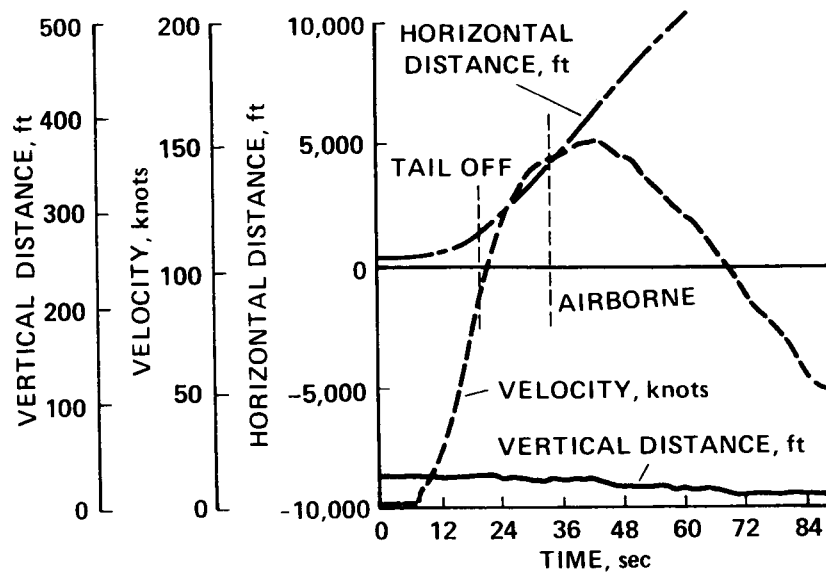


Figure 5.- RSRA fixed-wing taxi: radar data, flight 5, run 24.

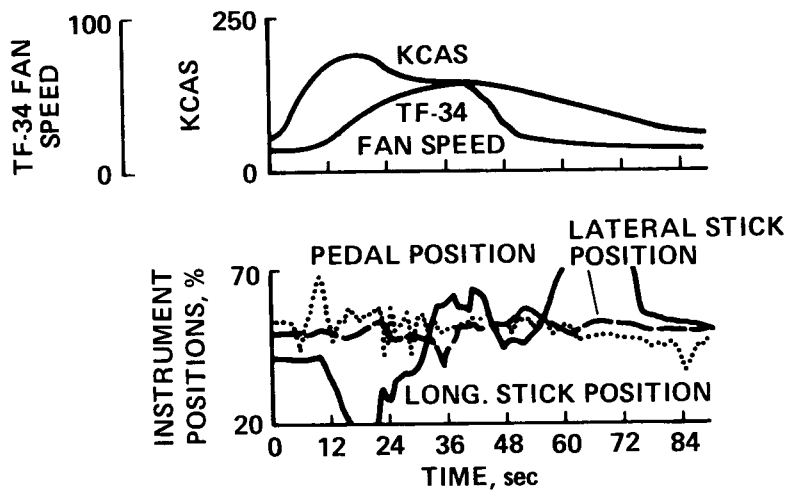


Figure 6.- RSRA fixed-wing taxi.

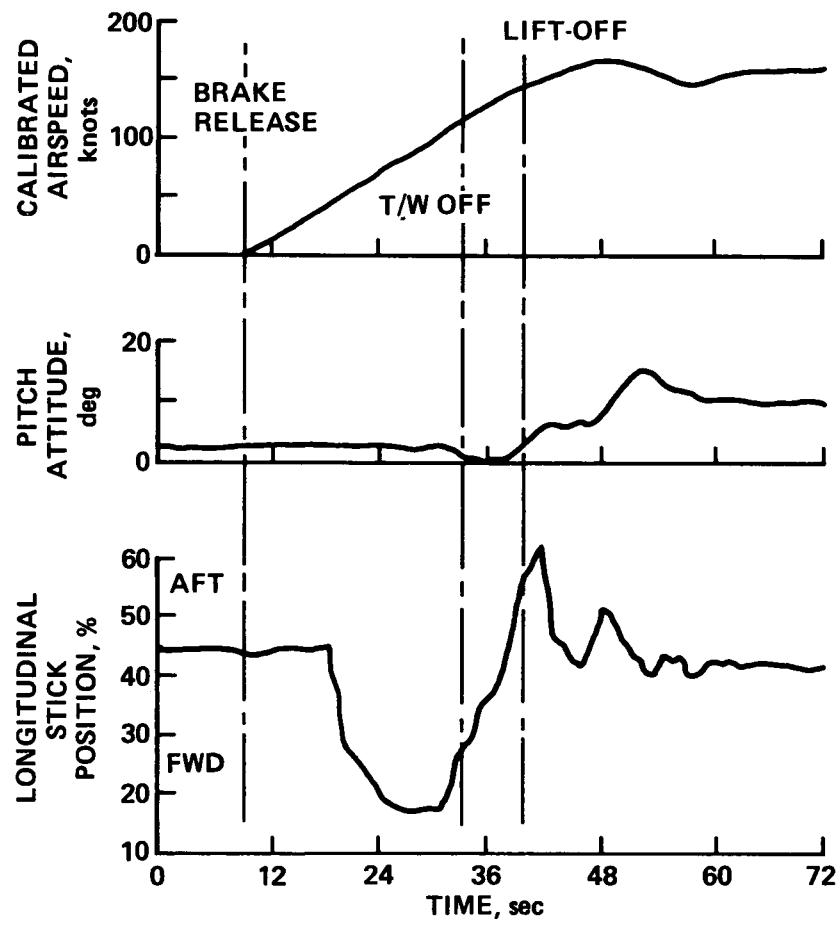


Figure 7.- RSRA fixed-wing takeoff, flight 6.

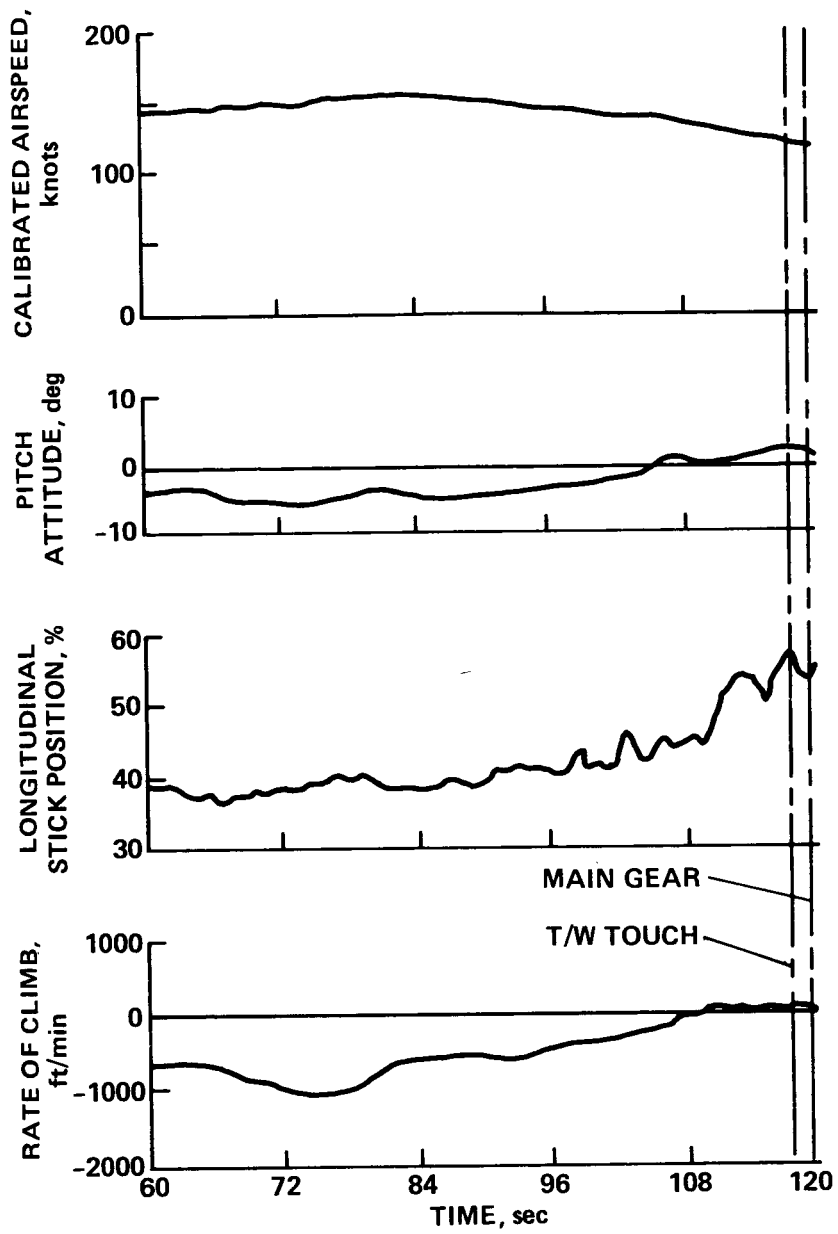


Figure 8.- RSRA fixed-wing final approach and touchdown, flight 6.

## 4. HANDLING QUALITIES

### Control Sensitivity

The control sensitivity of the RSRA was determined by using step and doublet control inputs. The ideal step input would be a square wave with a duration of 0.5 sec. The ideal doublet input would be two step inputs of equal amplitude and opposite direction, performed together with period at 1.5 sec. Figures 9 and 10 show typical examples of the two different types of input taken from flight data. The test inputs were made one axis at a time, keeping airspeed, altitude, and additional stick motion as constant as possible.

The amplitude of the test inputs was varied from 5% to 20% of the stick motion to check the linearity of the response. The inputs were made at 10,000-ft density altitude, at airspeeds of 160 and 205 KCAS, and in two aircraft configurations. The baseline test configuration consisted of a wing incidence of 5°, 5° of wing flaps, a tail-rotor speed of 94% (nominal rotor speed is 1243 rpm), main-rotor hub removed, and the yaw CPU in the 0% rotary-wing, 100% fixed-wing position. The second configuration included the main-rotor hub with weights attached to raise the gross weight from 26,000 lb to 28,000 lb and to change the vertical center of gravity from a waterline of 219 in. to 226 in. Table 2 shows the calculated moments of inertia for each configuration. The main purpose of the high gross weight configuration was to determine the effect of raising the vertical center of gravity on dynamic stability and to check the previous control-sensitivity data.

The data-reduction technique of the control-sensitivity data from the step and doublet inputs is described below. The data (angular acceleration versus control deflection) from the hub-off configuration, flights 9, 10, and 11, are plotted in figures 11 to 13, and the data from the hub-on configuration, flight 13, are plotted in figures 14 to 16. The angular acceleration plotted from the step inputs is the delta between the angular acceleration in trim flight condition and the maximum acceleration caused by the step input. The control deflection plotted from a step input is the delta between the trim control position and the maximum control deflection during the maneuver. Figure 9 illustrates how the data were extracted from a typical step input. The angular acceleration plotted from a doublet input is the delta between the angular acceleration in the trim flight condition and the angular acceleration at the instant that the angular rate goes to zero. The control deflection plotted from a doublet input is extracted in the same manner described above for the doublet acceleration data. Figure 10 illustrates how the acceleration and control position data are extracted from the maneuver time-history.

For each axis and each configuration, the data are divided into four different groups based on input type and airspeed. The slopes, which represent the control sensitivity, of each of the four groups of data were then determined using a simple regression; they are plotted in figures 17 to 19. The data show a distinct trend for the two different types of inputs. The doublets have a greater control sensitivity, which is attributed to the absence of aerodynamic damping created by taking data at the instant of zero angular rates. Aerodynamic stiffness also increases

apparent control sensitivity in yaw and pitch when using doublet inputs, a result of the weathervane effect. For this reason, step-input control sensitivity should be used as a conservative value for pitch and yaw.

For the case of a yaw doublet input, there was a 50% reduction in control sensitivity between the hub-off and the hub-on configuration. The configuration change did not have the same effect on the yaw step inputs, but the pitch and roll doublets showed good comparison between configurations. Therefore, the reduction in yaw-control sensitivity is attributed to a small change in the doublet input frequency between configurations. The average period of the doublet inputs for the hub-on configuration was 1.9 sec. At this input frequency, the control was near the maximum amplitude when the data were analyzed, resulting in a "large" control-position delta. The average period of the doublet inputs in the hub-off configuration was 2.25 sec. At this input frequency, the control was near the maneuver trim position when the data were analyzed, resulting in a "small" delta. The relative position of the yaw control coupled with the weathervane effects influences the results. An attempt to improve correlation between configurations was made by eliminating the weathervane effects from the measurement. The yaw acceleration owing to sideslip, as predicted from wind-tunnel data, was subtracted from the measured acceleration; this resulted in a decrease in control sensitivity for both configurations but in no improvement in correlation.

#### Control-System Rigging

The rigging characteristics of the fixed-wing control system for the fixed-wing configuration are identical to those of the compound configuration; they are shown in figures 20 to 22. The rigging characteristics of the tail-rotor control system were modified from those of the compound configuration, and they are shown in figure 23. The modification included changing the yaw CPU rocker assembly and adjusting the pitch link rods to obtain a tail-rotor pitch angle of  $0^\circ$  with the pedals at the mid-position. The main-rotor control system was disabled above the swash plate with the collective stick locked in a comfortable position for the pilot.

#### Flight Envelope

The objectives of this flight program were to develop a limited fixed-wing envelope, within the design limits, and to demonstrate, in preparation for the RSRA/X-wing flight program, that the RSRA could operate at high speed. In the process of gathering control-sensitivity and hub-drag data, several wing-incidence variations, significant load factors, and angles of bank were attained. The wing incidence was moved from  $0^\circ$  to  $10^\circ$  at 165 KCAS. The maximum load factor reached was 2.34 g's, and the maximum angle of bank attained was  $65^\circ$ , as shown in figure 24. The wing angle-of-attack data recorded as a function of airspeed and load factor are included in table 3. Documentation of the aeroelastic flight envelope is included as appendix C.

## Takeoff and Landing Procedures

The takeoff configuration consisted of a wing incidence of 5°, 15° of flaps, and a yaw CPU position of 100% rotary wing, 100% fixed wing for greater yaw control. The takeoff started with a gradual increase in power to approximately 80% fan speed. More power was not used because of the rapid acceleration obtained with this power level. As the airspeed increased, the longitudinal stick was moved forward to approximately 10% of full forward to raise the tail wheel off the ground. The tail wheel lifted off at a calibrated airspeed of about 100 knots. Once the tail wheel was off the ground, the longitudinal stick was adjusted to maintain a slightly nose-down pitch attitude. As the calibrated airspeed reached 135 knots, the longitudinal stick was moved aft to about 60%, at which point the aircraft rotated and lifted off. The directional control during the takeoff ground roll required pedal inputs of  $\pm 15\%$  of full travel with a period of about 1.5 sec for the entire ground roll. This is similar to the amount of directional control required for an RSRA takeoff in the compound configuration. A time-history plot of a typical takeoff is shown in figures 25 and 26. The runway distance required to reach takeoff was 2,900 ft (fig. 27).

If the aircraft is rotated before takeoff speed is attained, the tail wheel will contact the ground and result in a tail-wheel-last takeoff. This type of takeoff is undesirable, because the aircraft lifts off with a rapid nose-up pitch motion requiring a prompt stick-forward response from the pilot. The 2° nose-up ground attitude of the RSRA does not provide much margin during rotation; consequently, two tail-wheel-last takeoffs were made during the test program.

The fixed-wing landing configuration consists of a wing incidence of 5°, 25° of flaps (full flaps), and yaw CPU in the 100% rotary wing, 100% fixed-wing position. An approach speed of about 140 KCAS was used with a rate of descent of about 500 ft/min. A fan speed of 45% and a longitudinal stick position of about 41% should maintain this condition with a pitch attitude of 2° nose-down. Once over the threshold, the aircraft is slowed to a touchdown speed of 115 knots and rotated to a nose-up pitch attitude of 2° for a three-point landing. Tail-wheel-first landings occurred because of the difficulty in judging the aircraft pitch attitude and aircraft height above the ground. A typical time-history of a landing is shown in figures 28 and 29. The stopping distance from touchdown to a full stop is 4,500 ft (fig. 30).

## Longitudinal Trim

The aircraft longitudinal trim data--pitch attitude, longitudinal stick position, wing angle of attack, total TF-34 thrust, and predicted data--are plotted in figure 31. The flight data include both the hub-on and hub-off configurations. The predicted data are calculated by the Sikorsky JENHEL simulation program. The predicted data represent the RSRA with the hub-on and the main-rotor blades removed. The data show good correlation between flight data and predicted data. The major effect of adding the rotor hub is an increase in thrust required to overcome the

increase in drag, and a slightly larger angle of attack to compensate for the added weight.

The effects of wing incidence on longitudinal trim for both the hub-on and hub-off configuration are plotted in figure 32. The data show similar results for both configurations. The pitch attitude decreases with increasing wing incidence. Fan speed increases with increasing wing incidence.

TABLE 2.- RSRA FIXED-WING MOMENTS OF INERTIA

	Hub off, slugs/ft <sup>2</sup>	Hub and weights on, slugs/ft <sup>2</sup>
I <sub>x</sub>	22,741	26,192
I <sub>y</sub>	104,419	107,874
I <sub>z</sub>	115,274	115,278

TABLE 3.- WING ANGLE OF ATTACK, LOAD FACTOR, AND CALIBRATED AIRSPEED

KCAS	Load factor, g	Wing angle of attack, deg
206	2.34	14
209	2.00	11.5
164	1.48	15.3
172	1.61	15.9
165	1.54	16.2
183	1.93	16.1
166	1.65	16.3
173	1.54	13.8
221	2.04	9.0
167	1.53	15.5
172	1.39	15.1

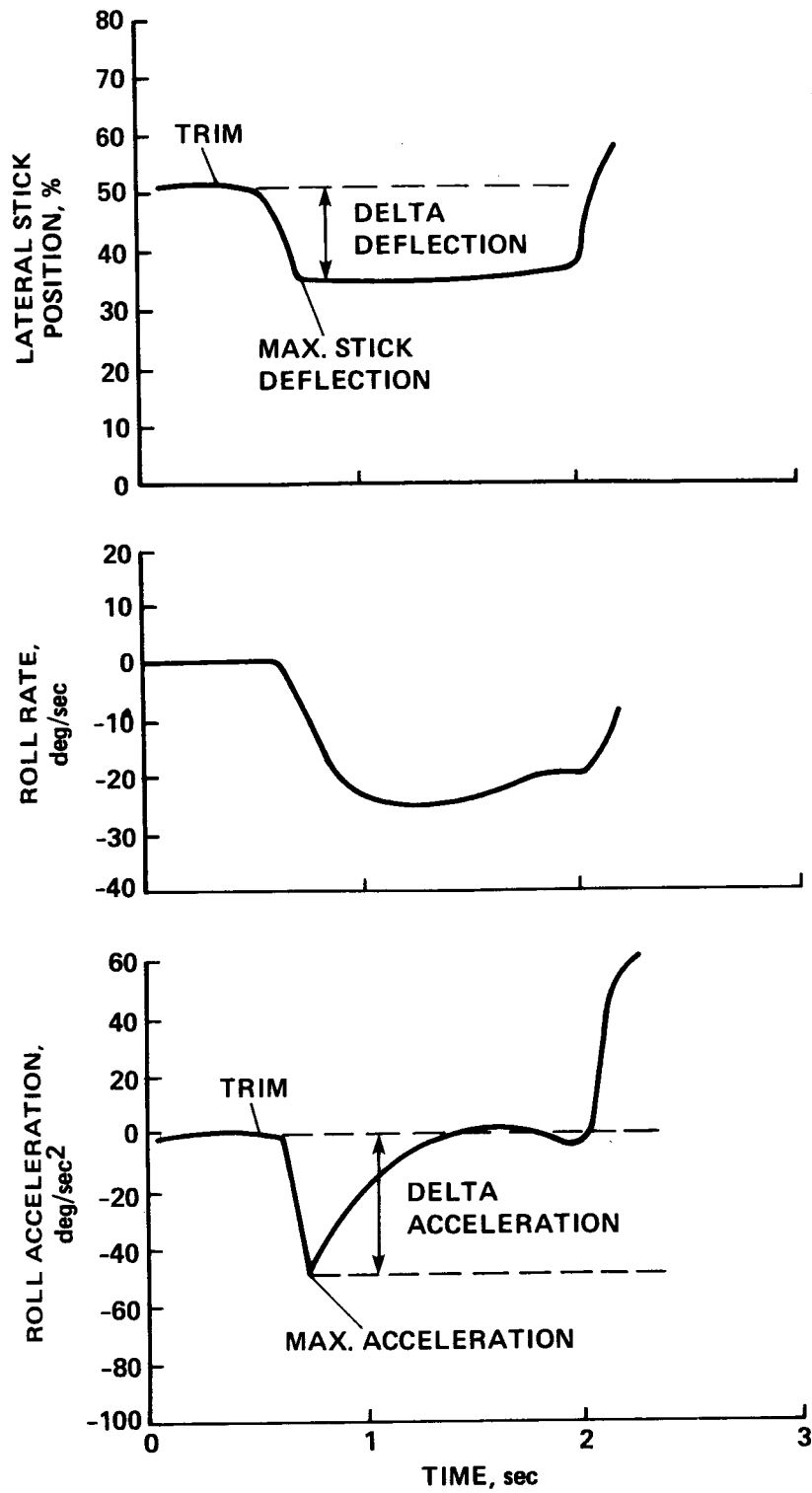


Figure 9.- Typical step input: flight 11, run 51.

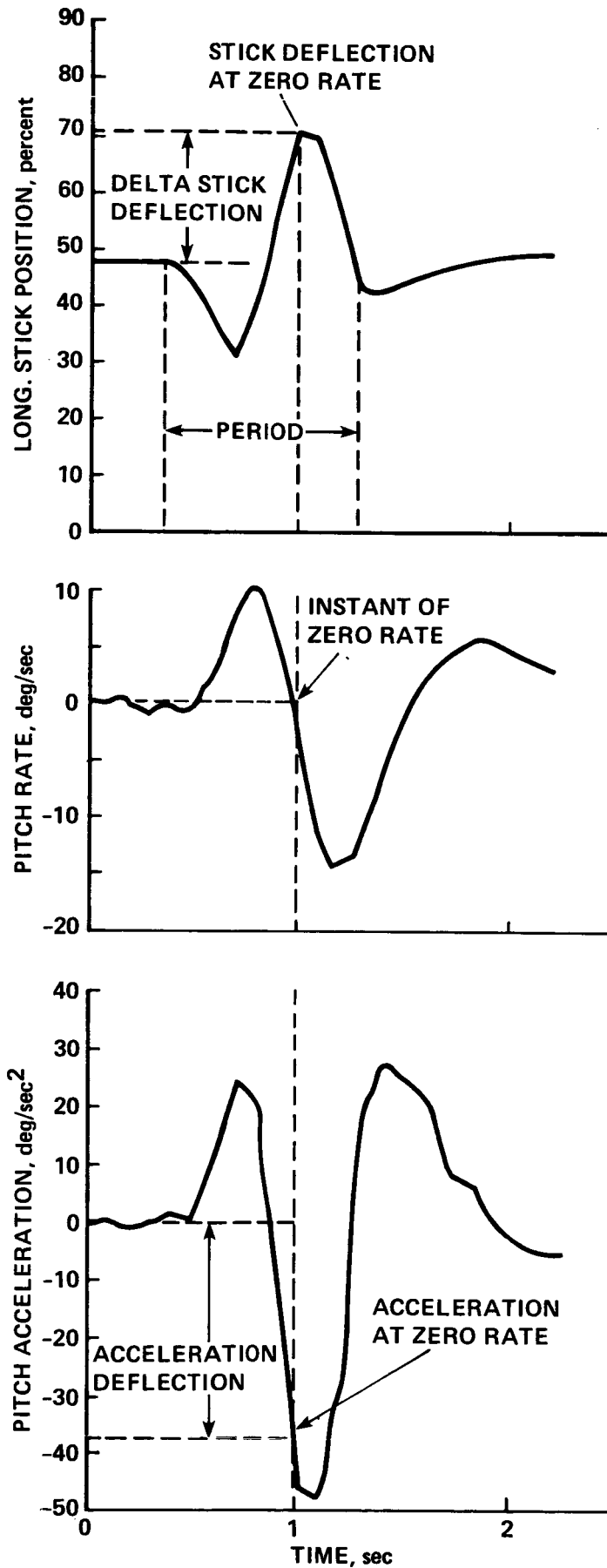


Figure 10.- Typical doublet input: flight 13, run 29.

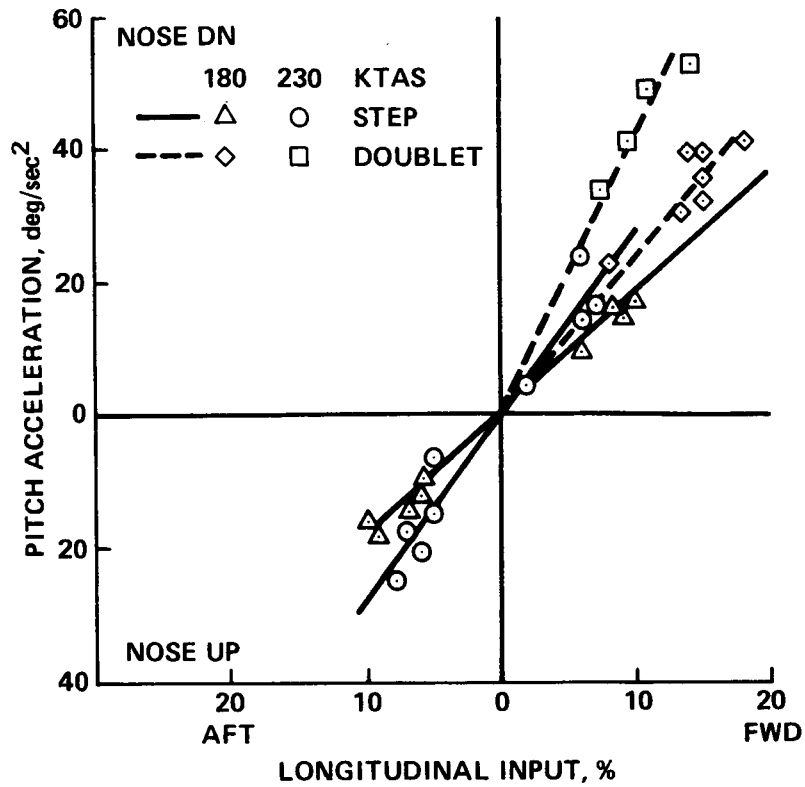


Figure 11.- Hub-off pitch acceleration versus longitudinal stick input.

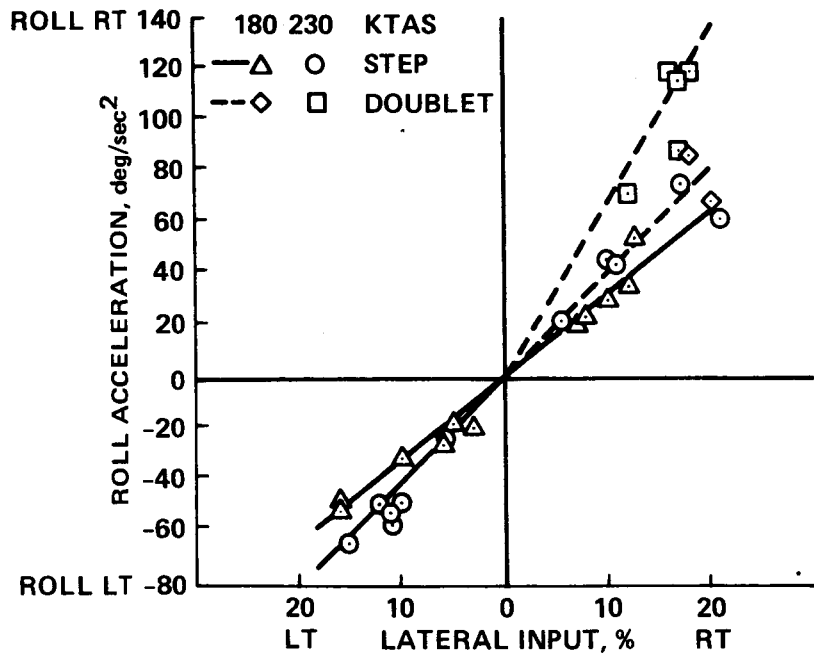


Figure 12.- Hub-off roll acceleration versus lateral stick input.

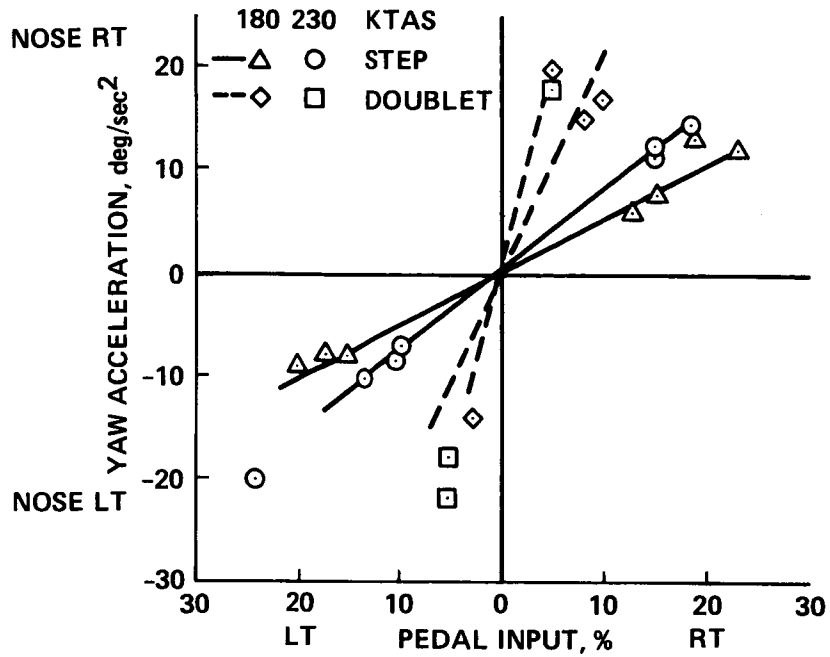


Figure 13.- Hub-off yaw acceleration versus pedal input.

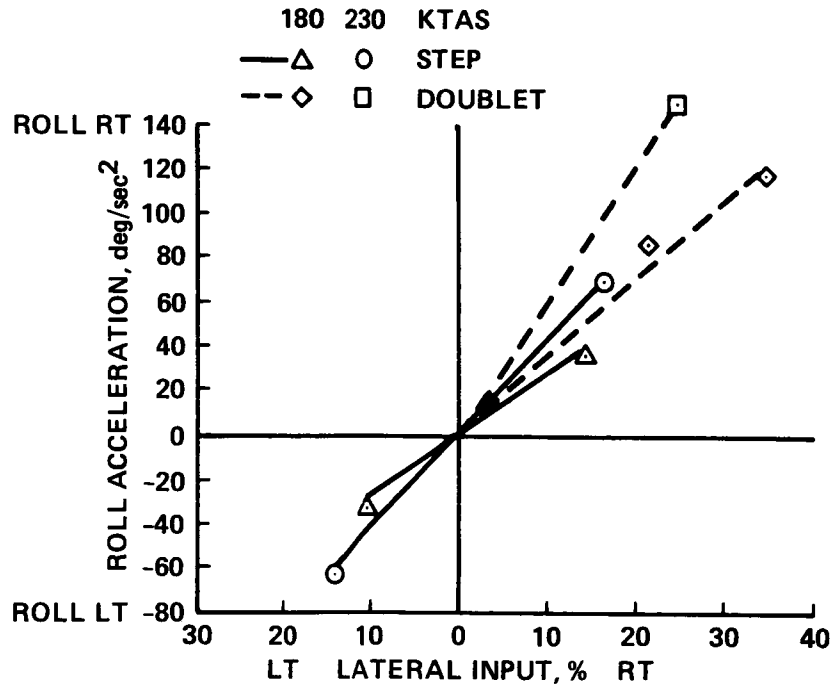


Figure 14.- Hub-On roll acceleration versus lateral stick input.

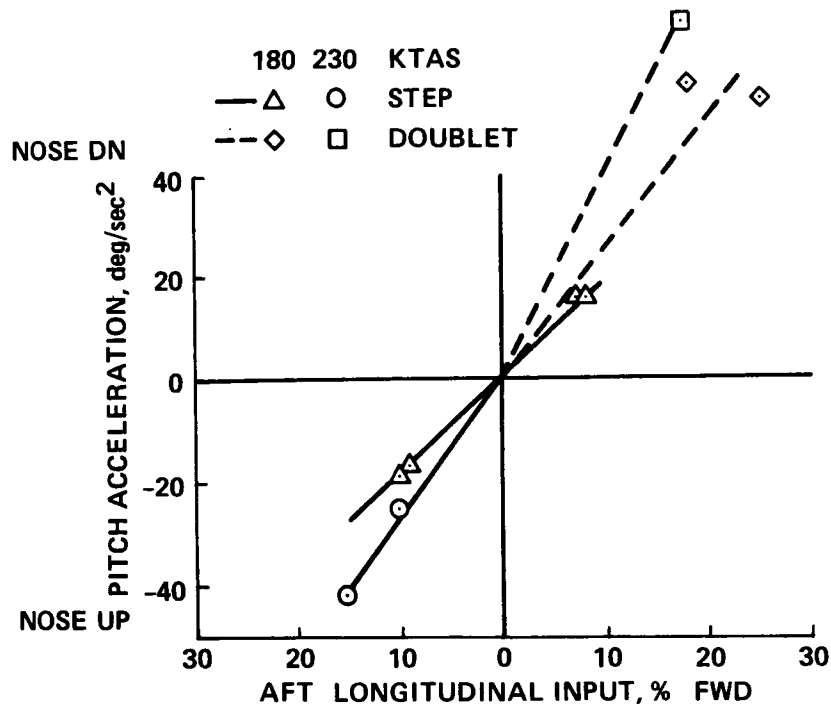


Figure 15.- Hub-On pitch acceleration versus longitudinal stick input.

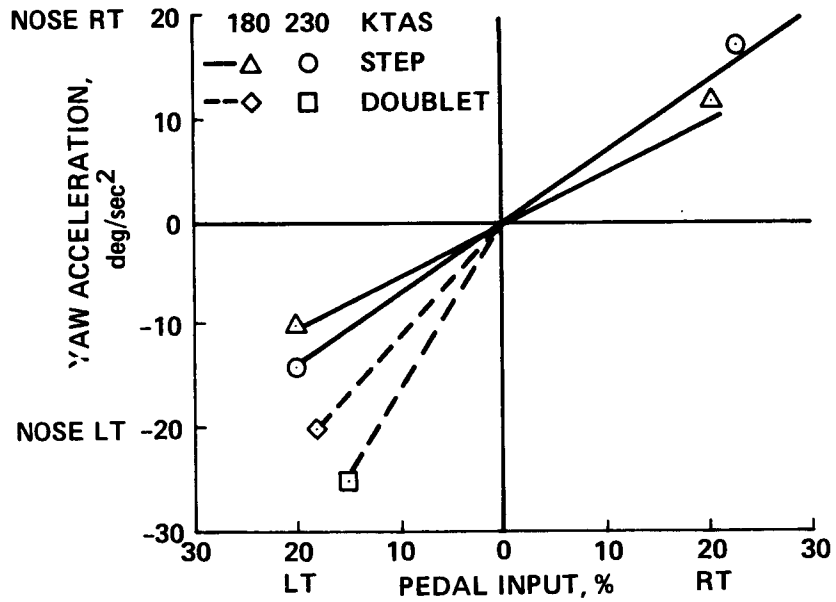


Figure 16.- Hub-on yaw acceleration versus pedal input.

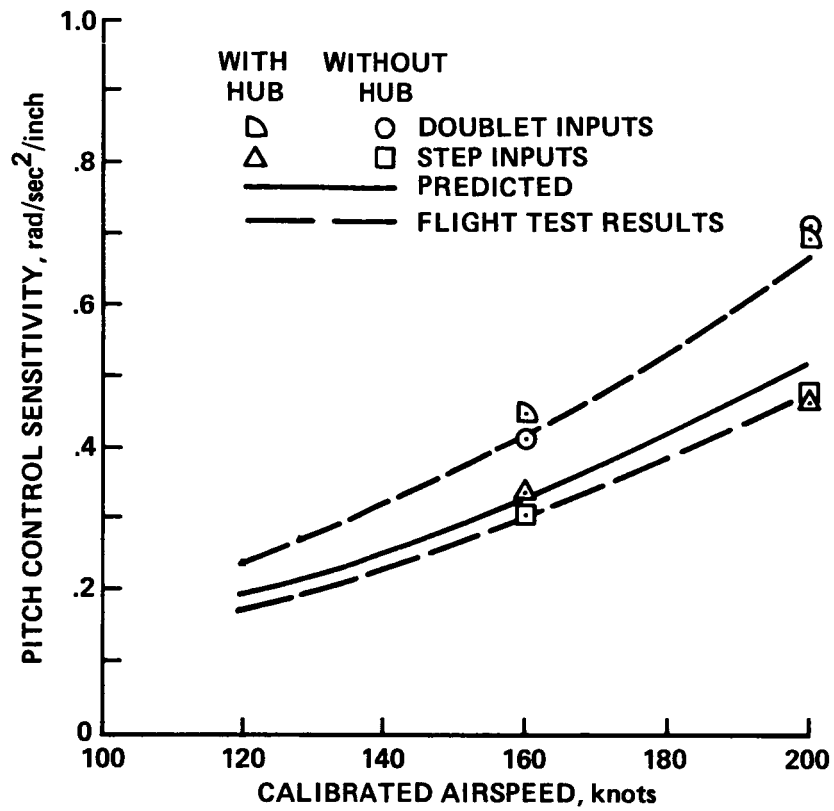


Figure 17.- Longitudinal control power versus calibrated airspeed.

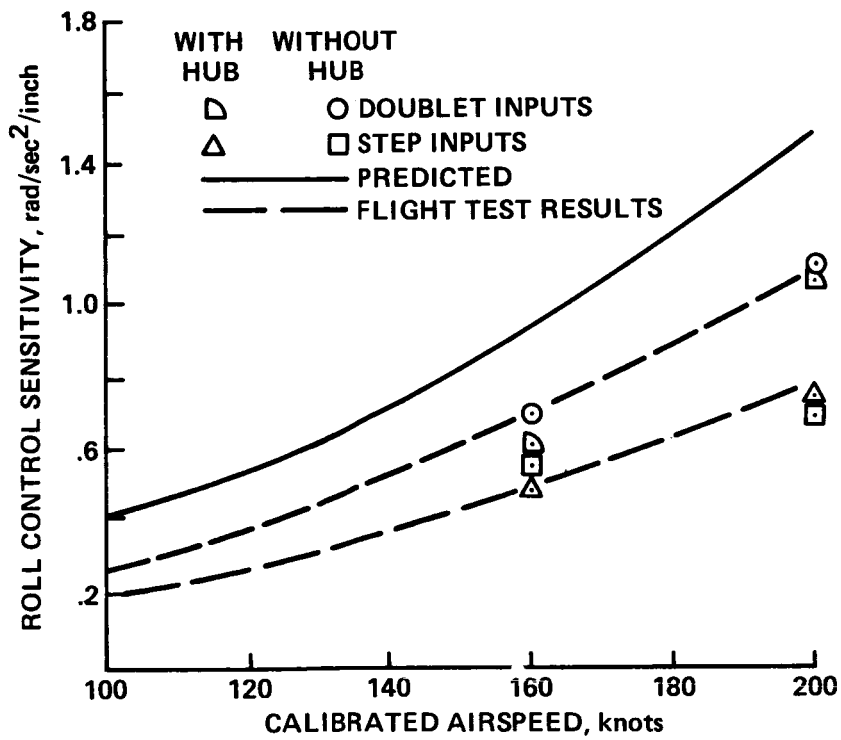


Figure 18.- Lateral control power versus calibrated airspeed.

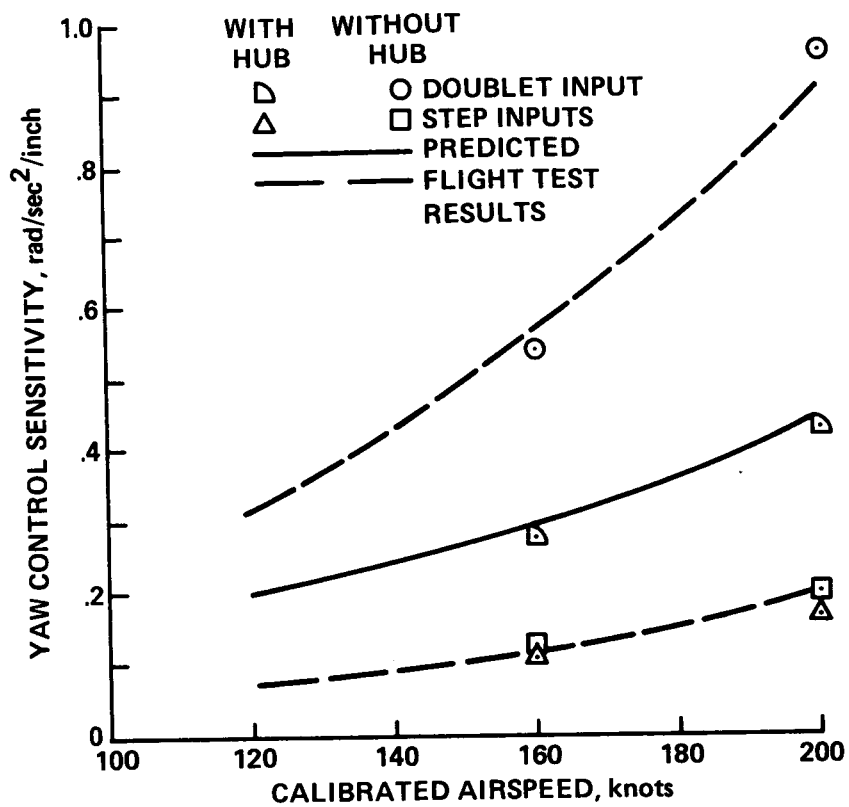


Figure 19.- Yaw control power versus calibrated airspeed.



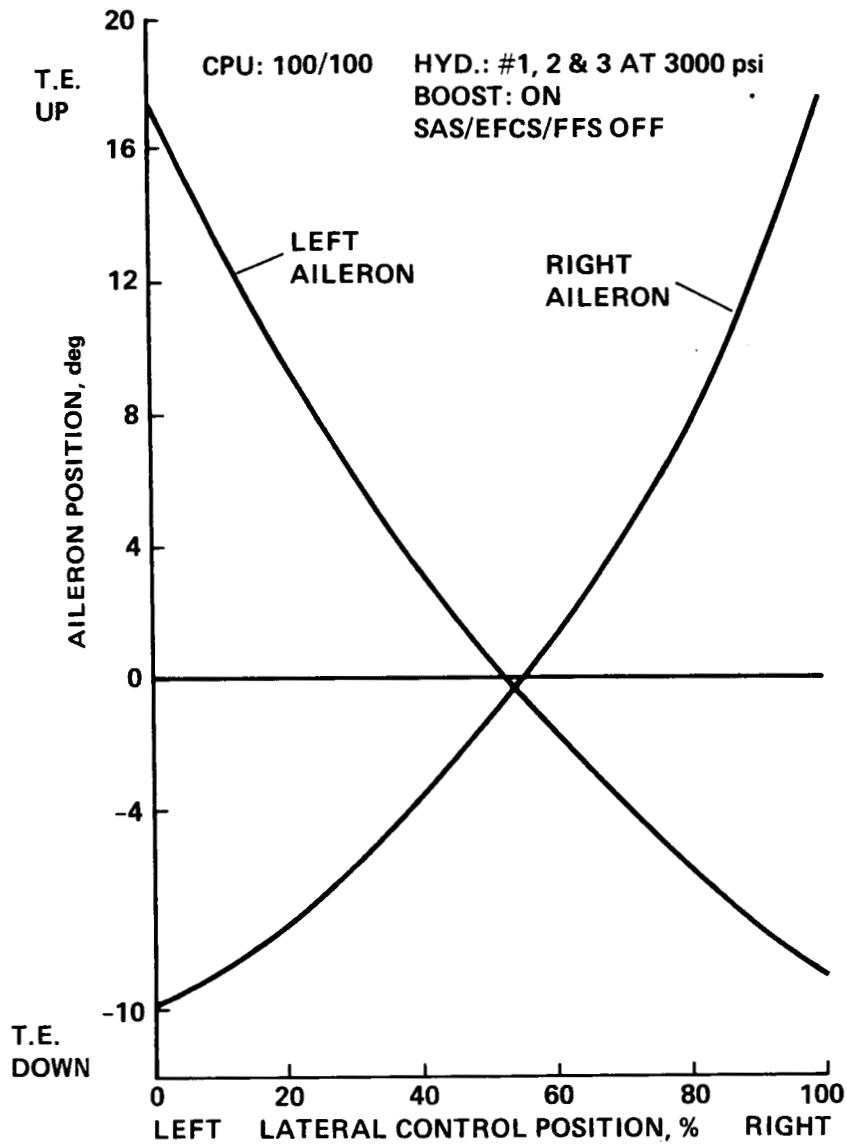


Figure 21.- Aileron rigging characteristics: fixed-wing configuration.

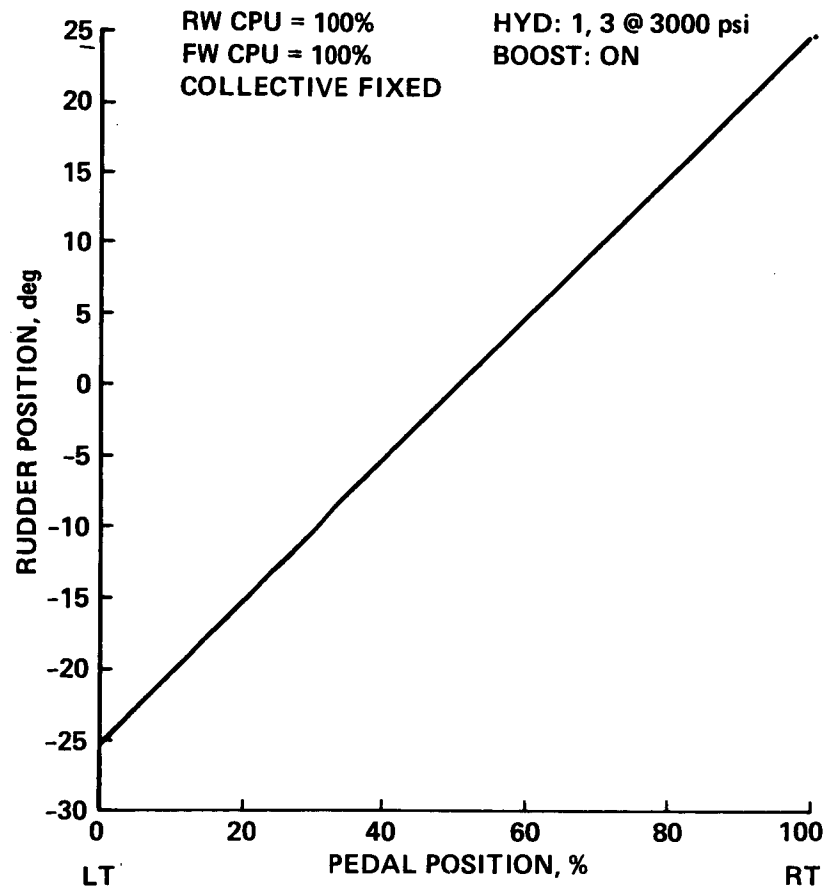


Figure 22.- Rudder rigging characteristics: fixed-wing configuration.

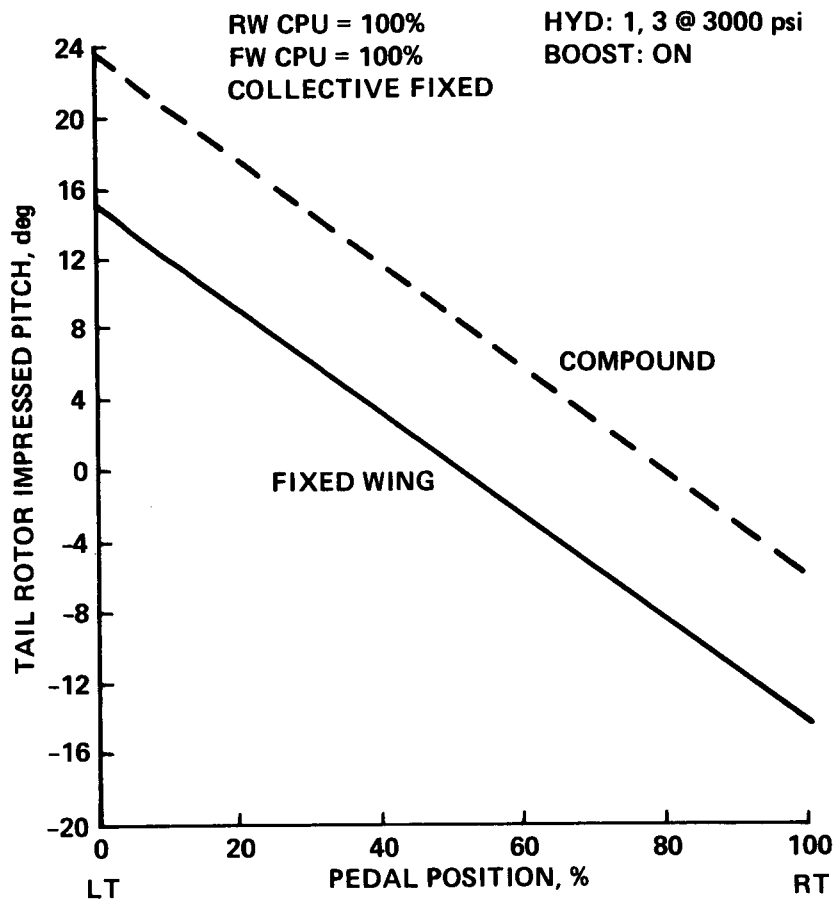


Figure 23.- Tail-rotor rigging characteristics.

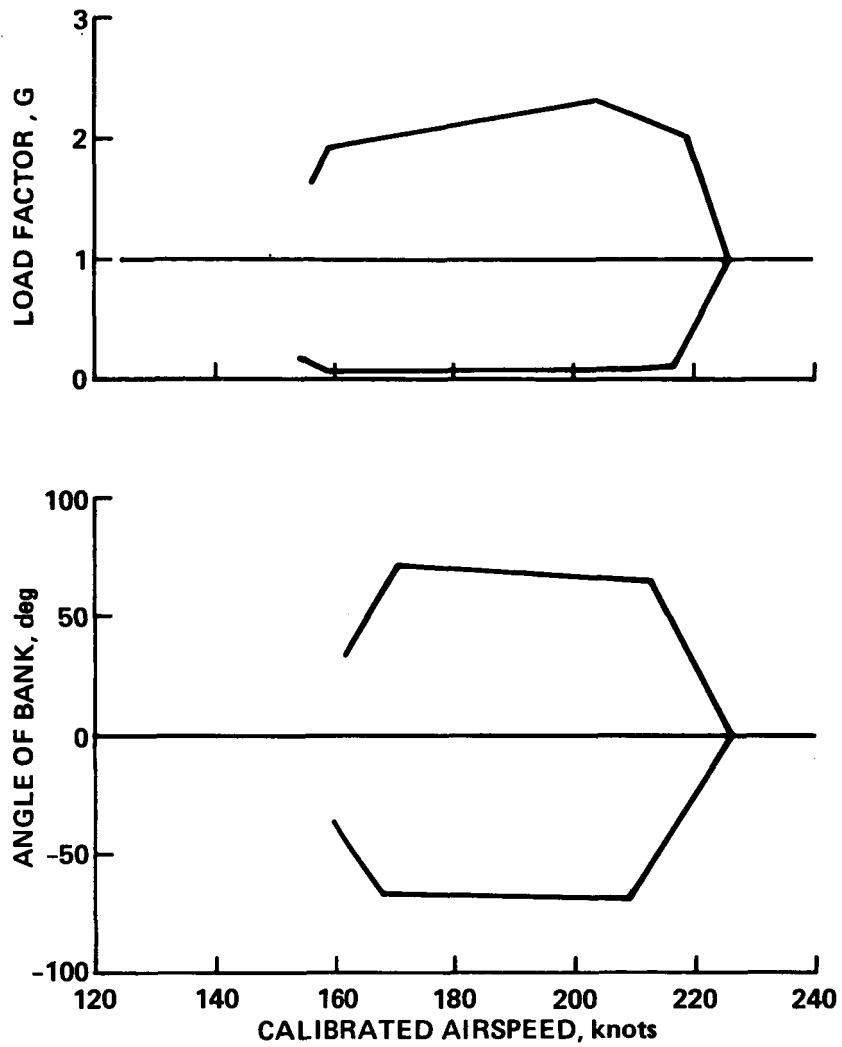


Figure 24.- Flight envelope for fixed-wing configuration: load factor and angle of bank versus calibrated airspeed.

FLIGHT NO. 14; RUN NO. 16

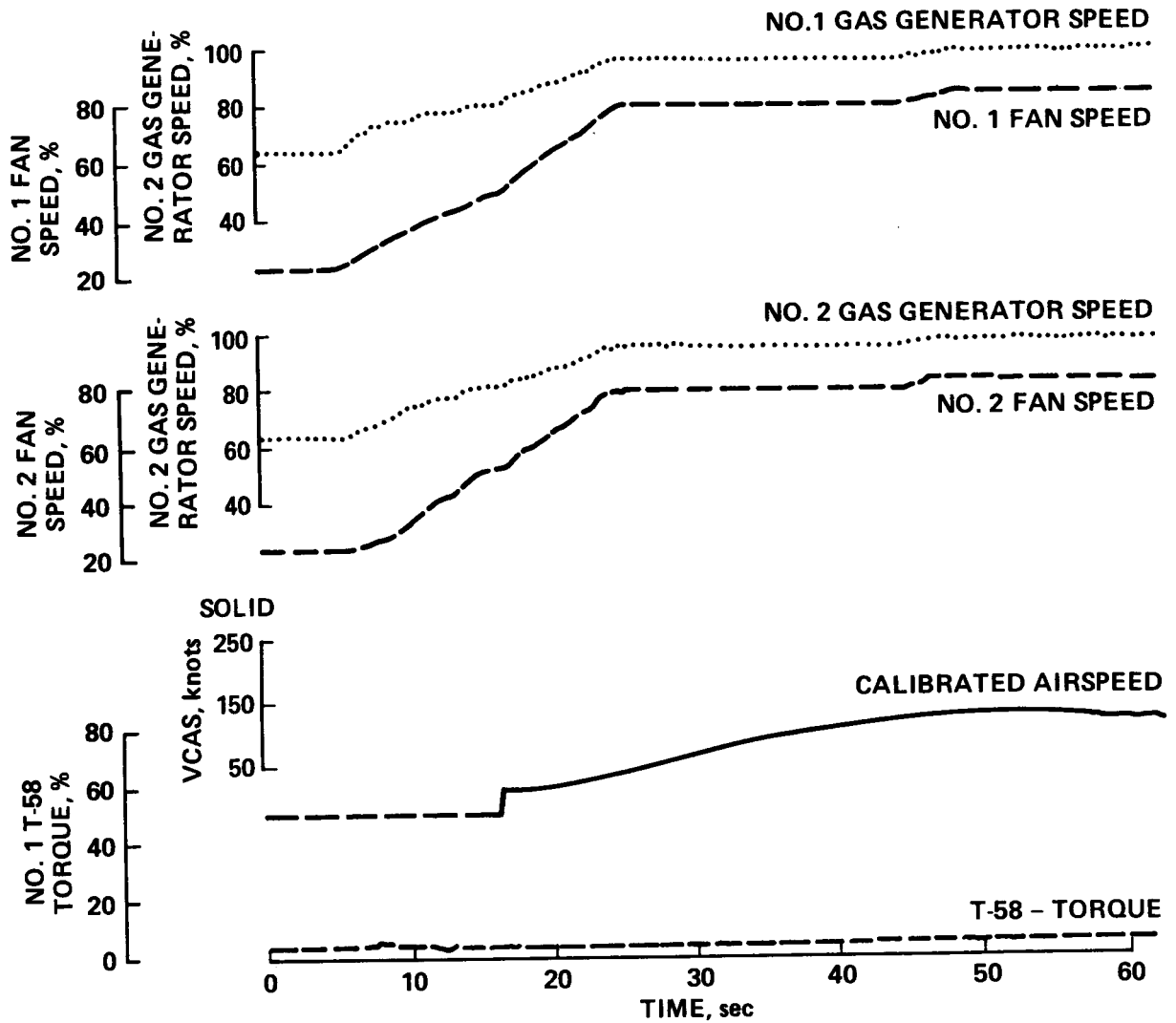


Figure 25.- Takeoff performance: 5° wing incidence, 15° flaps.

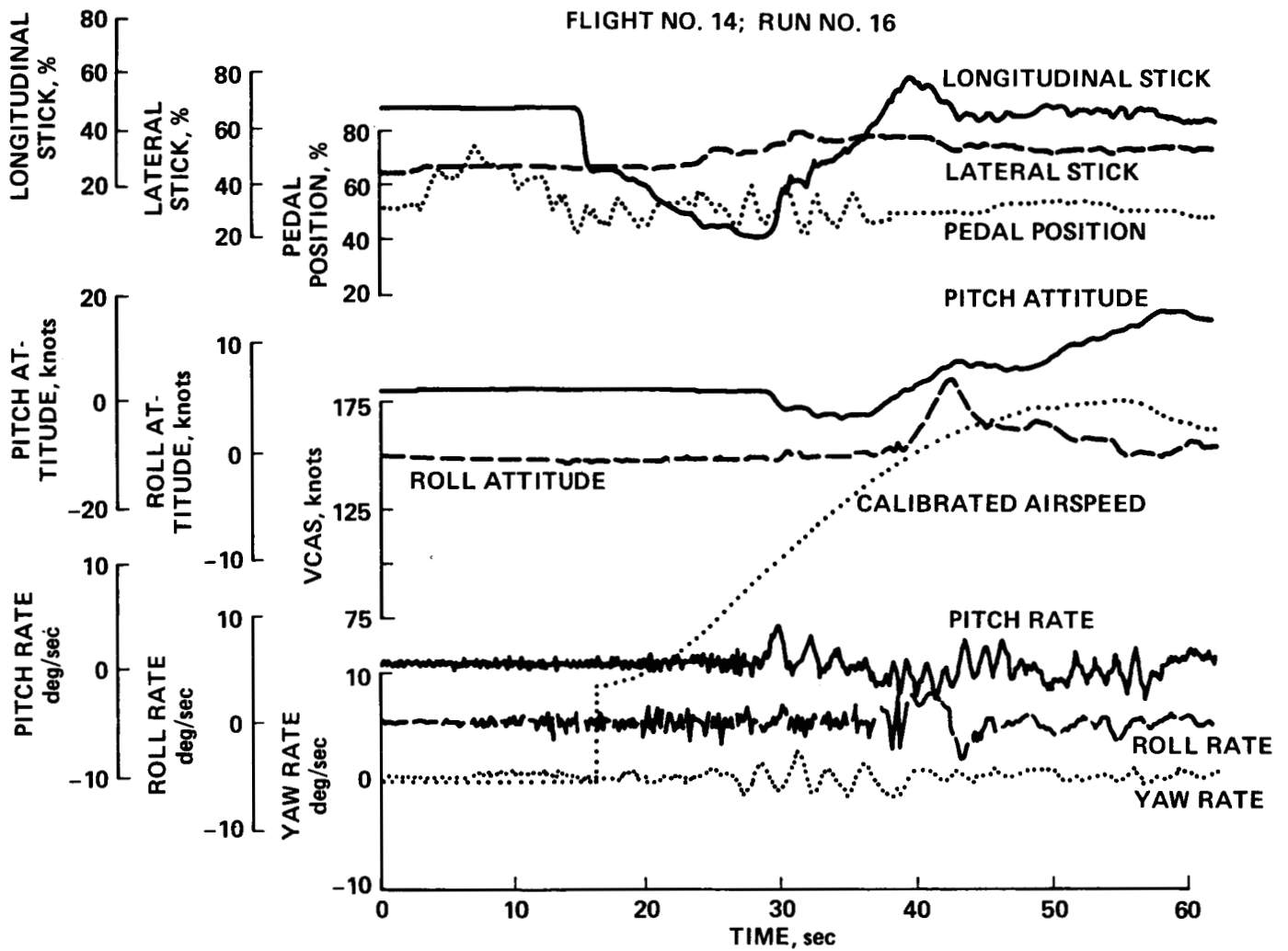


Figure 26.- Takeoff handling qualities: 5° wing incidence, 15° flaps.

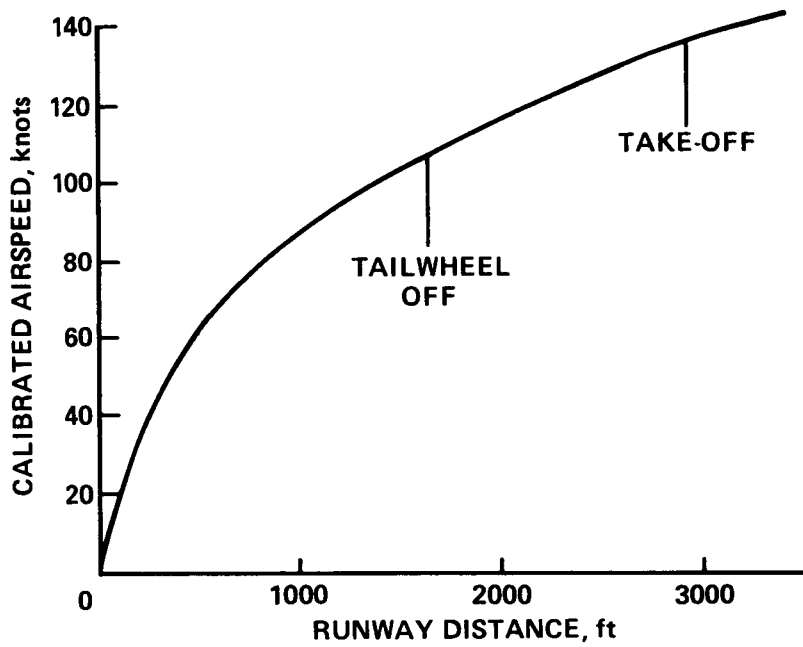


Figure 27.- Calibrated airspeed versus runway distance.

FLIGHT NO. 15: RUN NO. 49

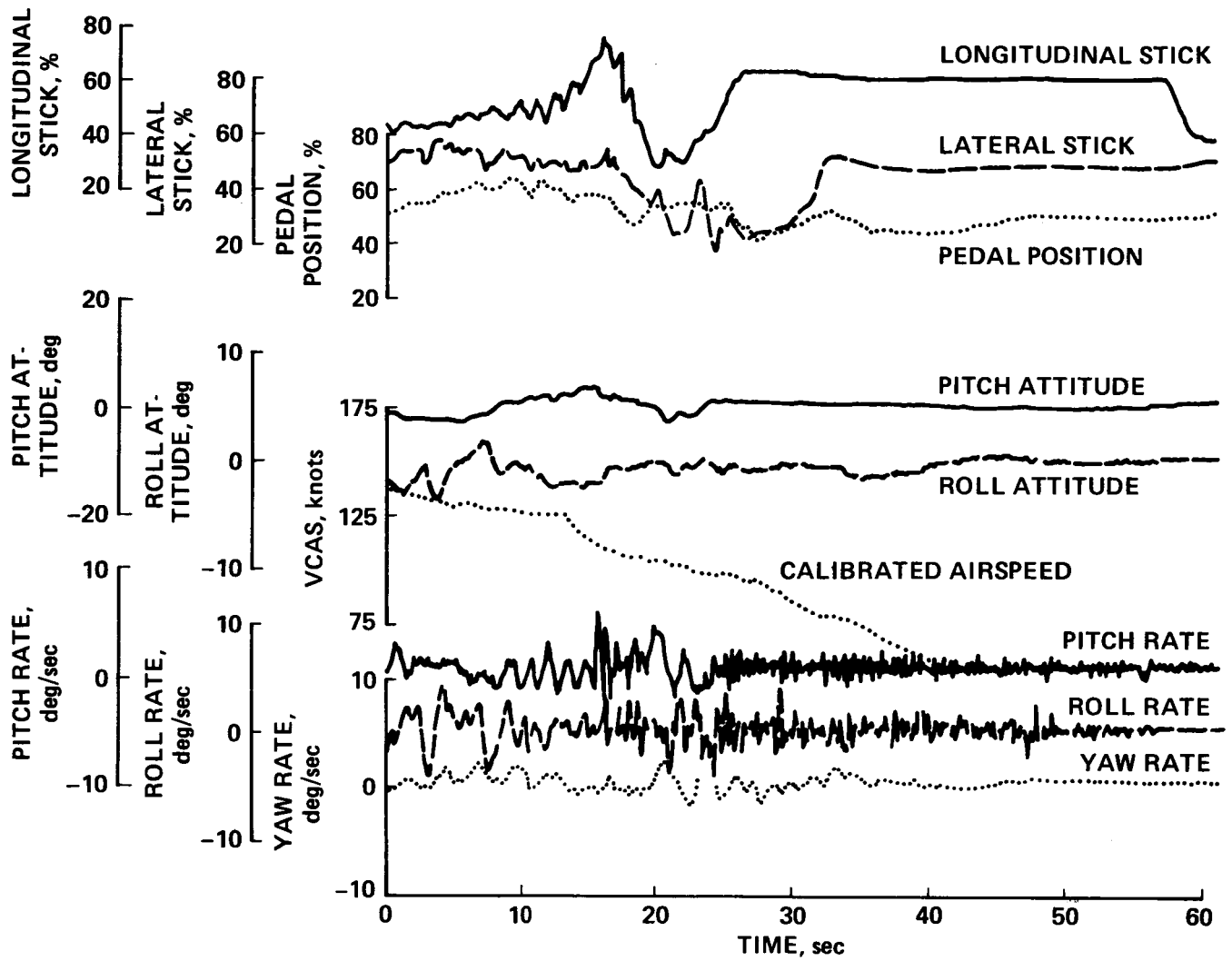


Figure 28.- Landing handling qualities: 5° wing incidence, 25° flaps.

FLIGHT NO. 15; RUN NO. 49

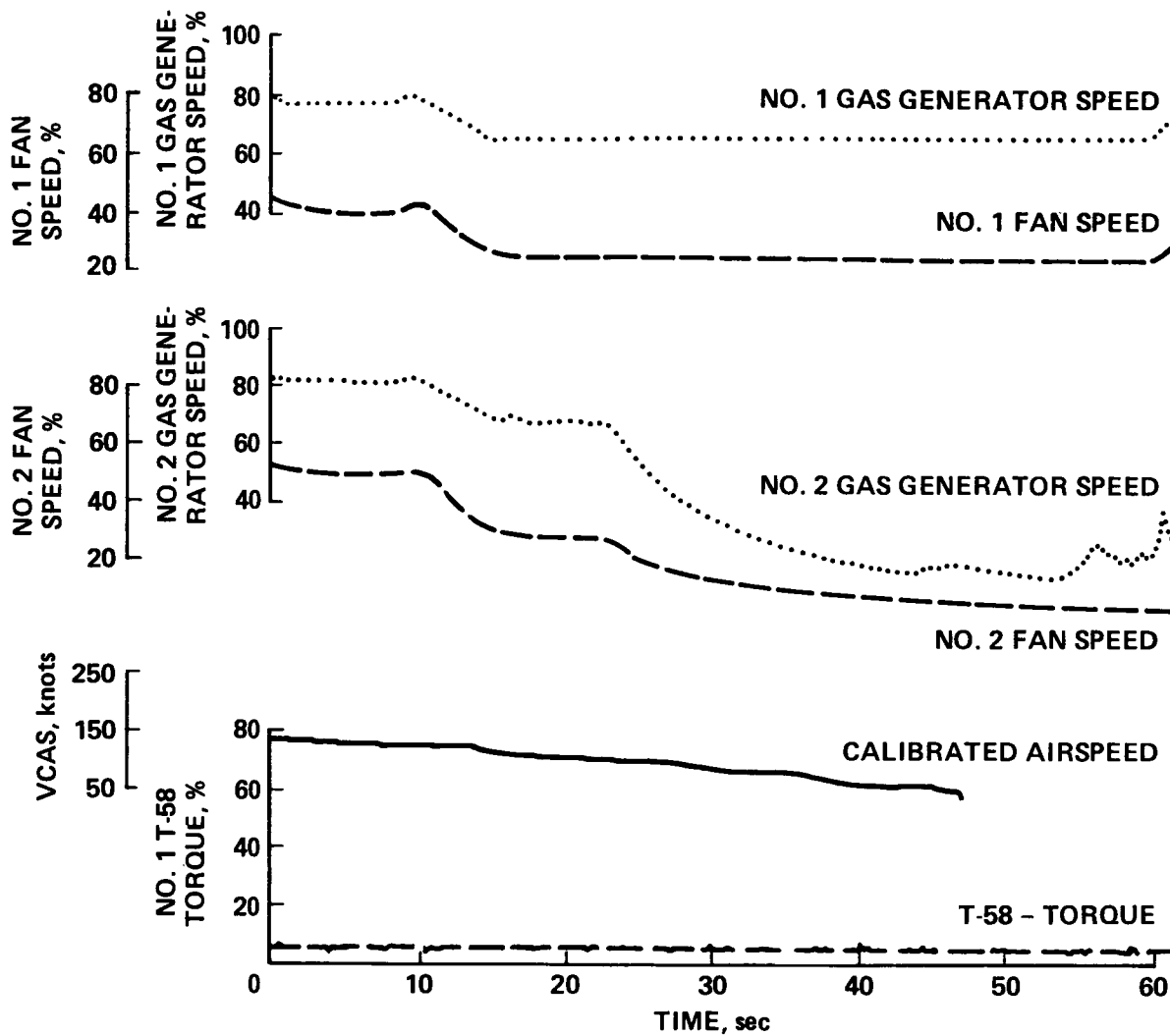


Figure 29.- Landing performance: 5° wing incidence, 25° flaps.

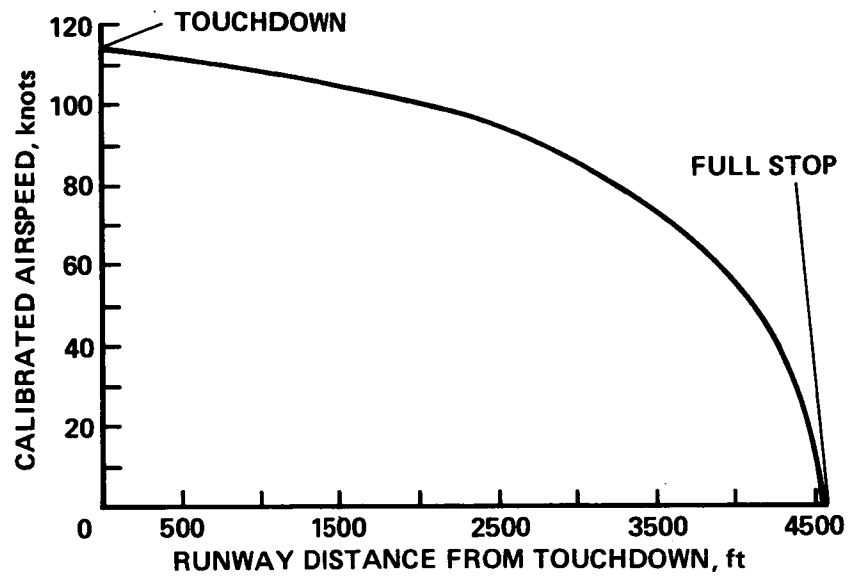


Figure 30.- Calibrated airspeed versus runway stopping distance.

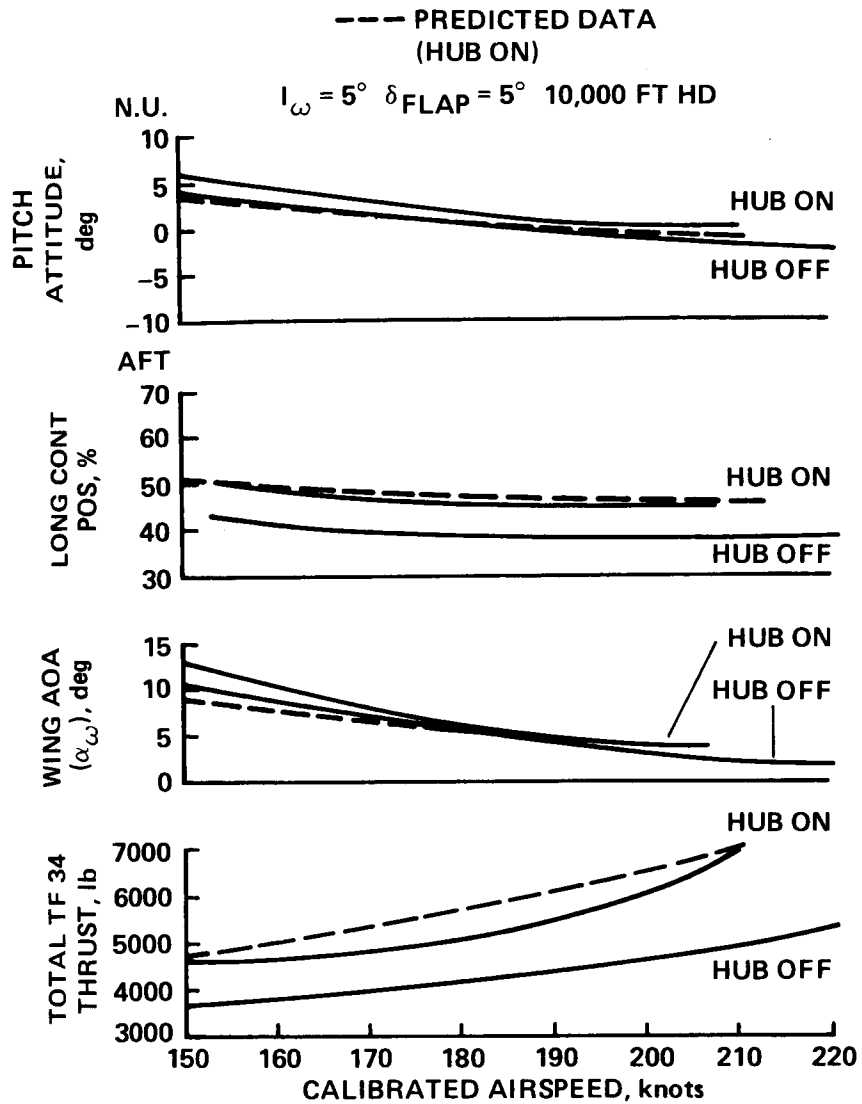


Figure 31.- Level-flight longitudinal trim, test and predicted:  $I_w = 5^\circ$ ,  $\alpha_{flap} = 5^\circ$ , 10,000-ft  $H_d$ .

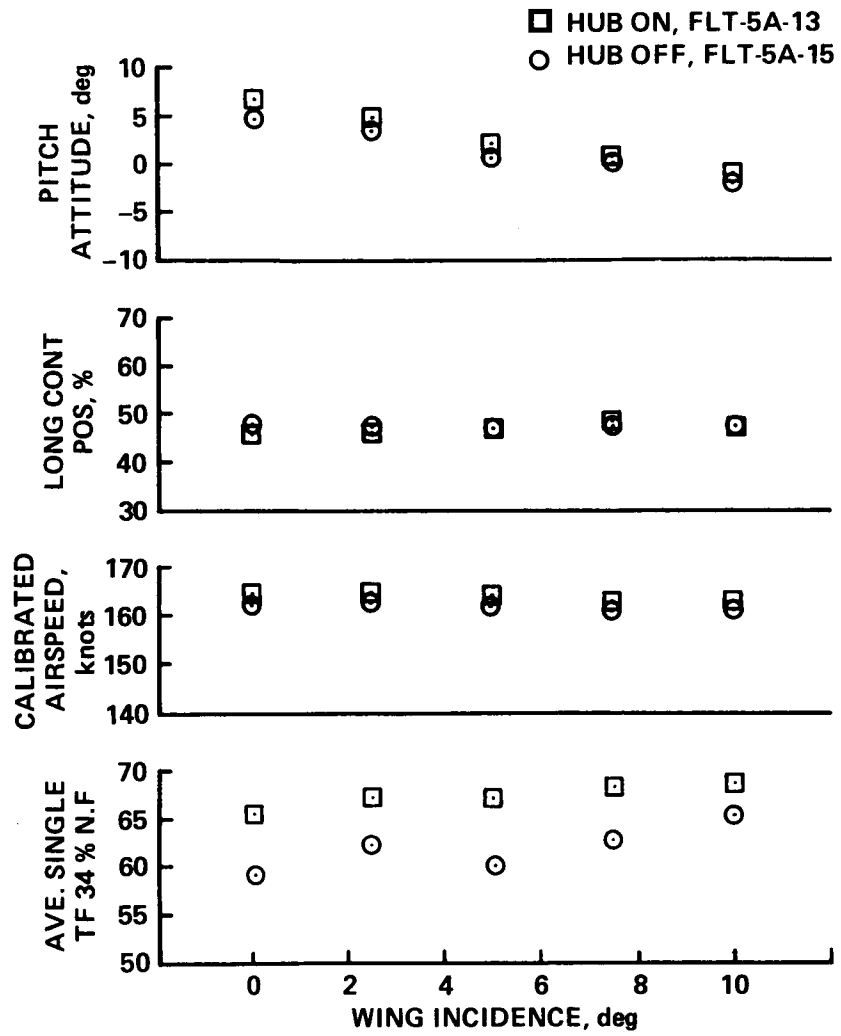


Figure 32.- Effect of wing incidence on longitudinal trim: 165 KCAS, 10,000 ft H<sub>d</sub>.

## 5. VIBRATION

Three factors affected crew comfort and airframe vibration during the program:

1. Wing-wake impingement on the stabilator with the wing at 5° incidence and the flaps at 0°. This was alleviated by deflecting the flaps to 5°.
2. With the main-rotor hub and weight installed, the resulting turbulence excited the stabilizer, rudder, and tail-rotor gear-box.
3. During flight 12, the right-side wing-root fairing peeled back at the high-speed test point, causing vibration in the wing and turbulence over the stabilator which excited the airframe.

### Engine Vibration

The TF-34 thrust engine vibration levels were monitored at locations specified by General Electric. The data are shown in figure 33 as a function of percent fan speed; the vibration levels were below the specified limit of 2.5 in./sec at all engine speeds.

### Crew Comfort

Figures 34 and 35 show cockpit vibration as a function of airspeed. Without the main-rotor hub installed, the aircraft was smooth. With the main-rotor hub and weight installed, the aircraft was rough. The frequency analysis shown in figure 36 illustrates the increase in vibration levels affected by turbulence from the hub-on configuration. Since these frequencies were low, they represented relatively large displacement and, therefore, an uncomfortable environment for the pilots.

### Airframe Vibration

Figures 37 through 41 present data recorded at various airframe locations which were primarily used to monitor airframe response during envelope expansion. The effect of the main-rotor hub and weight installation is evident in figures 37 (lateral only), 38, and 39. This excitation caused vibratory motions of the empennage that were visible to the chase pilot and that showed up on film. The shake was not steady, but of an aperiodic in-and-out nature. Attempts to reduce the shaking by changing the flap setting, wing incidence, and sideslip (small) were not successful. The shake was uncomfortable for the pilots (see fig. 36), but did not cause undue fatigue damage to the empennage attachment points. However, only two flights, 12 and 13, were completed in the hub-on configuration to acquire required data.

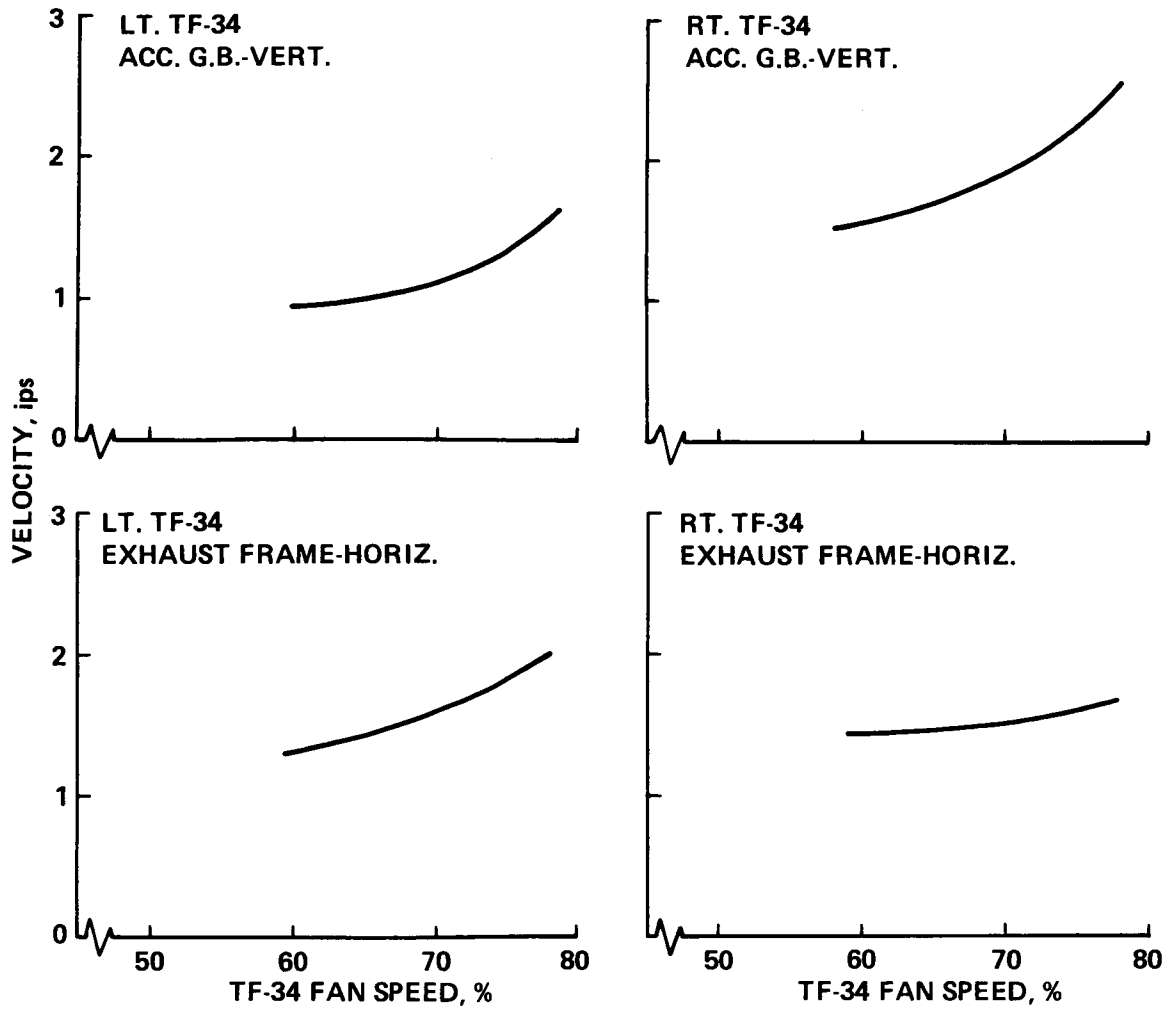


Figure 33.- TF-34 engine vibration: complex waveform, faired data.

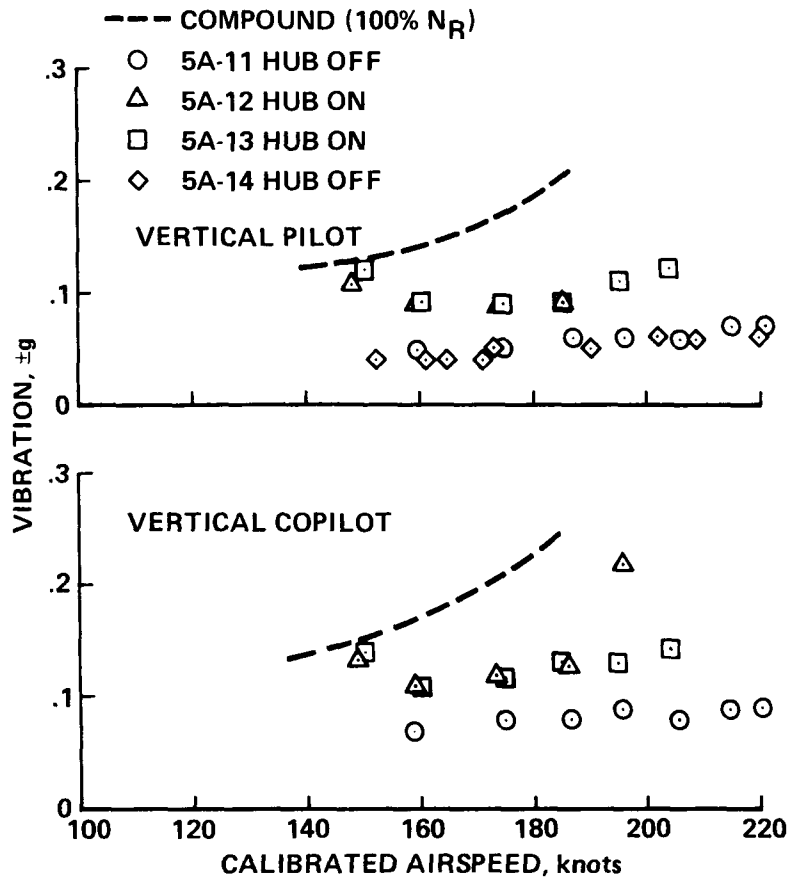


Figure 34.- Cockpit vertical vibration: 94%  $N_R$ , complex waveform.  
 (a) Vertical: pilot; (b) vertical: copilot.

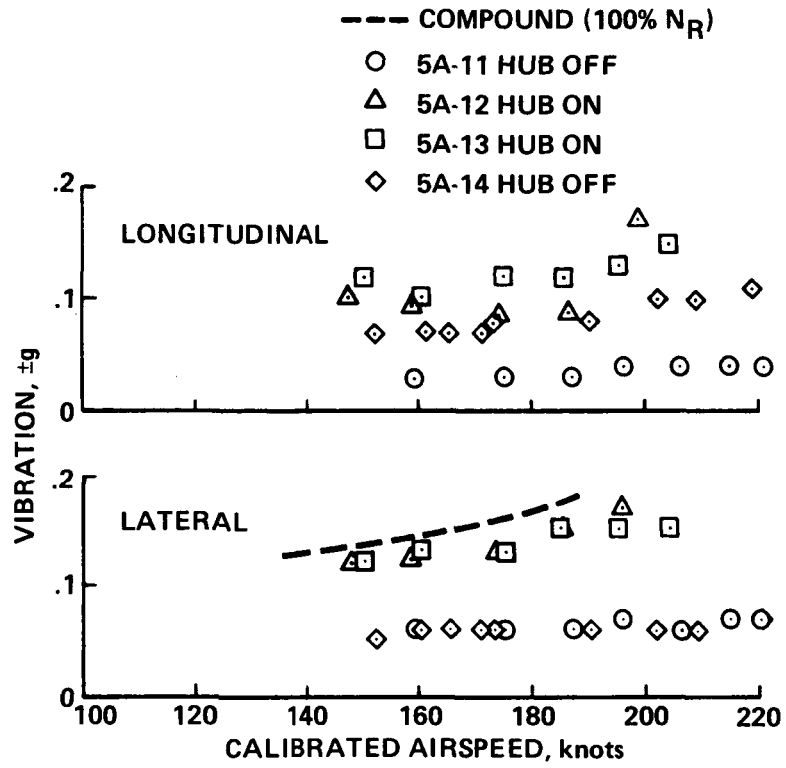


Figure 35.- Cockpit lateral and longitudinal vibration: 94%  $N_R$ , complex waveform. (a) Longitudinal; (b) lateral.

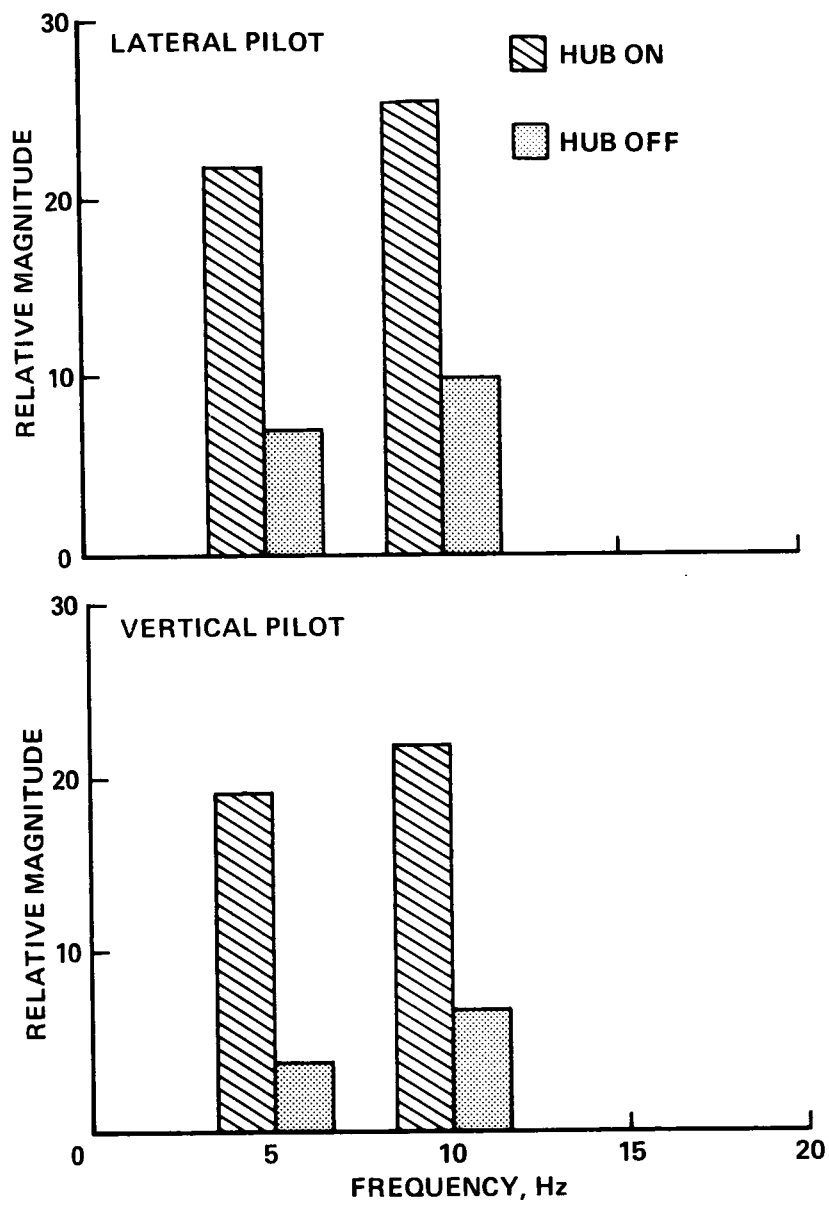


Figure 36.- Cockpit floor low-frequency spectrum: 196 KCAS, 94%  $N_R$ . (a) Lateral pilot; (b) vertical pilot.

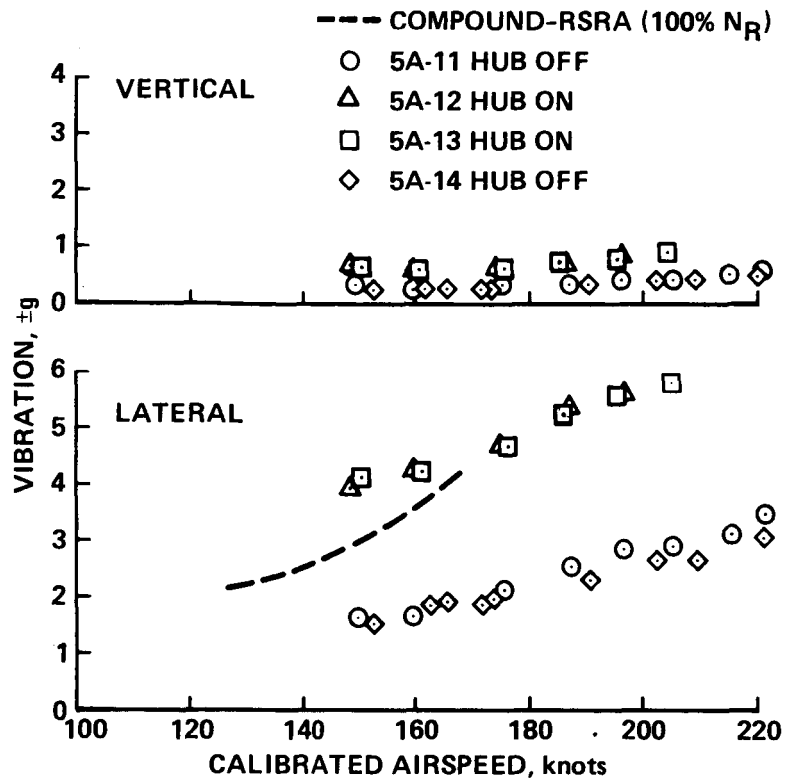


Figure 37.- Tail-rotor gear box vibration: 94%  $N_R$ ; complex waveform.  
 (a) Vertical; (b) lateral.

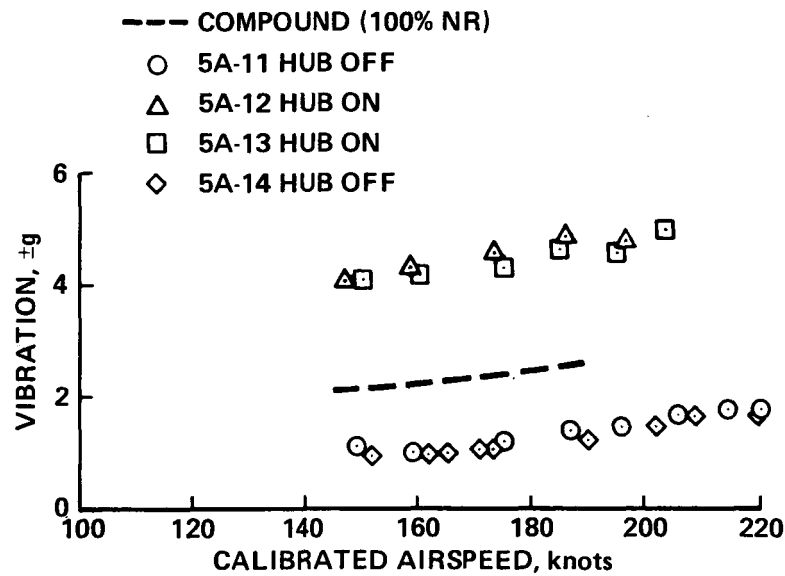


Figure 38.- Top-tail-pylon centerline lateral vibration: 94%  $N_R$ , complex waveform.

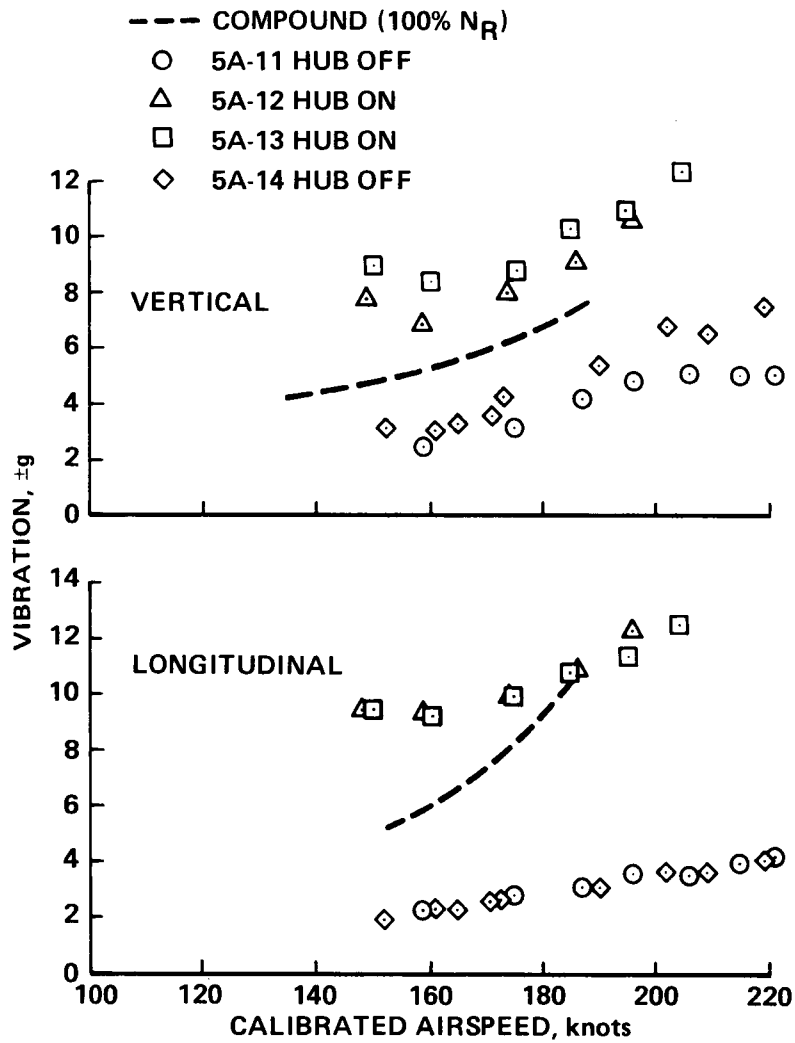


Figure 39.- Upper stabilizer right-tip vibration: 96%  $N_R$ , complex waveform.  
 (a) Vertical; (b) longitudinal.

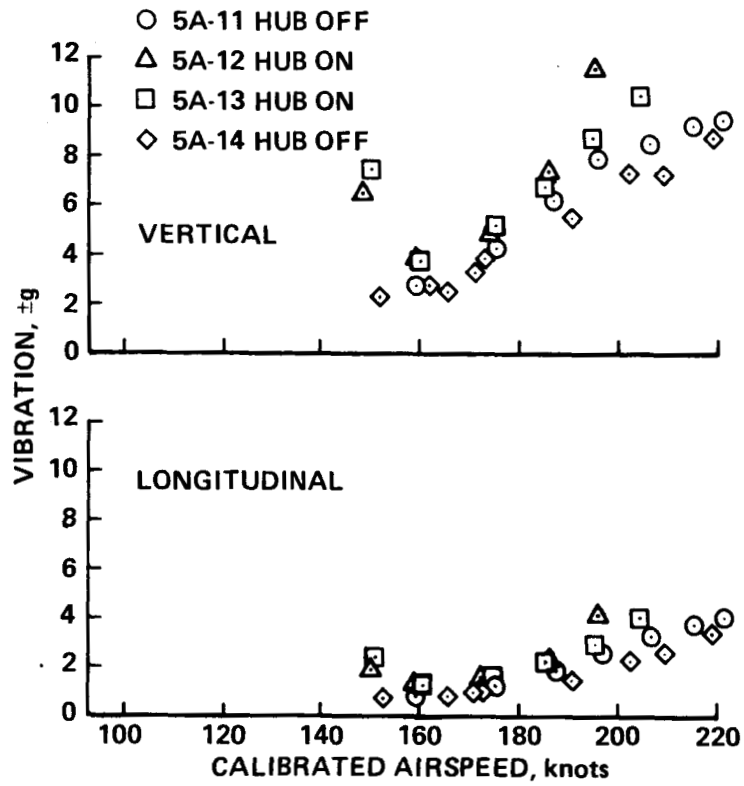


Figure 40.- Lower stabilizer right-tip vibration: 94%  $N_R$ , complex waveform.  
 (a) Vertical; (b) longitudinal.

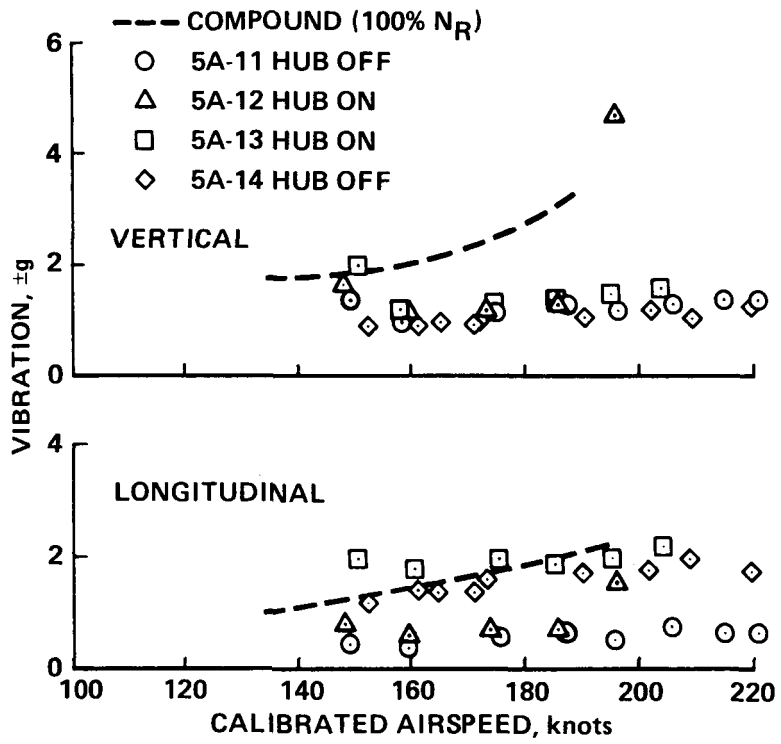


Figure 41.- Right wing-tip vibration: 94%  $N_R$ , complex waveform. (a) Vertical; (b) longitudinal.

## 6. STRUCTURES

The three factors that affected crew comfort and the airframe vibrations reported in section 5 also affected airframe vibratory loads and stresses.

### Stabilator and Stabilizer Loads and Stresses

The same method of analyzing stabilator loads, stresses, and fatigue damage as reported in reference 5 were applied. Figure 42 shows that the damage accumulated was very low [the portion of the curve under flight-test plan (FTP) 5A]. Figures 43 through 45 show the derived loads and stresses in the stabilator attachment and backup structure. The sensitivity to the main-rotor mass installation and wing-root fairing failure is quite evident. Figure 46 presents the stabilizer attachment stresses and also shows a high sensitivity to turbulence. Permissible fatigue damage accumulation on the drag box has been approved to 75% and on the tang and lugs to 50%.

### Tail Rotor

The tail rotor was monitored primarily to ensure that there were no instabilities present as the high-speed envelope was expanded. To this end, the rotor speed was reduced to 94% in order to stay below a tip speed of Mach 1, and the control phase unit was changed after each takeoff so that the rotor was in flat pitch above 150 KIAS (no control inputs). Figures 47 and 48 are data of two primary measurements; they show no abnormal response. Figure 49 presents tail-rotor load-cell data and confirms the high sensitivity to turbulence caused by the main-rotor mass. Some fatigue damage was accumulated in the latter configuration.

### Flight-Control Loads

Figures 50 through 53 show the various flight-control loads. Stabilator, elevator, and aileron loads were acceptable for all conditions tested; however, the aileron load was significantly affected by the wing-root fairing failure in flight 12 at the high-speed point. The rudder control load (fig. 52) was very sensitive to the main-rotor-hub turbulence, and some minimal fatigue damage was accumulated in this configuration.

### Airframe Damage Summary

Table 4 documents the total fatigue damage to date of airframe components and structure with the exception of the stabilator. The components and structure listed (parameters) are those identified by analysis, experience, or test as having potential for fatigue damage. The  $E_w$  in the second column of table 4 is defined as the vibratory stress value for which higher values cause accountable fatigue damage and

lower values can be termed "infinite life." Infinite life is defined as  $10^8$  cycles or more. "Damage (%)" is the damage fraction in percent of the total number of cycles to predicted failure of the component. It is planned that components be replaced when 50% damage is accumulated unless extenuating circumstances warrant other removal limits to be assigned, such as is the case of the lower horizontal stabilator attachment area. In this area, damage to 75% on the drag box is approved, based on inspectability, inspection interval, and crack growth rate.

Fatigue damage accumulation on flights 14 and 15 are included to indicate the rate of damage accrual in the hub-off configuration.

TABLE 4.- DAMAGE TRACKING

Parameter	$E_w (\pm)$	Dam., % 5A-14 <sup>a</sup>	Dam., % 5A-15 <sup>b</sup>	Accumulated dam., %
M.R. SHAFT BNDG LO #1	12800 lb/in. <sup>2</sup>	N.C.	N.C.	7.2061
M.R. STA SCISS LD	220 lb	N.C.	N.C.	0.9086
M.R. PUSH ROD LD UPPER	625 lb	N.C.	N.C.	0.6864
M.R. DAMPER MOM.	27500 lb-in.	N.C.	N.C.	0.0166
M.R. ROT SCISS LD	285 lb	N.C.	N.C.	0.0081
M.R. DRAG CELL	1640 lb @ 7K STY	0.0	0.0	0.0179
M.R. BLADE BR-6	6350 lb/in. <sup>2</sup>	N.C.	N.C.	0.4247
M.R. BLADE BR-7	6350 lb/in. <sup>2</sup>	N.C.	N.C.	0.1142
M.R. RT LAT STA WASH LD	1250 lb	N.C.	N.C.	0.1466
M.R. LT LAT STA WASH LD	1250 lb	N.C.	N.C.	0.1120
M.R. LIFT A	2150 lb	0.0	0.0	0.0451
M.R. LIFT B	2150 lb	0.0	0.0	0.001
M.R. LIFT C	2150 lb	0.0	0.0	0.0067
M.R. LIFT D	2150 lb	0.0	0.0	0.0158
M.R. GB Q CELL E	2200 lb @ 4K STY	0.0	0.0	0.0042
M.R. GB Q CELL F	2200 lb @ 4K STY	0.0	0.0	0.0041
T.R. THRUST CELL N	630 lb @ 1500 STY	0.000125	0.000056	11.0592
T.R. PITCH BND #5	90 lb	0.0	0.0	0.08738
T.R. SPIN EDGE #1 MOM	5200 lb-in.	0.0	0.0	0.00001
T.R. STA CONT LD	300 lb	0.0	0.0	0.0027
T.R. BLADE - P2	4025 lb/in. <sup>2</sup>	0.0005	0.00056	0.00541
UP HORIZ STAB #1	1130 lb/in. <sup>2</sup>	0.000077	0.00128	1.0944
UP HORIZ STAB #2	1130 lb/in. <sup>2</sup>	0.000029	0.00141	0.9933
LO HORIZ STAB #3	2000 lb/in. <sup>2</sup>	N.C.	N.C.	
LO HORIZ STAB #4	2000 lb/in. <sup>2</sup>	N.C.	N.C.	
↓ #9	↓	0.0002	0.00154	0.00993
#10		0.00077	0.00216	0.01433
#18		N.C.	N.C.	0.0019
#23		N.C.	N.C.	0.0007
#29		0.0006	0.0038	0.0143
#30		0.0004	0.0004	0.00846
↓ #1	↓	N.C.	N.C.	0.0003

<sup>a</sup>Flight Test Plan 5A, flight 14. N.C. = not carried.

<sup>b</sup>Flight Test Plan 5A, flight 15. N.C. = not carried.

TABLE 4.- CONCLUDED.

Parameter	$E_w (\pm)$	Dam., % 5A-14	Dam., % 5A-15	Accumulated dam., %
LO HORIZ STAB #32	2000 lb/in. <sup>2</sup>	0.00002	0.0	0.000333
TPLN 225	4900 lb/in. <sup>2</sup>	0.0	0.0	0.00219
	@ 5K STY			
TPLN 226	↓	0.0	0.0	0.00002
TPLN 229		0.0	0.0	0.00001
TPLN 230		0.0	0.000067	0.1753
ELEV CONT ROD LT	305 lb	GAG	GAG	NO S/N CURVE
ELEV CONT ROD RT	305 lb	GAG	GAG	NO S/N CURVE
RT AILERON CONT ROD	94 lb	0.00288	0.0043	1.4696
LT AILERON CONT ROD	94 lb	0.00338	0.0069	1.4738
RUDDER CONT ROD	195 lb	0.000017	0.000084	0.0340
LO HORIZ STAB LIFT LT	2000 lb/in. <sup>2</sup>			
LO HORIZ STAB LIFT RT	2000 lb/in. <sup>2</sup>			
LG AXIAL STRUD LD	437 lb	0.0013	0.000634	0.0165
HORIZ STAB ACT	1010 lb	0.0	0.0	0.0302

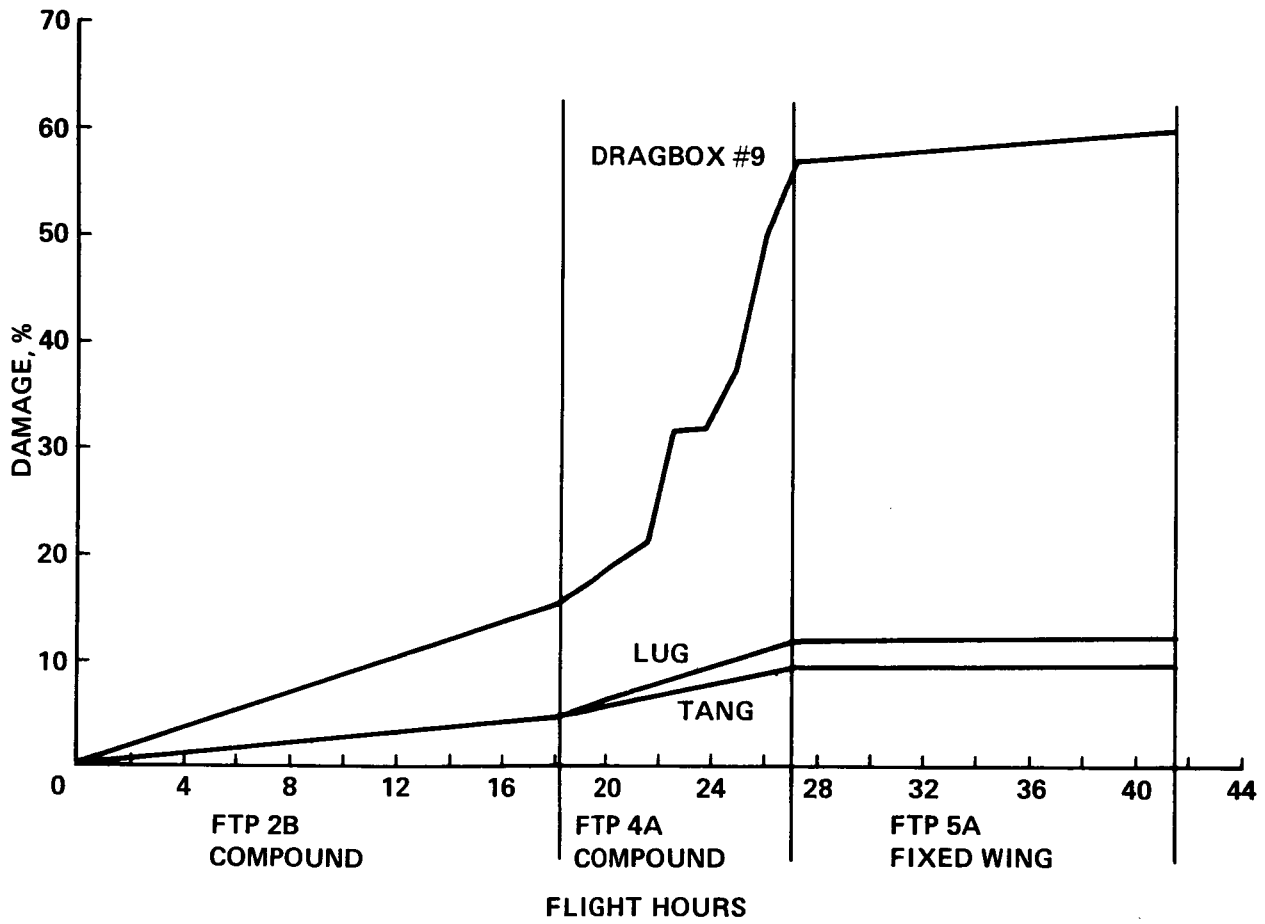


Figure 42.- Percent damage: stabilator lugs and backup structure.

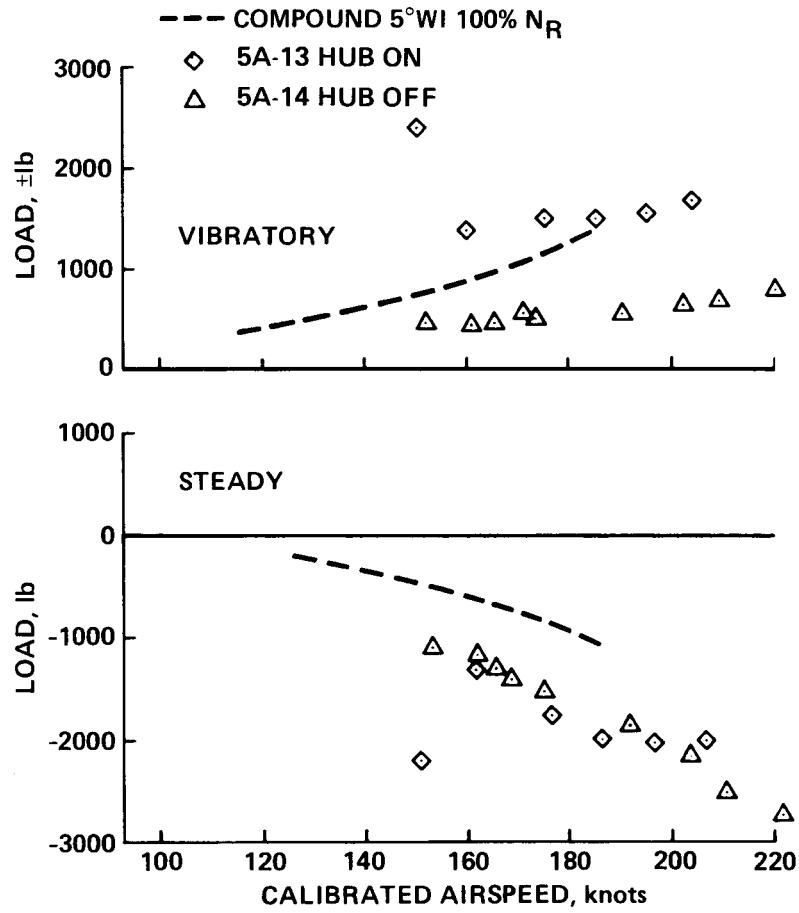


Figure 43.- Derived stabilator lug vibration load: 94% N<sub>R</sub>, 5° wing incidence.

(a) Vibratory. (b) Steady.

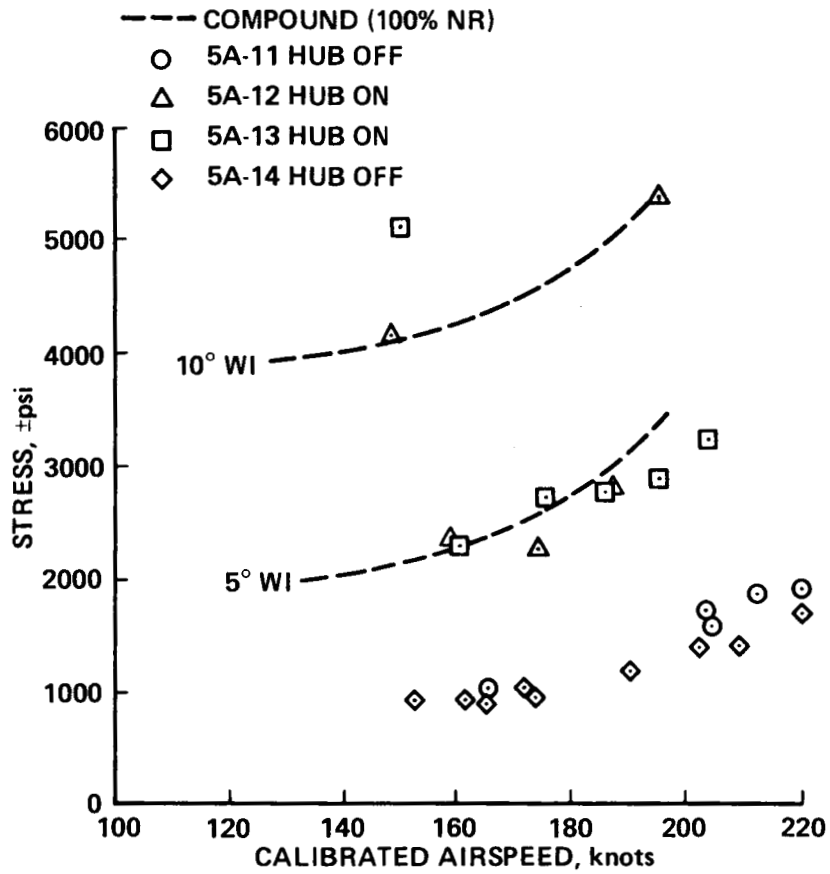


Figure 44.- Derived stabilator dragbox vibratory stress.

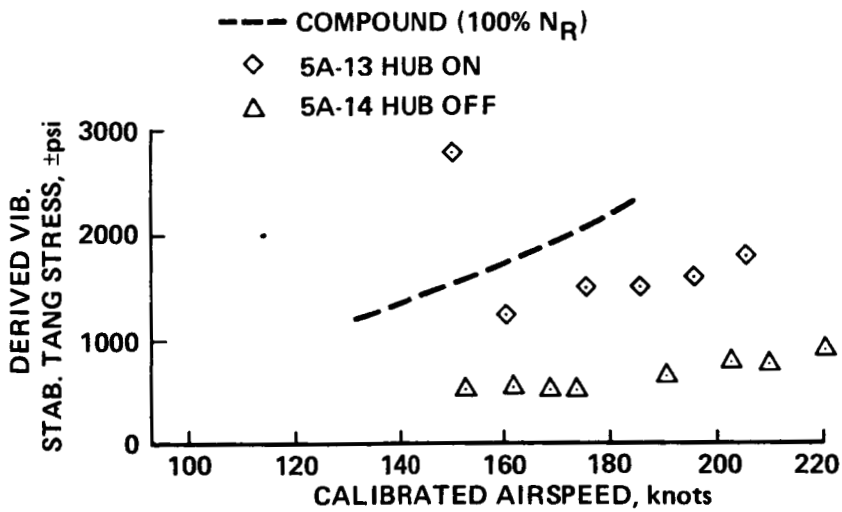


Figure 45.- Derived stabilator tang vibratory stress: 94% NR, 5° wing incidence.

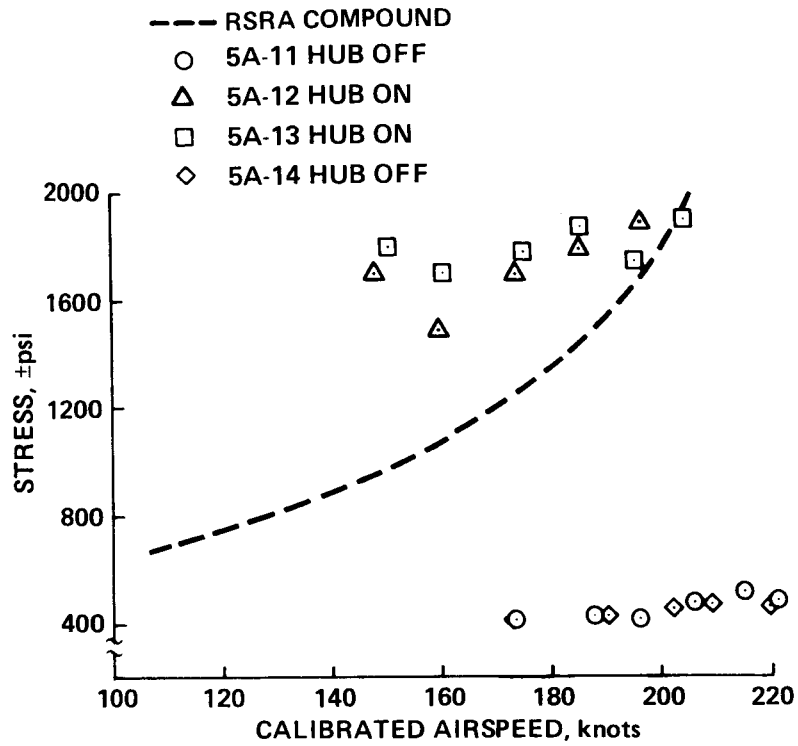


Figure 46.- Upper stabilizer attachment vibratory stress: upper stabilizer No. 1.

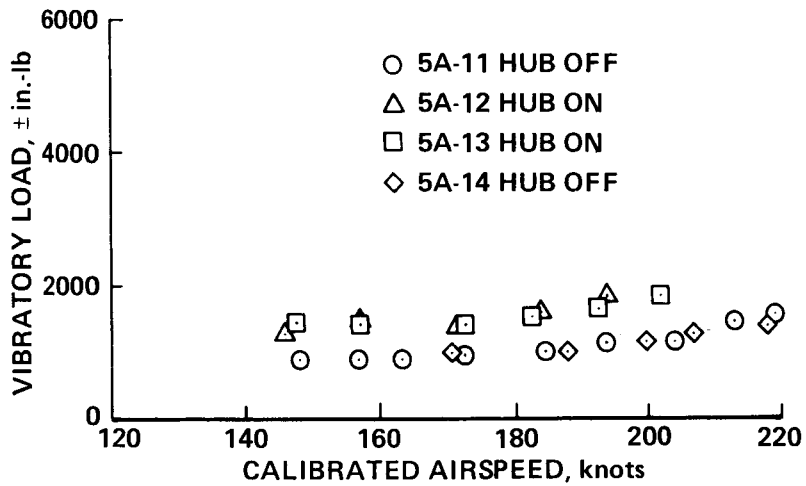


Figure 47.- Tail-rotor spindle edgewise bending versus calibrated airspeed.

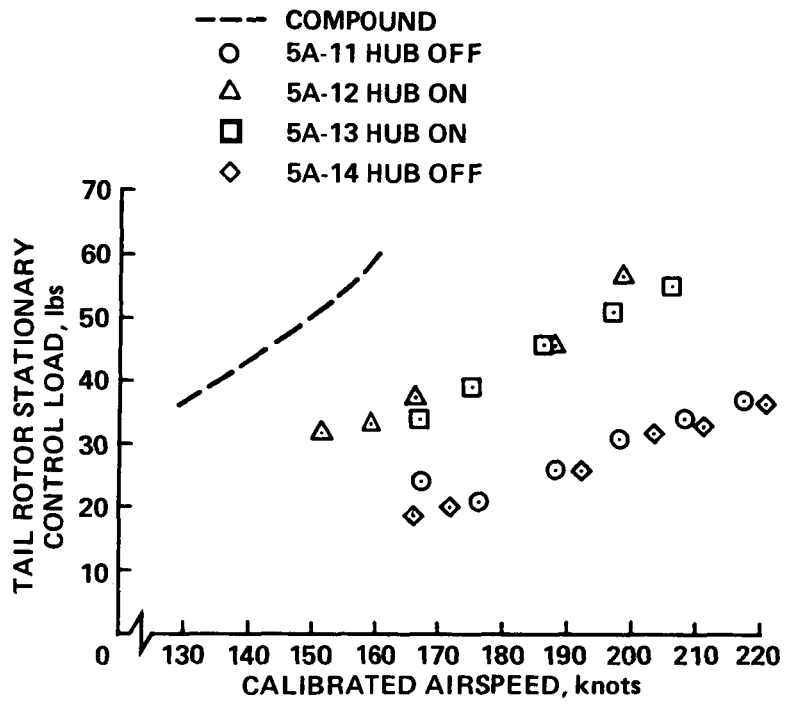


Figure 48.- Tail-rotor stationary control load versus CAS.

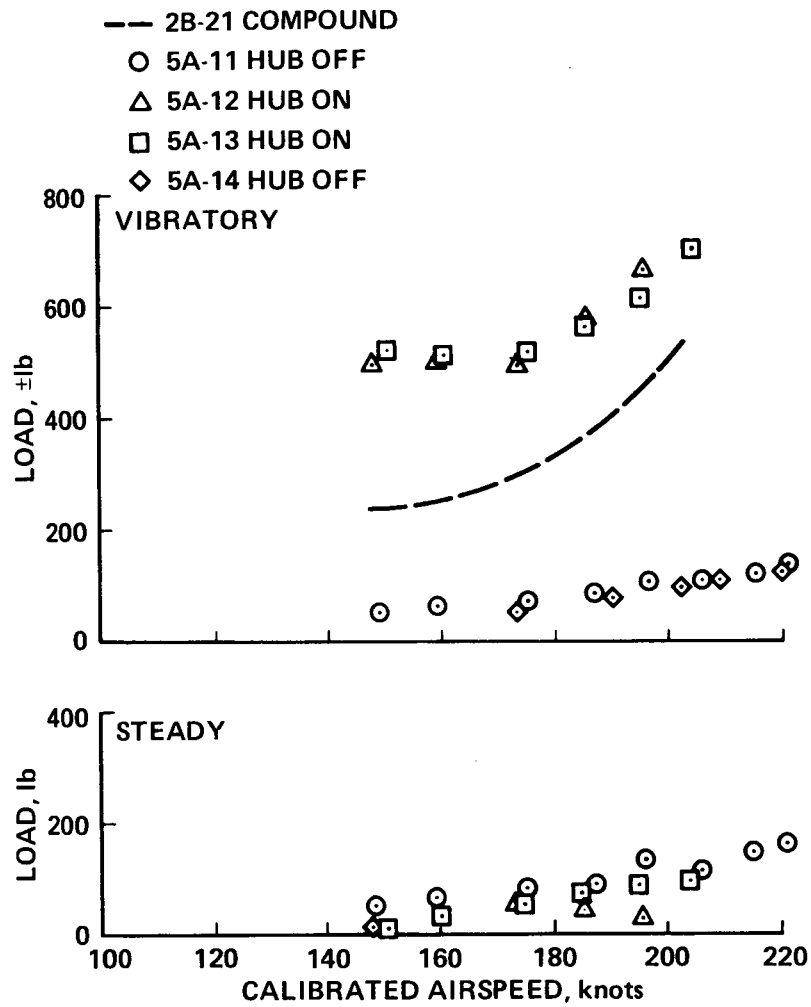


Figure 49.- Tail-rotor thrust load-cell load (a) Vibratory; (b) steady.

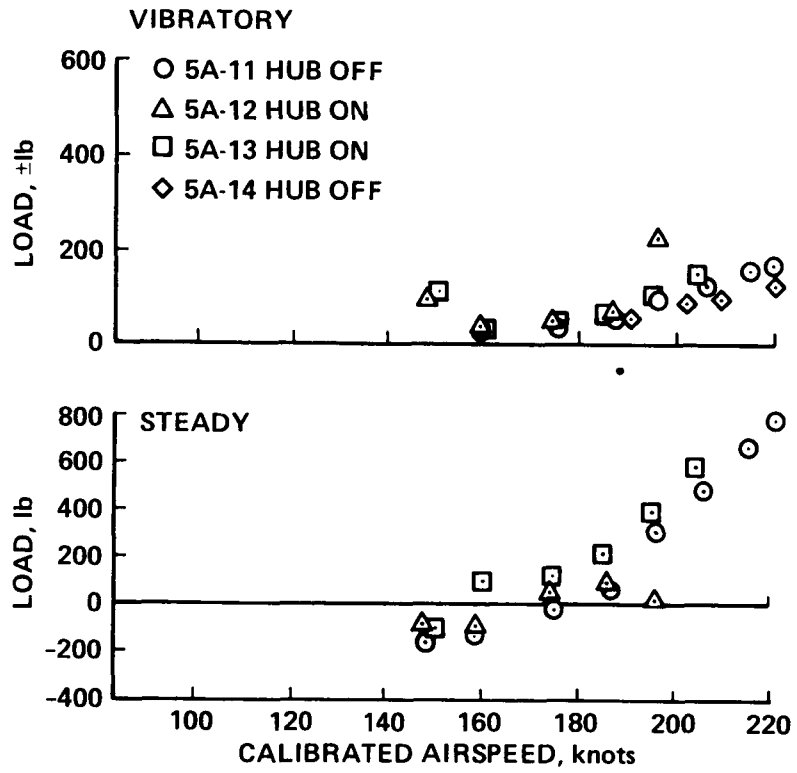


Figure 50.- Horizontal stabilator control load. (a) Vibratory; (b) steady.

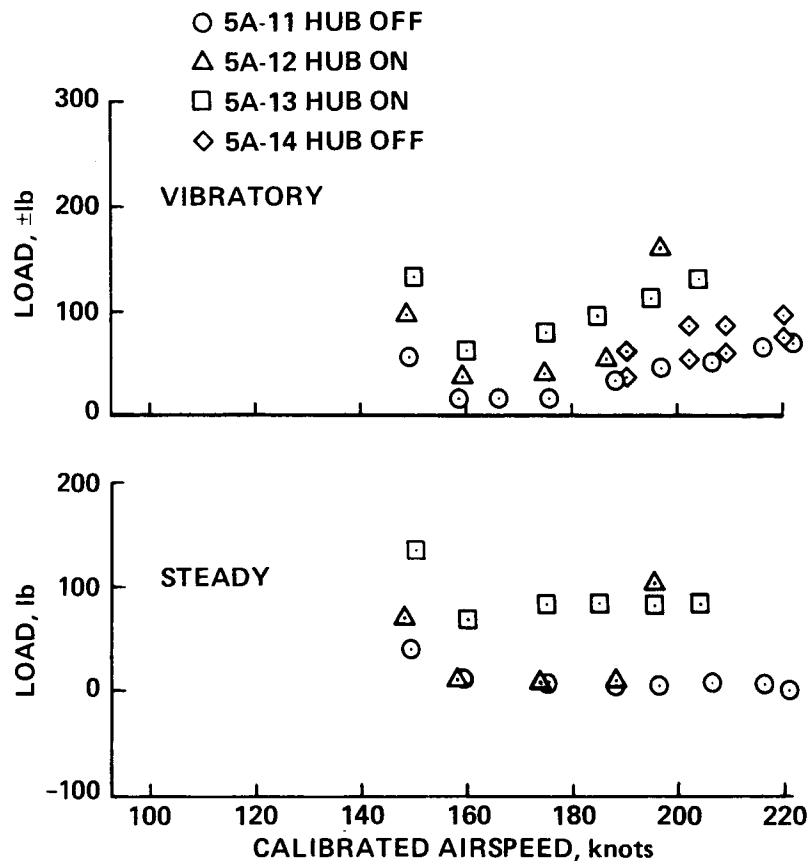


Figure 51.- Elevator control load. (a) Vibratory; (b) steady.

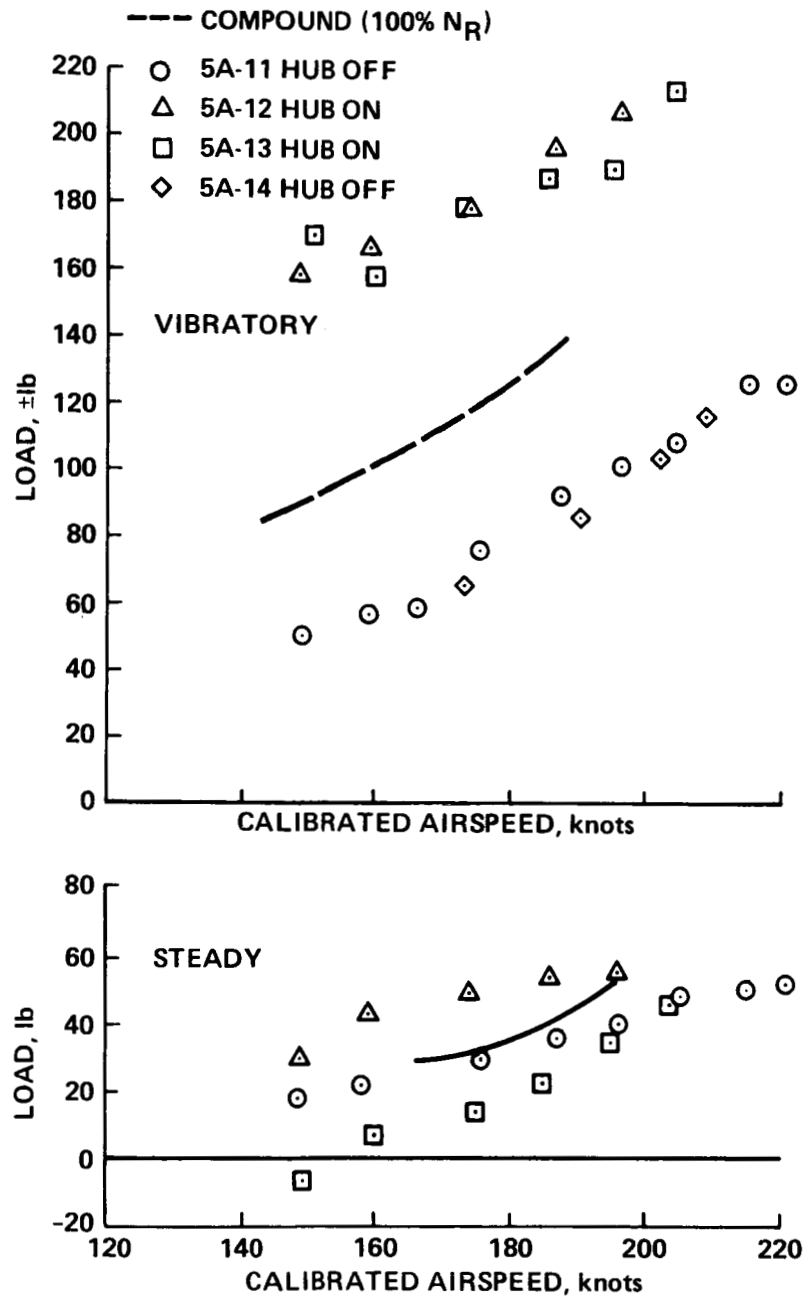


Figure 52.- Rudder control-rod loads. (a) Vibratory; (b) steady.

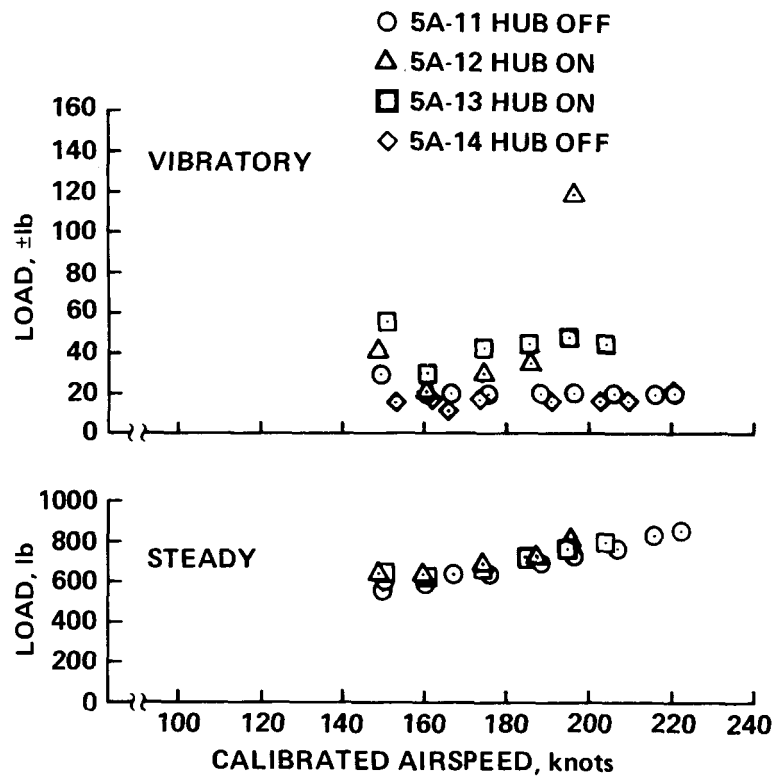


Figure 53.- Aileron control-rod load: right. (a) Vibratory; (b) steady.

## 7. PERFORMANCE

One objective of the RSRA fixed-wing flight-test plan was to obtain limited level-flight performance and trim data. The level-flight performance data consist of speed sweeps flown at 10,000-ft density altitude. The speed sweeps were always the first test points on the flight card, so as to reduce the variation in aircraft gross weight. The biggest weight change, 5% of start-up gross weight, occurred during the final high-speed runs. Performance data were taken in both aircraft configurations, hub-on and -off, at 5° wing incidence with 5° flap. In addition to the nominal wing incidence data, a wing incidence sweep was also conducted at 165 KCAS (192 KTAS).

The performance data presented here have been dimensionally analyzed. The values have all been referenced to sea level standard day conditions. The hub-on data are referenced to 27,000 lb, and the hub-off data are referenced to 25,000 lb. Figure 54 presents the speed-thrust polar for both the hub-on and hub-off configurations. The flight test did not completely define the thrust curve for either configuration at the high- or the low-speed ends. This was due to the desire to stay well away from potential stall/spin flight conditions, at the low end, and to maintain tail-rotor Mach number below unity at the high end. Because of excessively high vibration levels, the RSRA was limited to 239 KTAS when in the hub-on configuration. A discussion of the vibration problem is presented in section 5. Figures 54 and 55, showing power-turbine inlet temperature versus fan speed, have been extrapolated out to the engine limits. This provides the maximum speeds that the RSRA could achieve in the fixed-wing configuration for the three engine-limit conditions, neglecting tail-rotor supersonic drag effects, for both hub-on and -off.

Figure 56 presents the TF-34 fuel consumption versus fan speed, and figure 57 presents the wing angle of attack versus airspeed, thus completing the basic performance documentation. The effects of wing incidence on wing angle of attack and on TF-34 fan speed, at a nominal airspeed of 194 knots, are presented in figures 58 and 59, respectively. As can be seen, the wing angle of attack and fan speed increase with increasing wing incidence. This is the result of the fuselage pitching nose-down to maintain trim. The effects of the more nose-down fuselage attitude are an increased fuselage down-load and drag, and an increased component of engine thrust directed downward. It is this increased lift requirement that causes the increased wing angle of attack and the increased drag that results in the higher fan speed.

The level-flight trim data were presented in section 4. An airspeed calibration was obtained by repeated comparison with the calibrated airspeed of the King Air chase plane. This resulting correction is several knots more than the previous correction for the compound. The correction is plotted in figures 60 and 61 for the pilot indicator and telemetry, respectively.

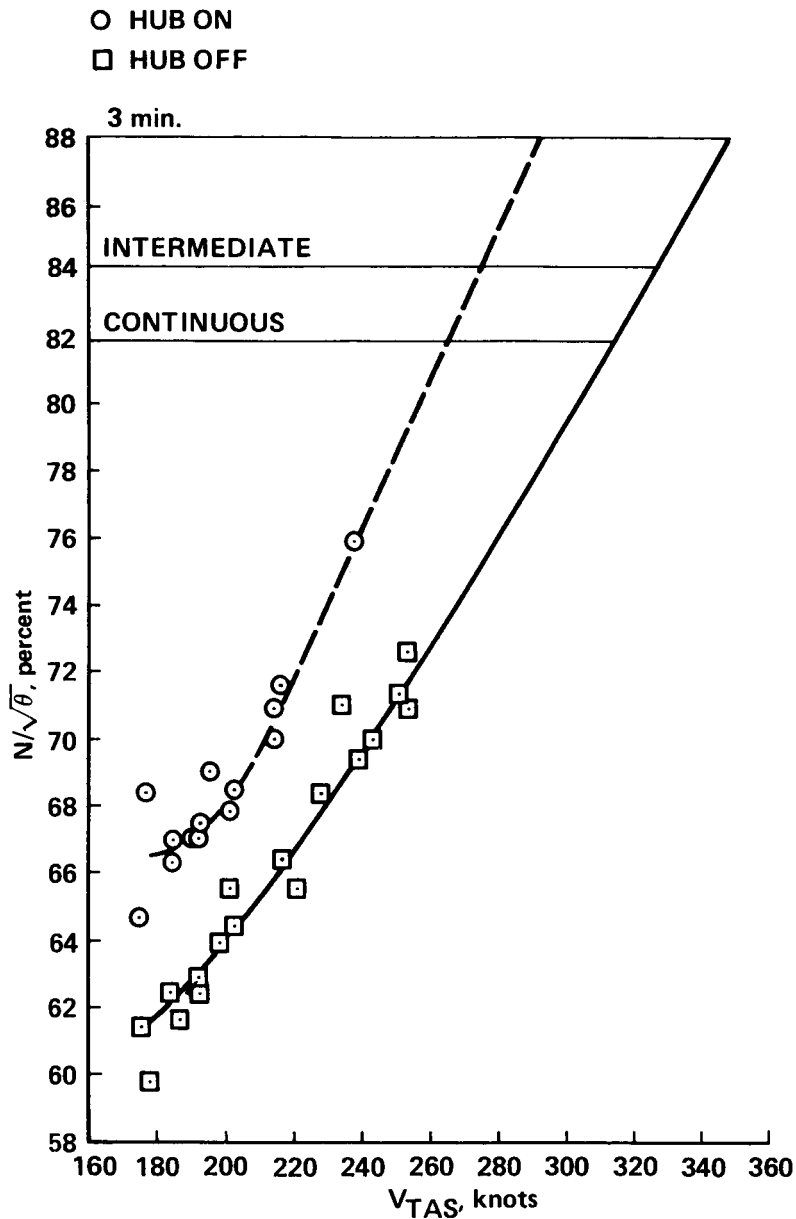


Figure 54.- TF-34 fan speed versus true airspeed:  $I_w = 5^\circ$ , level flight.

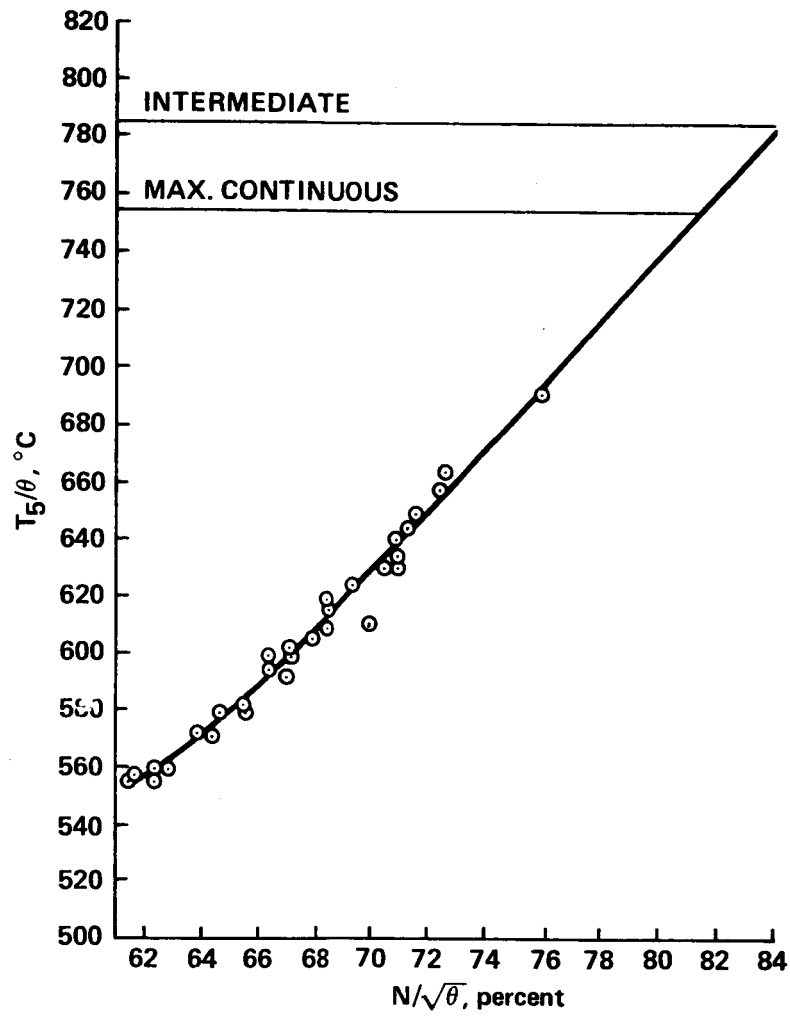


Figure 55.- TF-34 power-turbine inlet temperature versus fan speed.

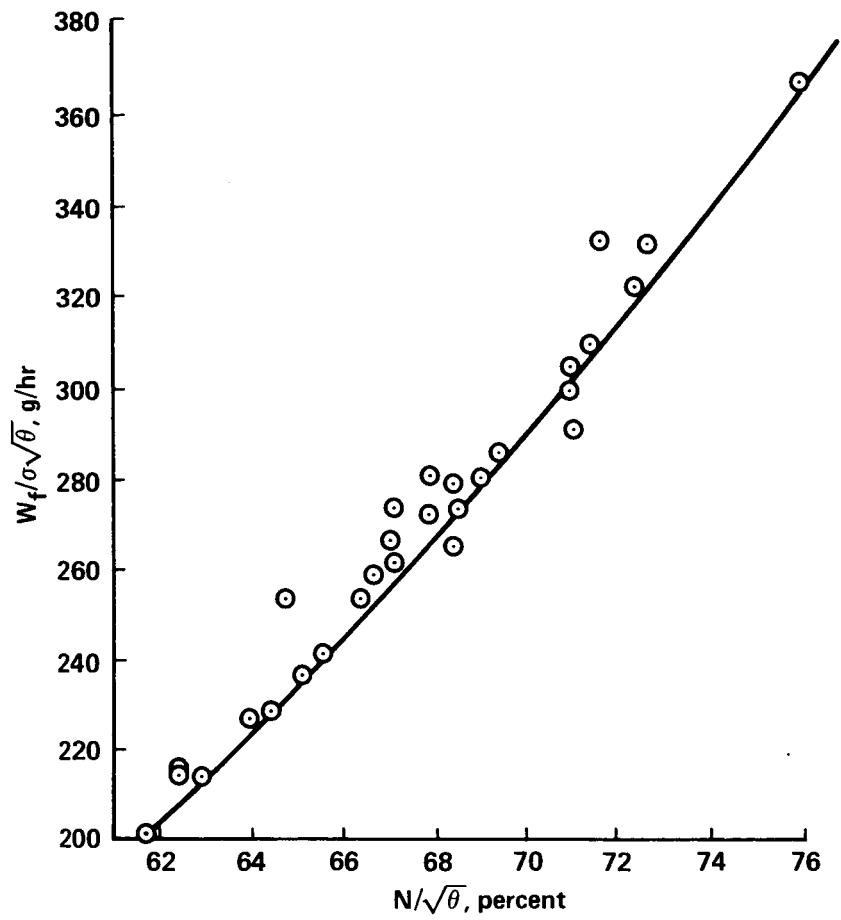


Figure 56.- TF-34 fuel consumption versus fan speed.

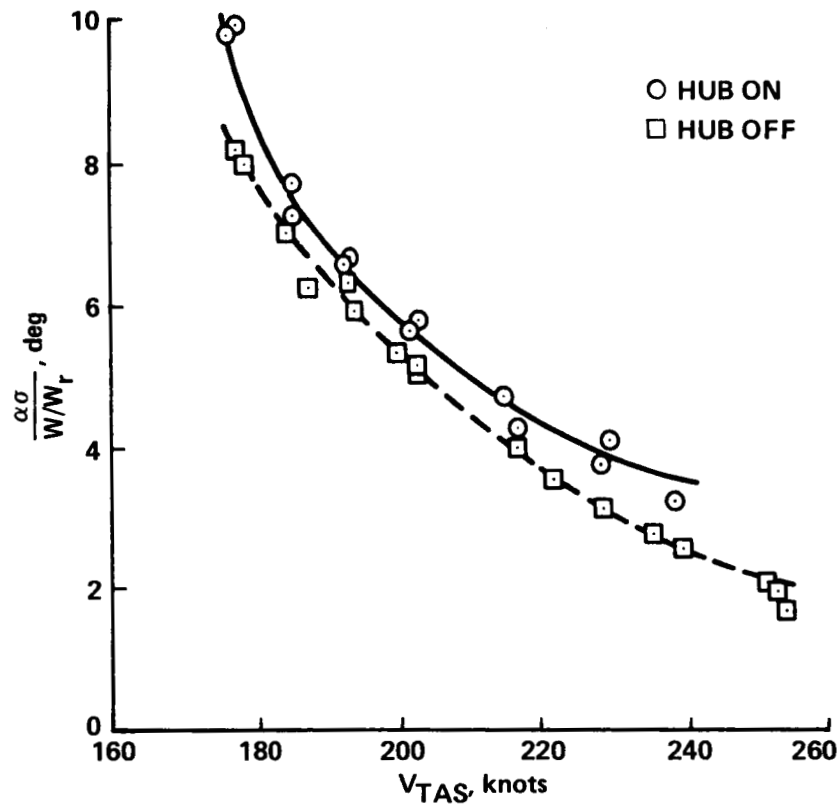


Figure 57.- Wing angle of attack versus true airspeed in level flight.

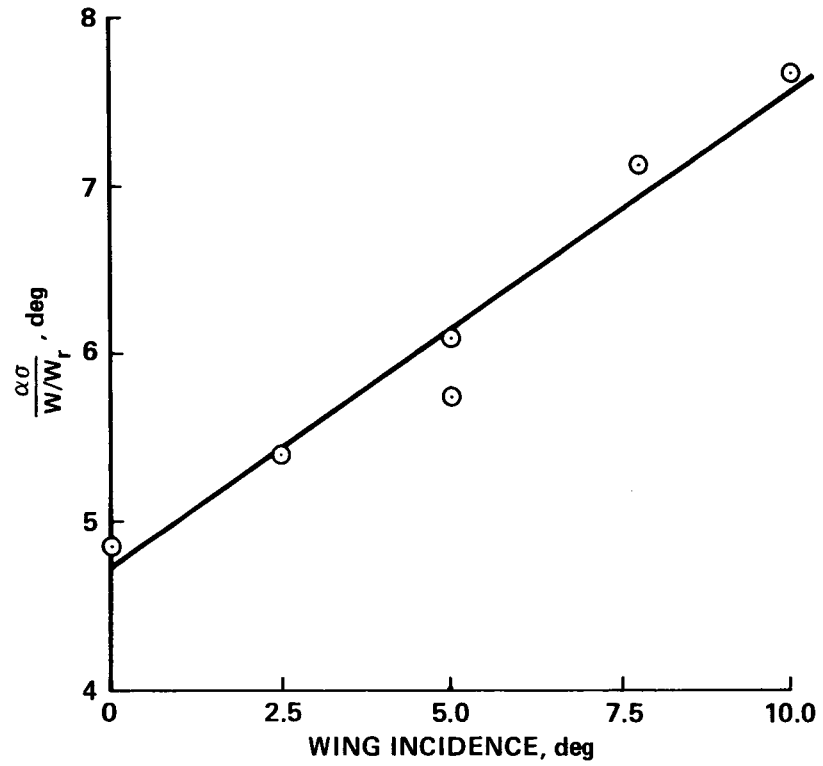


Figure 58.- Effect of wing incidence on wing angle of attack: 194 KTAS, hub on.

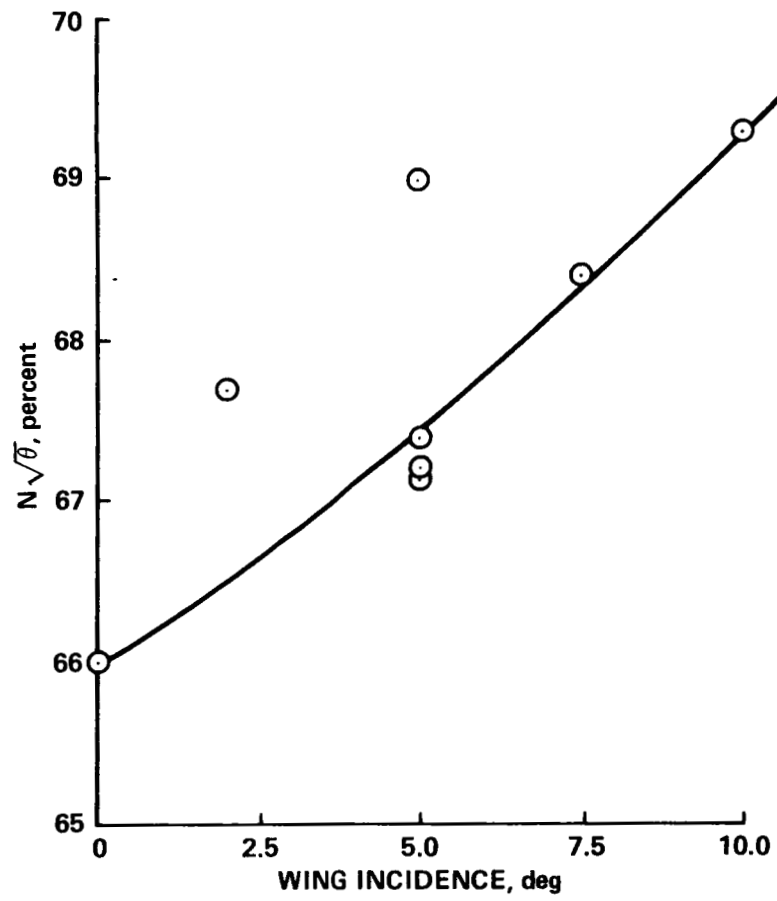


Figure 59.- Effect of wing incidence on fan speed: level flight at 194 KTAS, hub on.

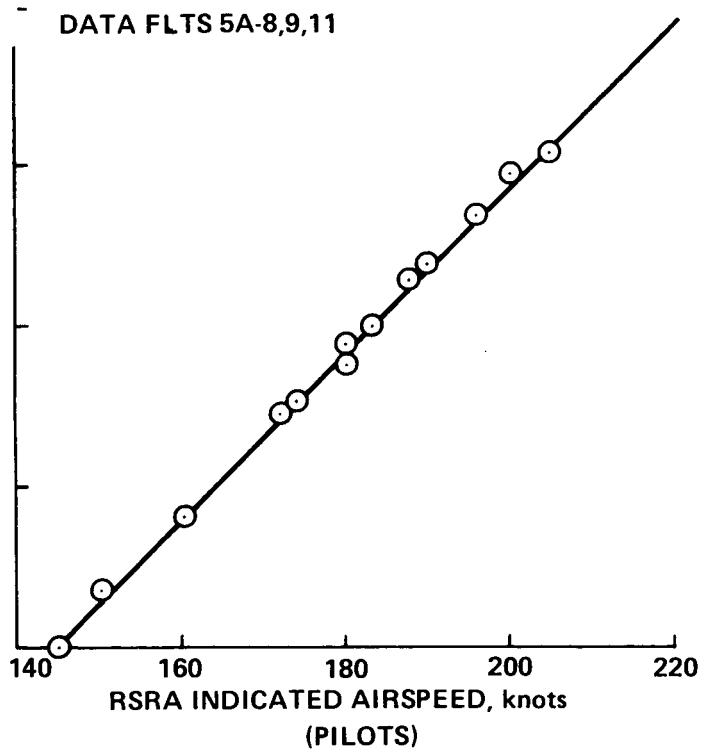


Figure 60.- Pilot's indicated airspeed versus King Air chase plane calibrated airspeed.

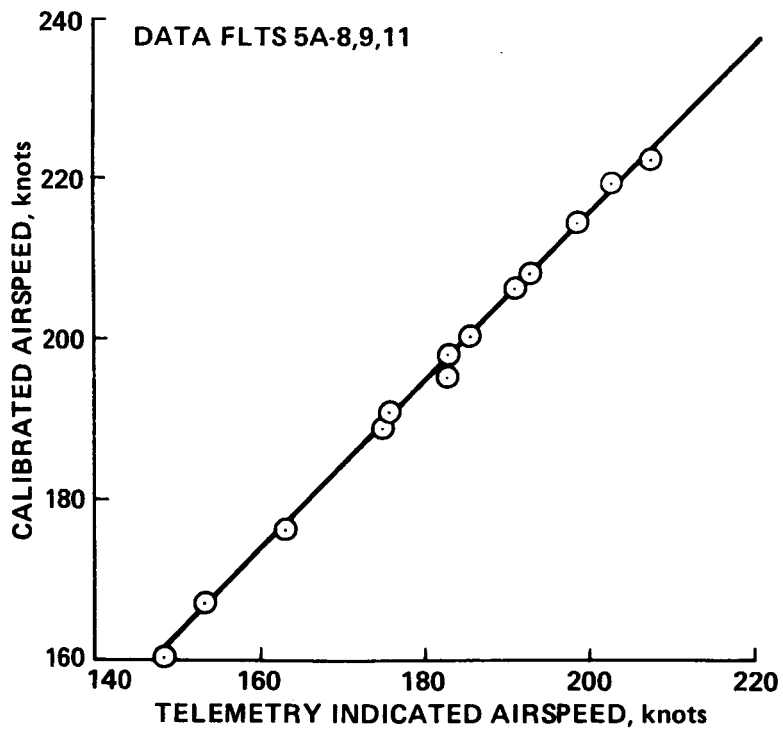


Figure 61.- Telemetry indicated airspeed versus King Air chase plane calibrated airspeed.

## 8. ACOUSTICS

The gathering of flyover acoustic data was part of the RSRA fixed-wing flight-test plan. The objective of the acoustic tests was twofold: (1) to obtain the acoustic signature of the RSRA without the main rotor, and (2) to study the tail-rotor noise without main-rotor effects and interactions. These goals are not achievable with any other rotorcraft. Only sample data are presented here, but a detailed report of this aspect of the RSRA/fixed-wing flight test will be published separately.

The test was conducted according to recognized international standards for acoustics testing. The microphone layout (fig. 62) was set up along the flyby line on Rogers Dry Lake bed. The test matrix (table 5) consisted of straight and level flyby speed sweeps, and 3° glide-slope speed sweeps. Two tail-rotor tip speeds, 723 ft/sec and 676 ft/sec, during the straight and level flybys were flown. At the lower tip speed, the tail rotor was set at flat pitch, leaving only the rudder for yaw control. However, the pilot had full authority over both the tail rotor and the rudder at the high tip speed setting. Results from the 145 knot flybys are shown in figure 63 for high tip speed and in figure 64 for low tip speed. Figure 65 presents data from a 175-KIAS low-tip-speed flyby. The figures present a 1/3 octave spectrum of the RSRA at three distances from the center microphone. Each data set is a single sample taken over 0.125 sec. Table 6 presents the A-weighted and flat-weighted decibel readings that correspond to the figures presented above.

TABLE 5.- RSRA FIXED-WING ACOUSTIC TEST MATRIX

Condition	Indicated airspeed, knots				
	135	145	155	165	175
$V_{TR} = 723$ ft/sec	X	X		X	X
$V_{TR} = 676$ ft/sec	X	X		X	X
3° glide slope	X		X		X

TABLE 6.- A-WEIGHTED AND FLAT-WEIGHTED dB READINGS

Flyby	Overhead	Mid	Far
145 knots, high tip speed	96.2/97.5	85.2/90.2	71.8/78.8
145 knots, low tip speed	99.0/100.0	82.2/87.5	72.8/80.0
175 knots, low tip speed	105.0/105.0	91.0/95.8	74.8/81.2

Note: These data are preliminary, and have not been compensated for temperature and humidity effects, or for altitude variations. The resultant Doppler shifts have been accounted for in the labeling on the 3rd octave plots.

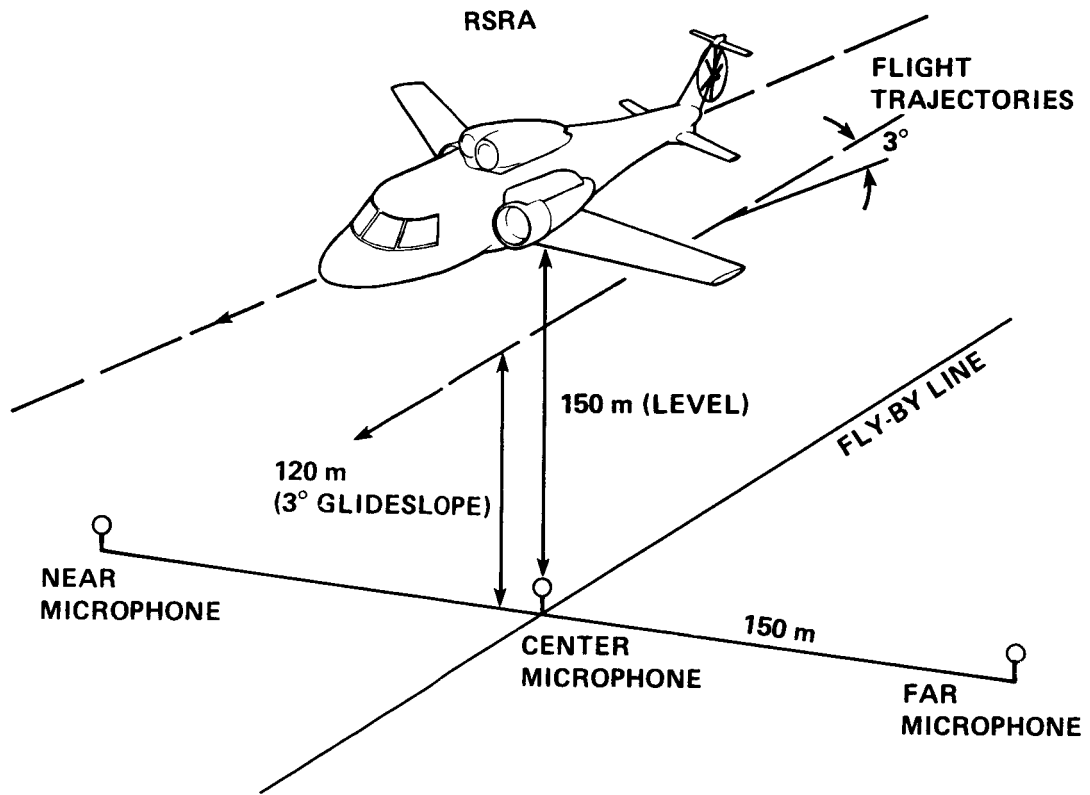


Figure 62.- Acoustic ground array setup.

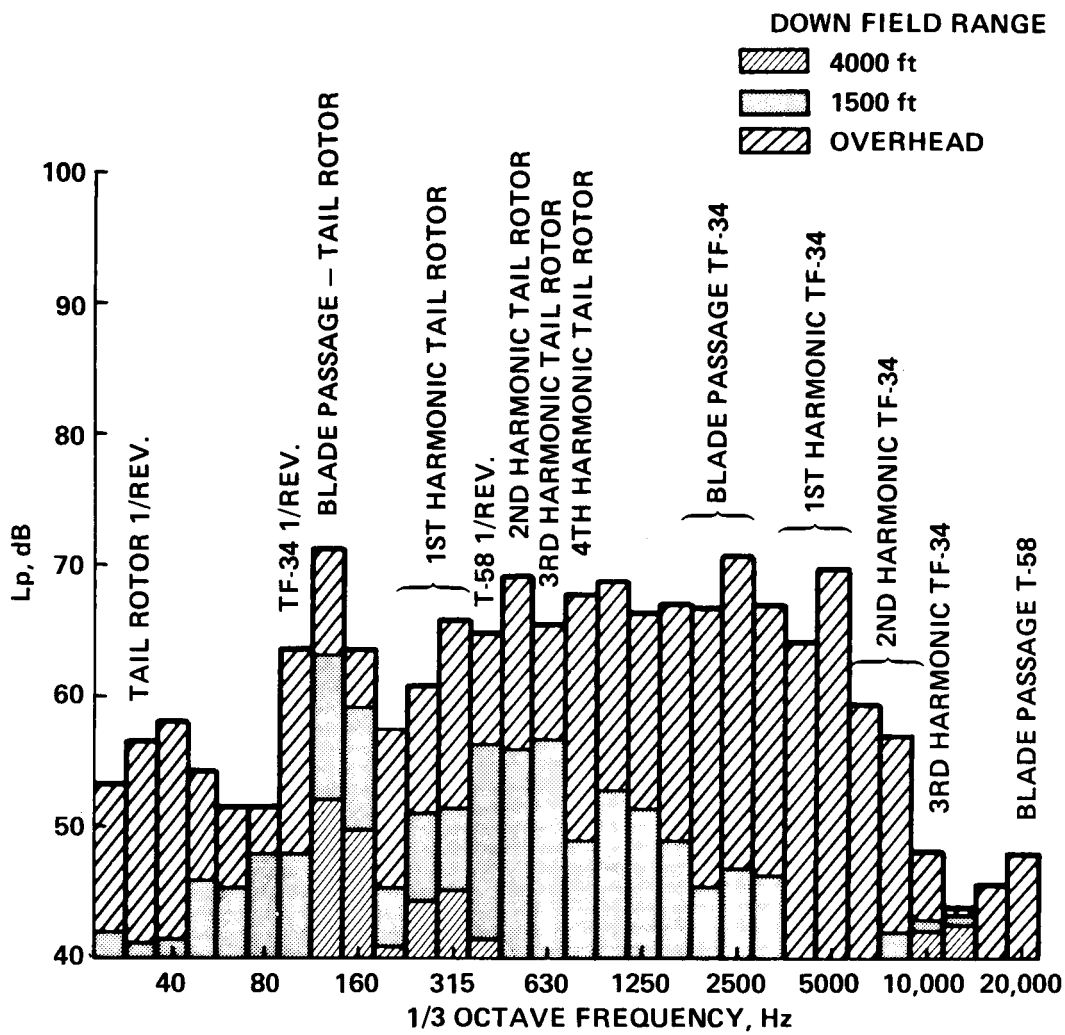


Figure 63.- Third-octave band spectrum of centerline microphone: 145-KIAS, level flyby with high tip speed.

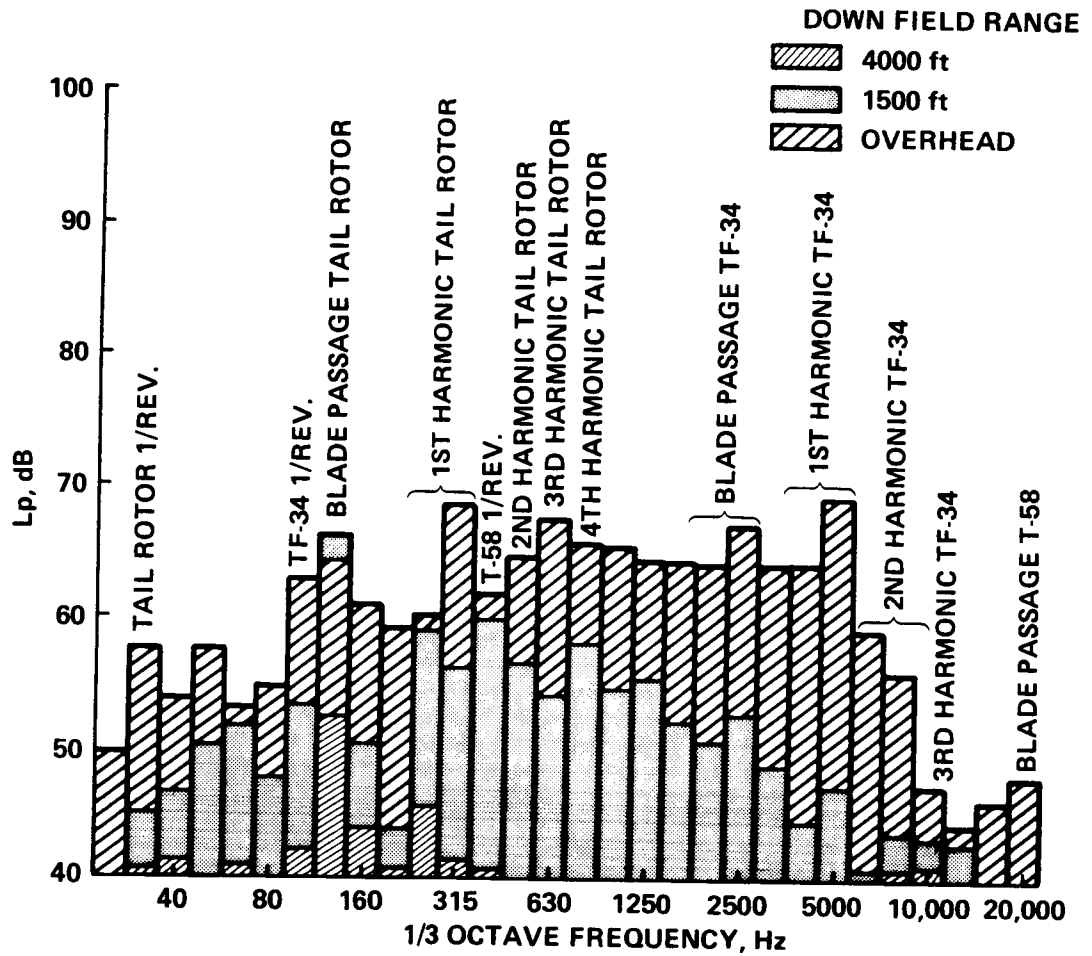


Figure 64.- Third-octave band spectrum of centerline microphone: 145-KIAS, level flyby with low tip speed.

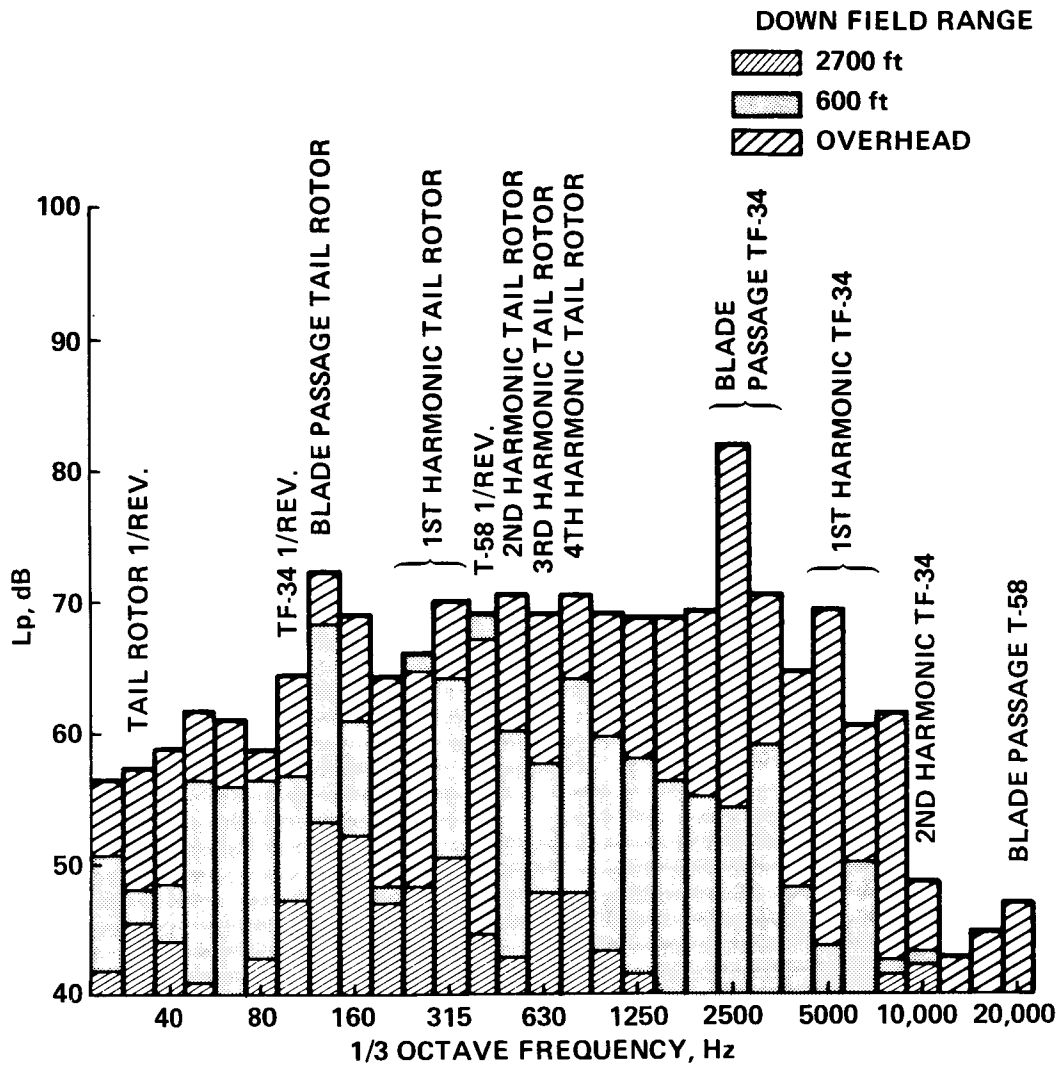


Figure 65.- Third-octave band spectrum of centerline microphone: 175 KIAS, level flyby with low tip speed.

## 9. MAIN-ROTOR HUB DRAG

The fixed-wing flights presented an opportunity to measure hub drag with the rotor-load measurement system. Figure 66 shows raw hub-drag data plotted against airspeed. In figure 67, the same data are shown converted to equivalent flat-plate area and plotted against dynamic pressure  $Q$ . Both figures clearly show the increase in drag caused by the hub. The load measurement system would ideally measure zero drag when the hub is removed, but the exposed shaft stub, air flowing to the unsealed pylon and around the transmission, and other similar effects sum to several hundred pounds of residual drag.

To investigate the effects of angle of attack, separate sets of data were taken by changing the wing incidence without changing airspeed. This had the effect of changing the fuselage angle of attack at constant dynamic pressure. All such data points were taken at a reference airspeed of 166 KCAS, yielding a dynamic pressure of  $92 \text{ lb/ft}^2$ . The results are shown in figure 68.

Hub-lift data were taken at the same time as hub-drag data. Figures 69 through 71 show the hub-lift data in the same formats and plotted to the same scales as the hub drag (figs. 68-70). Note that the vertical axes have been shifted slightly to more clearly show the zero-lift data.

Although not a problem for drag measurements, the large changes in hub weight between the hub-off and hub-on configurations shifted the hub-lift tare values significantly. Corrections were made by taking preflight and postflight reference data with the aircraft standing still on the ground, and subtracting the hub lift thus measured from all flight data to get true lift values.

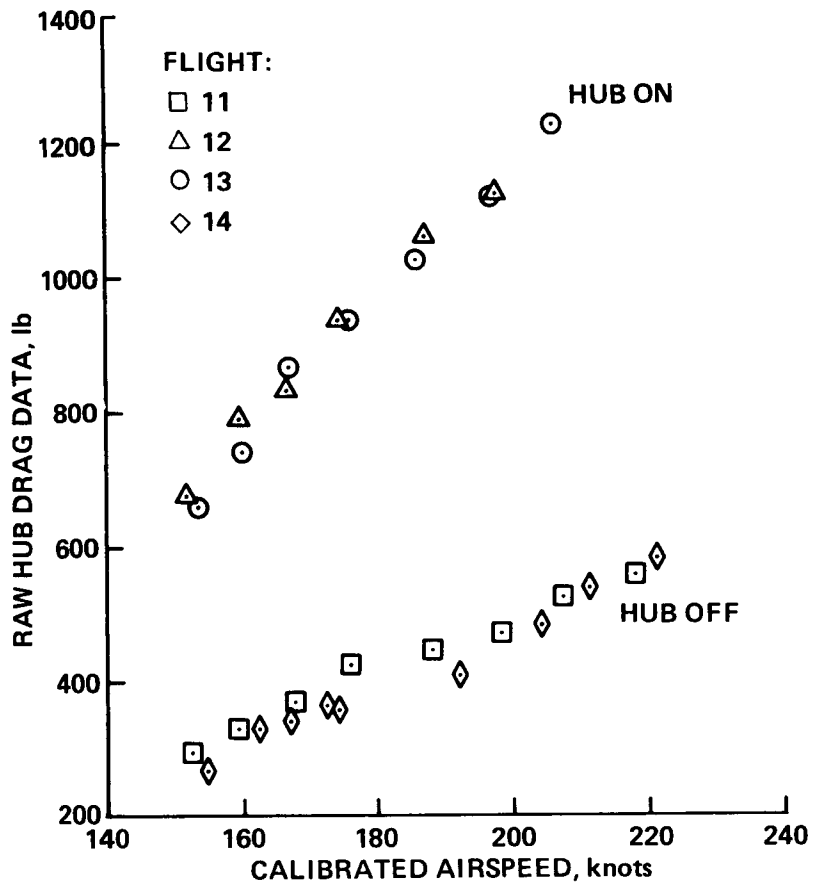


Figure 66.- Measured hub drag versus airspeed.

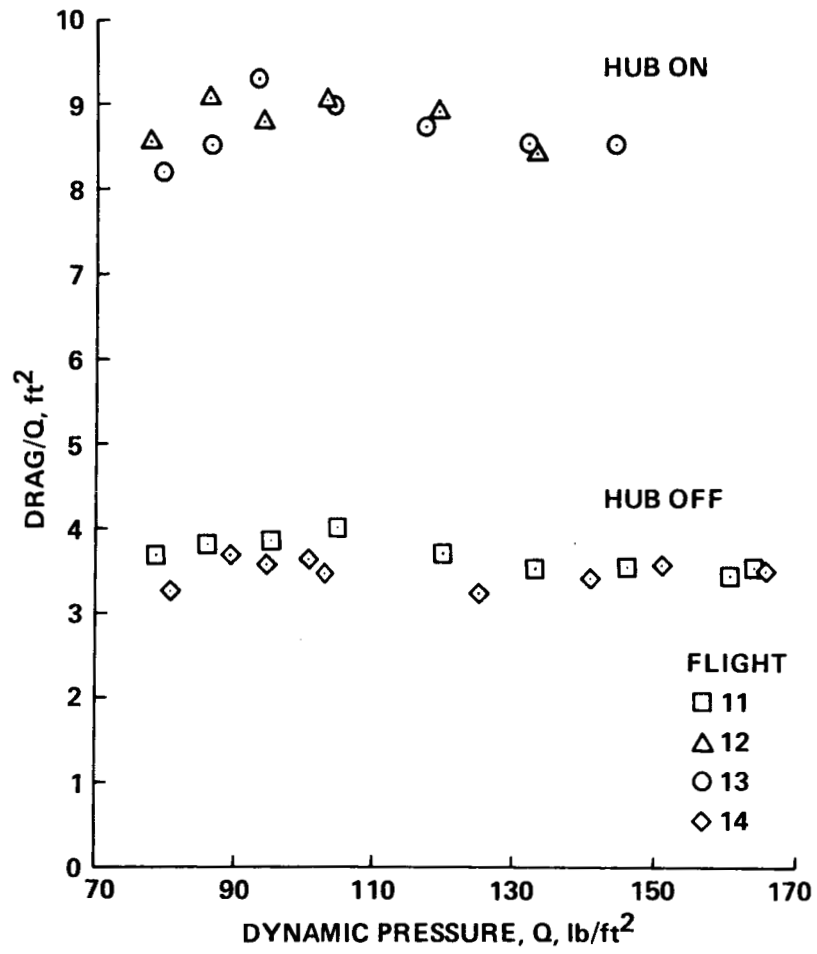


Figure 67.- Normalized hub drag versus dynamic pressure.

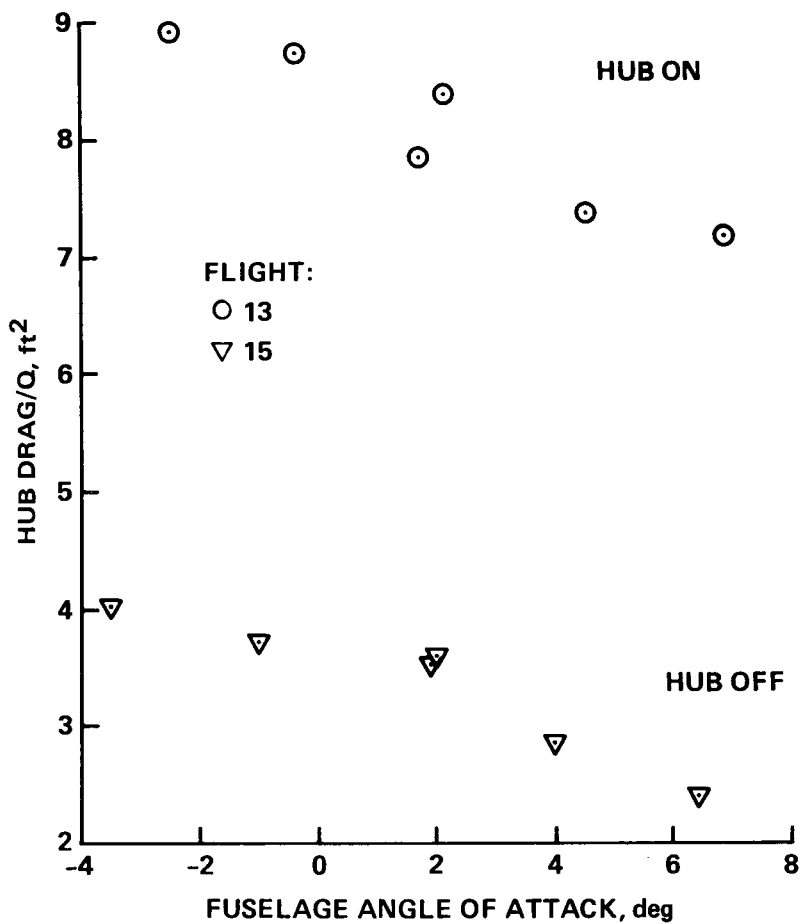
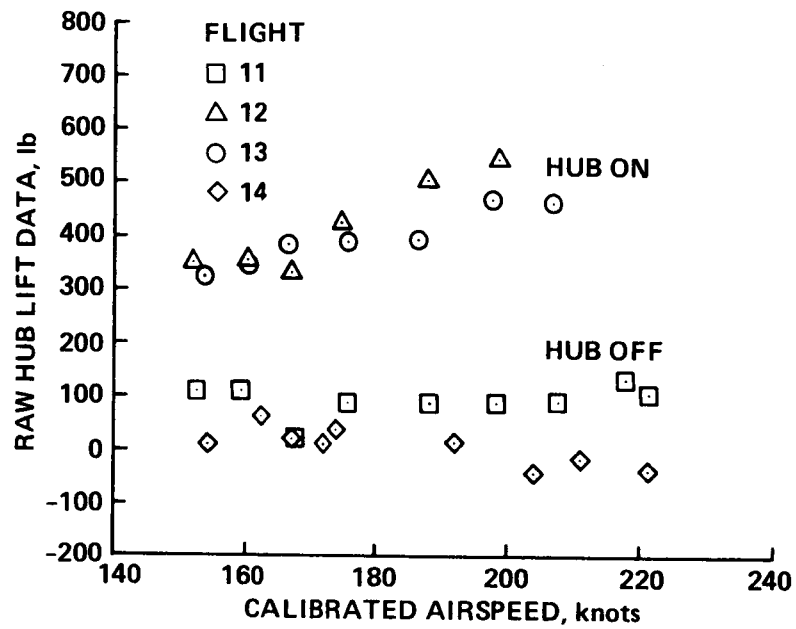


Figure 68.- Normalized hub drag versus angle of attack at constant dynamic pressure.



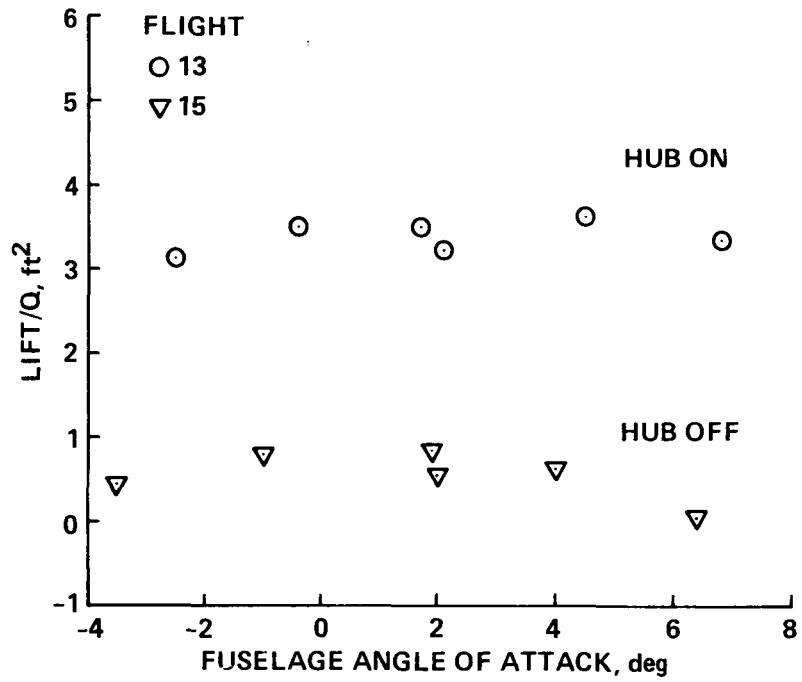


Figure 71.- Normalized hub lift versus angle of attack at constant dynamic pressure.

## 10. CONCLUSIONS

The principal results of these fixed-wing flight tests are summarized below:

1. With the emergency SAS off, the fixed-wing flying characteristics of the RSRA are satisfactory for speeds up to 261 KTAS with the tail rotor on and a gross weight of 28,000 lb.
2. The flaps should be extended to 5° to prevent unnecessary lower stabilator vibrations.
3. The landing gear can be safely extended and retracted up to 170 KCAS.
4. The RSRA fixed-wing operating envelope is expanded to 261 KTAS (226 KCAS) with the rotor hub removed.
5. The RSRA fixed-wing, rotor-hub installed, emergency flight envelope is expanded to 242 KTAS (209 KCAS).
6. The load-factor capability was demonstrated to 2.34 g at 206 KCAS.
7. Wake turbulence from the installed main-rotor hub with weights causes vibration of the empennage.

## APPENDIX A

### AIRCRAFT DESCRIPTION

The Rotor Systems Research Aircraft (RSRA) is a test vehicle designed to operate in three configurations: as a pure helicopter, as a compound helicopter, and as a fixed-wing aircraft. Figure A1 is a general arrangement drawing of the compound configuration. The fixed-wing configuration is identical, except that the main rotor and, optionally, the tail rotor are removed. Figure A2 is a general arrangement of the helicopter configuration. Table A1 gives areas of the aerodynamic surfaces, and table A2 lists dimensions and other general data. Figure A3 shows the general arrangement of the GE TF-34 thrust engines.

The RSRA is designed as a test bed to provide a full-scale, real-world environment for research on new rotor concepts. It can also be used to investigate phenomena associated with rotors in general, and it has the additional capability to fly as a fixed-wing aircraft. This fixed-wing capability is used when the test rotor is not providing the required lift or thrust or when the test rotor is severed from the airframe for emergency reasons, thus allowing safe return of the aircraft.

The RSRA fixed-wing configuration (FW) has four main engines. Two GE T-58-10 engines power the main transmission and tail rotor. The main transmission provides power for hydraulic systems 1, 2, and 3 and all electrical power. Two GE TF-34 turbofan engines provide forward thrust, and the left engine pressurizes hydraulic system 4.

The RSRA has a variable incidence wing. The wing is hinged at the aft spar on each side of the fuselage and is activated by two hydraulic actuators at the approximate 1/4-chord line on either side of the fuselage. Full design travel of the actuators provides  $+15^\circ$  to  $-9^\circ$  incidence change. For the purposes of the FW evaluation, internal stops limited the downward travel to  $0^\circ$  incidence.

The RSRA has two horizontal tail surfaces. The smaller, upper stabilizer is fixed. The lower surface is a stabilator with a geared elevator to increase effectiveness. The lower stabilator is controlled by the pilot's longitudinal stick through  $\pm 8^\circ$  incidence. In addition to the stabilator, the pilot has control of wing ailerons, rudder, wing flaps, and a drag brake at the tail. The RSRA has provisions for computer flight control, but the computer was not installed for this evaluation.

The pilots are seated side by side. The right pilot, who is the safety pilot (SP), has direct mechanical hydraulic control of the aircraft; the left pilot, who is the evaluation pilot (EP), has control of the aircraft through an electrical hydraulic force feel system (FFS) when that system is activated. An emergency escape system (EES) is provided for the pilots. The EES is a pyrotechnic system which severs the main-rotor blades (the blade severance device was deactivated for this evaluation) and then vertically ejects the crew with Martin-Baker US10LT ejection seats.

The RSRA fuel system is designed to operate to 12,000 ft on suction alone. The total fuel-system capacity is 654 gal (4,446 lb) of JP-5 in two fore and aft tanks located in the center fuselage. This capacity is adequate for test flights of 1 hr with an 800 lb reserve.

The RSRA (FW) is designed to attain, without the tail rotor, 300 knots in level flight and 360 knots in a dive. It is designed to +4 g to -1.5 g load factors.

A more detailed description of the RSRA and RSRA systems is given in reference 6.

TABLE A1.- AERODYNAMIC SURFACE AREAS

Wing area, total	369.9 ft <sup>2</sup> (34.36 m <sup>2</sup> )
Wing flap area, total	57.8 ft <sup>2</sup> (5.37 m <sup>2</sup> )
Aileron area, total	35.7 ft <sup>2</sup> (3.32 m <sup>2</sup> )
Horizontal tail area	
Lower (compound)	88.3 ft <sup>2</sup> (8.20 m <sup>2</sup> )
Upper (compound)	17.2 ft <sup>2</sup> (1.60 m <sup>2</sup> )
Upper (helicopter)	35.4 ft <sup>2</sup> (3.29 m <sup>2</sup> )
Lower stabilizer (to elevator hinge)	61.8 ft <sup>2</sup> (5.74 m <sup>2</sup> )
Elevator	26.48 ft <sup>2</sup> (2.46 m <sup>2</sup> )
Vertical tail area, total	100.8 ft <sup>2</sup> (9.36 m <sup>2</sup> )
Fin (to rudder hinge)	81.3 ft <sup>2</sup> (7.55 m <sup>2</sup> )
Rudder	19.5 ft <sup>2</sup> (1.81 m <sup>2</sup> )
Main rotor blade area (1 blade)	40.5 ft <sup>2</sup> (3.75 m <sup>2</sup> )
Main rotor geometric disc area (total)	3019 ft <sup>2</sup> (280.47 m <sup>2</sup> )
Main rotor blade geometric solidity ratio	0.0775
Tail rotor blade area	3.24 ft <sup>2</sup> (0.30 m <sup>2</sup> )
Tail rotor geometric disc area	88.3 ft <sup>2</sup> (8.20 m <sup>2</sup> )
Tail rotor geometric solidity ratio	0.184

TABLE A2.- DIMENSIONS AND GENERAL DATA  
[From ref. 6]

<b>Wings</b>	
Span, maximum	45.1 ft (13.75 m)
Chord	
At root	115.2 in. (2.83 m)
At construction tip	76.8 in. (1.95 m)
Mean aerodynamic	100.8 in. (2.56 m)
Airfoil at root	63 <sub>2</sub> 415
Airfoil at construction tip	63 <sub>2</sub> 415
Thickness	15%
Incidence	
At root	Variable, +15° to -9° (0.262 to -0.157 rad)
At construction tip	Variable, +15° to -9° (0.262 to -0.157 rad)
Sweepback at 25%, chord	3.0° (0.052 rad)
Dihedral	7.0° (0.122 rad)
Aspect ratio	5.52
Ailerons	
Span	46 in. (1.17 m)
Chord (average percent wing chord)	30%
High lift and drag increasing device	
Type	Single slotted flap
Span, exclusive of cutouts	64.7%
Chord (average percent wing chord)	30%
<b>Tail</b>	
Lower horizontal (compound only)	
Span	22.5 ft (6.86 m)
Chord (MAC)	3.9 ft (1.19 m)
Airfoil	NACA 0015
Incidence	Variable, ±8° (±0.140 rad)
Sweep of leading edge	0
Dihedral	0
Aspect ratio	5.73
Elevator	
Span (percent of tail span)	100%
Chord (percent of tail chord)	30%
Upper horizontal (compound only)	
Span	8.58 ft (2.62 m)
Chord (MAC)	2.05 ft (0.62 m)
Airfoil	NACA 0015
Incidence	Ground adjustable, ±5° (±0.087 rad)
Sweep of leading edge	12.5° (0.218 rad)
Dihedral	0
Aspect ratio	4.29

TABLE A2.- CONTINUED.

Upper horizontal (helicopter only)	
Span	13.25 ft (4.04 m)
Chord (MAC)	2.78 ft (0.85 m)
Airfoil	NACA 0015
Incidence	Ground adjustable, $\pm 5^\circ$ ( $\pm 0.087$ rad)
Sweep of leading edge	$12^\circ$ (0.209 rad)
Dihedral	0
Aspect ratio	4.97
Vertical	
Airfoil	NACA 0015
Sweep at 25% chord	$48^\circ$ (0.838 rad)
Aspect ratio	3.62
Rudder tab cord	8 in. (0.20 m)
Height over highest fixed part of aircraft	
Reference line level	20.1 ft (6.13 m)
Three-point	17.9 ft (5.46 m)
Height over highest part of tail	20.1 ft (6.13 m)
Height in hoisting attitude	18 ft (5.49 m)
Length, maximum	
Reference line level	70.6 ft (21.52 m)
Three-point	70.6 ft (21.52 m)
Length from hoisting sling to farthest aft part of tail, reference line level, rudder neutral, elevator down	
	48.6 ft (14.81 m)
Distance from wing MAC quarter chord point to lower horizontal tail MAC quarter chord point	
	28.57 ft (8.71 m)
Distance from centerline of main rotor to lower horizontal tail MAC quarter chord point	
	29.57 ft (9.01 m)
Ground angle	$2.45^\circ$ (0.043 rad)
Wheel size	
Main wheels	24 X 8.00-13
Auxiliary wheel (tail)	18 X 5.5
Tire size	
Main wheels	24 X 8.00-13
Auxiliary wheel (tail)	18 X 5.5, Type VII
Tread of main wheels	10.8 ft (3.29 m)
Wheel base	40.9 ft (12.47 m)
Vertical travel, extended/compressed	
Main wheels	
Right gear	10.5 in. (0.26 m)
Left gear	12 in. (0.30 m)
Tail wheel	12 in. (0.30 m)

TABLE A2.- CONCLUDED.

Angle between lines joining center of gravity with point of ground contact of main wheel tires, static deflection of 1W (front elevation)	64.16° (1.120 rad)
Angle of line through center of gravity and ground contact of main wheel tire to vertical line, reference line level, static deflection of 1W (side elevation)	28.79° (0.502 rad)
Maximum slope helicopter can be parked upon without overturning (nose downhill)	28.79° (0.502 rad)
Critical turnover angle	25.98° (0.453 rad)
D = diameter of main rotor	62 ft (18.90 m)
Number of blades main rotor	5
$W_g$ = geometric disk loading ( $W/A_g$ )	6.095
Airfoil section designation and thickness	NACA 0012 (modified)
Width--main-rotor blades (turning Length)	62 ft (18.90 m)
Maximum: main-rotor blades (at rest, one trailing)	73.6 ft (22.43 m)
Maximum: main-rotor blades turning	79.6 ft (24.26 m)
Height	
Over main-rotor blades at rest	14.5 ft (4.42 m)
Main-rotor clearance (ground to tip, rotor static)	11 ft (3.35 m)
Main-rotor clearance (ground to tip, rotor turning)	14.5 ft (4.42 m)
Main-rotor clearance (structure to tip, rotor static)	5 ft (1.52 m)
Main-rotor clearance (structure to tip, rotor turning)	7.5 ft (2.29 m)
Diameter tail rotor	10.6 ft (3.23 m)
Tail-rotor clearance (ground to tip, rotor turning)	5 ft (1.52 m)

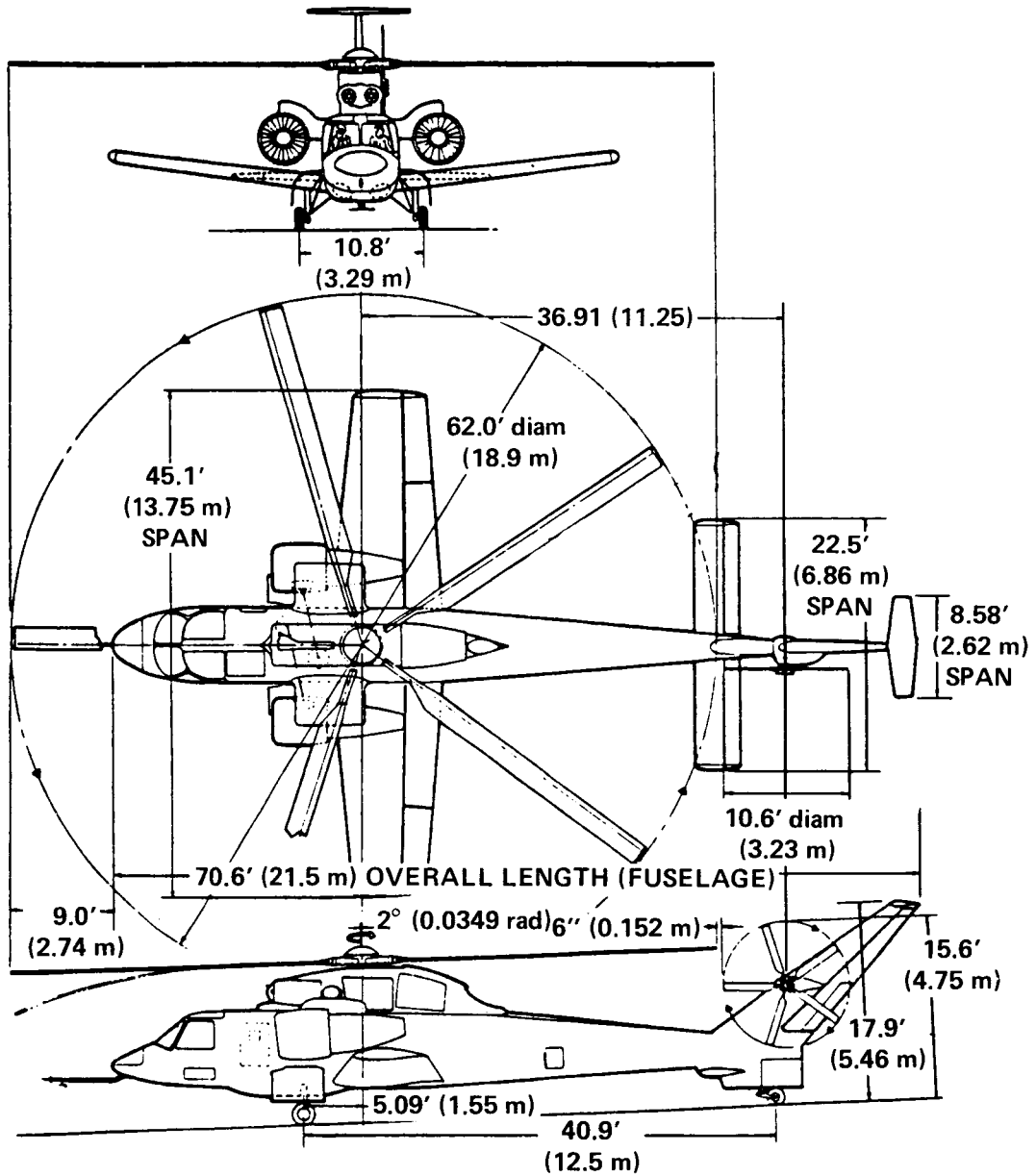
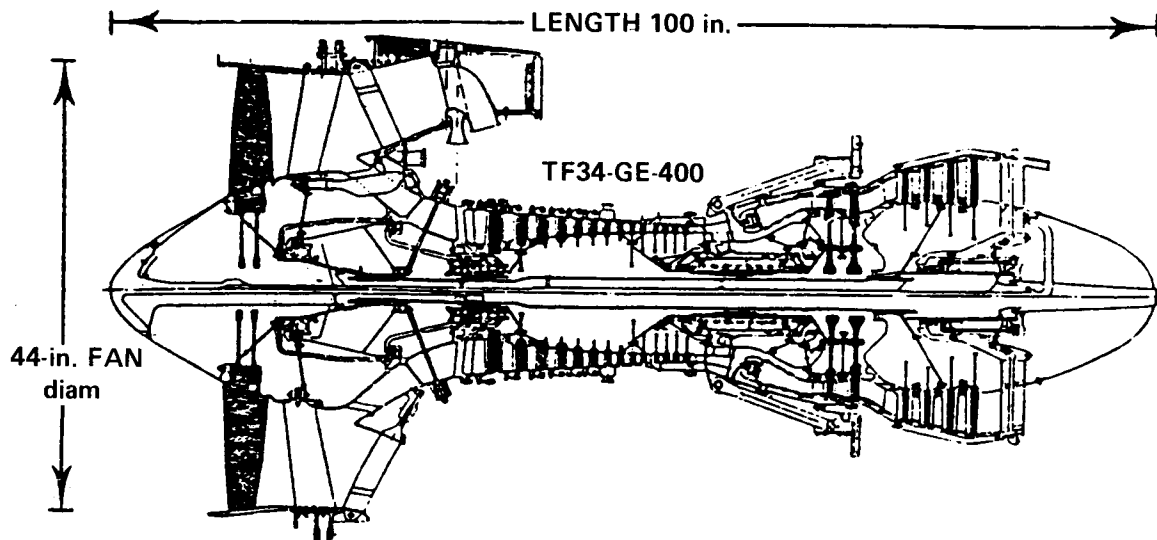


Figure A1.- RSRA in the compound configuration.





	<u>-2/-400</u>
APPLICATION:	S-3A
THRUST, lb:	9,275
(RSRA INSTALLATION):	8,250
WEIGHT, lb:	1,475
BYPASS RATIO:	6.2
OVERALL PRESSURE RATIO:	21
T4, °F:	2,240
LUBE OIL:	23,699

Figure A3.- TF-34 engine.

APPENDIX B

MEASURED PARAMETER LIST FOR THE RSRA 740: FIXED-WING TEST

<u>Mnemonic</u>	<u>Parameter</u>
ACTOTLB	Total fuel used, lb
AILPOSR	Right aileron position, deg
ATTACK	Aircraft angle of attack, deg
ATTACKW	Wing angle of attack, deg
ATXPR1	Transmission cowling aft pressure sensor 1, lb/in. <sup>2</sup>
ATXPR2	Transmission cowling aft pressure sensor 2, lb/in. <sup>2</sup>
ATXPR3	Transmission cowling aft pressure sensor 3, lb/in. <sup>2</sup>
AUXETOLB	Auxiliary engines fuel used, lb
CPULAT	Lateral CPU position, %
CPULONG	Longitudinal CPU position, %
CPUYAW	Yaw CPU position, %
DBOX9	Drag box No. 9, lb/in. <sup>2</sup>
DBOX15	Drag box No. 15, lb/in. <sup>2</sup>
DBOX20	Drag box No. 20, lb/in. <sup>2</sup>
DBOX21	Drag box No. 21, lb/in. <sup>2</sup>
DBOX22	Drag box No. 22, lb/in. <sup>2</sup>
DBOX23	Drag box No. 23, lb/in. <sup>2</sup>
DBOX24	Drag box No. 24, lb/in. <sup>2</sup>
ELEVCRDL	Left elevator control rod load, lb
ELEVCRDR	Right elevator control rod load, lb
FLAPPOS	Flap position, deg
FTXPR1	Transmission cowling forward pressure sensor 1, lb/in. <sup>2</sup>
FTXPR2	Transmission cowling forward pressure sensor 2, lb/in. <sup>2</sup>
FTXPR3	Transmission cowling forward pressure sensor 3, lb/in. <sup>2</sup>
HBOOM	Pressure attitude, ft
HEADING	Compass heading, deg
HSSASAL	Stabilizer electronic flight control system actuator lateral acceleration, g
HSSASAV	Stabilizer electronic flight control system actuator vertical acceleration, g
HSSTAL	Stabilator series trim actuator lateral acceleration, g
HSSTAV	Stabilator series trim actuator vertical acceleration, g
HZSTACT	Horizontal stabilizer actuator-rod load, lb
ICEBATH	Ice bath reference temperature, °C
ITATBOOM	Indicated total air temperature boom, °C
IW	Wing incident angle, deg
LAICR	Left aileron control-rod load, lb
LATCG	Lateral c.g. acceleration, g
LATSTKP	Lateral stick position, %
LATSTKPE	Lateral stick position (PE), %

LATTPYN	Lateral acceleration tail pylon, g
LCDLF	Lateral acceleration copilot floor, g
LGCG	Longitudinal acceleration of c.g., g
LGDLAL	Left landing-gear door aft lateral acceleration, g
LGDLFL	Left landing-gear door forward lateral acceleration, g
LGDRL1	Left landing-gear door 1, lb/in. <sup>2</sup>
LGDRL2	Left landing-gear door 2, lb/in. <sup>2</sup>
LGDRL3	Left landing-gear door 3, lb/in. <sup>3</sup>
LGDRL4	Left landing-gear door 4, lb/in. <sup>2</sup>
LGDRL5	Left landing-gear door 5, lb/in. <sup>2</sup>
LGDRL6	Left landing-gear door 6, lb/in. <sup>2</sup>
LGDRL7	Left landing-gear door 7, lb/in. <sup>2</sup>
LGDRL8	Left landing-gear door 8, lb/in. <sup>2</sup>
LGDRL9	Left landing-gear door 9, lb/in. <sup>2</sup>
LGLSTLD	Left landing-gear door strut load, lb
LGLTL	Left landing-gear lateral acceleration, g
LGRTL	Right landing-gear lateral acceleration, g
LGSTKP	Longitudinal stick position, %
LGSTKPE	Longitudinal stick position (PE), %
LHSLIFTL	Left lower horizontal stabilizer lift, lb/in. <sup>2</sup>
LHSLIFTR	Right lower horizontal stabilizer lift, lb/in. <sup>2</sup>
LHZSTB7	Lower horizontal stabilizer stress No. 7, lb/in. <sup>2</sup>
LHZSTB9	Lower horizontal stabilizer stress No. 9, lb/in. <sup>2</sup>
LHZSTB10	Lower horizontal stabilizer stress No. 10, lb/in. <sup>2</sup>
LHZSTB27	Lower horizontal stabilizer stress No. 27, lb/in. <sup>2</sup>
LHZSTB29	Lower horizontal stabilizer stress No. 29, lb/in. <sup>2</sup>
LTZSTB30	Lower horizontal stabilizer stress No. 30, lb/in. <sup>2</sup>
LTZSTB32	Lower horizontal stabilizer stress No. 32, lb/in. <sup>2</sup>
LOADFACT	Aircraft load factor, g
LOPF	Longitudinal acceleration pilot floor, g
LOSTTURT	Longitudinal acceleration upper right stabilizer, g
LOWGTPRT	Longitudinal acceleration right wing tip
LPF	Lateral acceleration pilot floor
LSBTVT	Left stabilizer tip vertical acceleration, g
LSTBEB15	Left lower stabilizer edgewise bending at BL 15, lb/in. <sup>2</sup>
LSTBEB40	Left lower stabilizer edgewise bending at BL 40, lb/in. <sup>2</sup>
LSTBNB15	Left lower stabilizer normal bending at BL 15, lb/in. <sup>2</sup>
LSTBNB40	Left lower stabilizer normal bending at BL 40, lb/in. <sup>2</sup>
LTBRKT	Left brake stack temperature, °C
LTGB	Lateral acceleration tail gearbox
MGBOILIN	Main-rotor gearbox oil-in temperature, °C
MGBOILOT	Main gearbox oil-out temperature, °C
MRDRAG	Main rotor drag, lb
MRBQCE	Main-rotor gearbox torque cell E, lb
MRBQCF	Main-rotor gearbox torque cell F, lb
MRLIFTA	Main-rotor transmission load cell A, lb
MRLIFTB	Main-rotor transmission load cell B, lb
MRLIFTC	Main-rotor transmission load cell C, lb

MRLIFTD	Main-rotor transmission load cell D, lb
MRψ	Main-rotor contactor
NO1AUXNF	No. 1 TF-34 engine power-turbine (fan) speed, %
NO2AUXNF	No. 2 TF-34 engine power-turbine (fan) speed, %
NO1AUXNG	No. 1 TF-34 engine gas-generator speed, %
NO2AUXNG	No. 2 TF-34 engine gas-generator speed, %
NO1AUXSL	No. 1 TF-34 engine speed-lever position, %
NO2AUXSL	No. 2 TF-34 engine speed-lever position, %
NO1AUXT5	No. 1 TF-34 engine T5 temperature, °C
NO2AUXT5	No. 2 TF-34 engine T5 temperature, °C
NO1AUXWF	No. 1 TF-34 engine fuel-flow rate, gal/min
NO2AUXWF	No. 2 TF-34 engine fuel-flow rate, gal/min
N1AXAGVV	No. 1 TF-34 accessory gearbox vertical acceleration, g
N2AXAGVV	No. 2 TF-34 accessory gearbox vertical acceleration, g
N1AXEFHV	No. 1 TF-34 exhaust frame horizontal acceleration, g
N2AXEFHV	No. 2 TF-34 exhaust frame horizontal acceleration, g
NO1FIT	No. 1 TF-58 fuel-in temperature, °C
NO2FIT	No. 2 TF-58 fuel-in temperature, °C
NO1FPCT	No. 1 engine free-turbine speed, %
NO2FPCT	No. 2 engine free-turbine speed, %
NO1QPCT	No. 1 engine torque, %
NO2QPCT	No. 2 engine torque, %
N1TFIT	No. 1 TF-34 fuel-in temperature, °C
N2TFIT	No. 2 TF-34 fuel-in temperature, °C
NO1T5	No. 1 engine T5, °C
NO2T5	No. 2 engine T5, °C
N1TEP2	No. 1 TF-34 pylon temperature No. 2, °F
N2TEP2	No. 2 TF-34 pylon temperature No. 2, °F
NO1WFGPH	No. 1 engine fuel-flow rate, gal/min
NO2WFGPH	No. 2 engine fuel-flow rate, gal/min
NR	Main-rotor speed, %
PEDP	Pedal position, %
PITCHACC	Aircraft pitch acceleration, g
PITCHATT	Aircraft pitch attitude, deg
PITCHRAT	Aircraft pitch rate, deg/sec
QTAL1	No. 1 engine aft torque-tube lateral acceleration, g
QTAV1	No. 1 engine aft torque-tube vertical acceleration, g
RAICR	Right aileron input control-rod load, lb
ROCBOOM	Rate-of-climb boom, ft/min
ROLLACC	Aircraft roll acceleration, g
ROLLATT	Aircraft roll attitude, deg
ROLLRAT	Aircraft roll rate, deg/sec
ROTETOLB	Rotor engines fuel used, lb
RSTBLG	Right stabilizer tip longitudinal acceleration, g
RSTBVT	Right stabilizer tip vertical acceleration, g
RSTBEB15	Right lower stabilizer edgewise bending at BL 15, lb/in. <sup>2</sup>
RSTBEB40	Right lower stabilizer edgewise bending at BL 40, lb/in. <sup>2</sup>
RSTBNB15	Right lower stabilizer normal bending at BL 15, lb/in. <sup>2</sup>

RSTBNB40	Right lower stabilizer normal bending at BL 40, lb/in. <sup>2</sup>
RTBRKT	Right brake stack temperature, °C
RUDPOS	Rudder position, deg
SIDESLIP	Aircraft sideslip angle, deg
SPFASST	Force automatic system servo surface temperature, °C
STABPOS	Stabilator position, %
THRUSTLT	No. 1 TF-34 thrust load cell, lb
TPYLN134	Tail pylon stress No. 134, lb/in. <sup>2</sup>
TPYLN139	Tail pylon stress No. 139, lb/in. <sup>2</sup>
TPYLN140	Tail pylon stress No. 140, lb/in. <sup>2</sup>
TPYLN225	Tail pylon stress No. 225, lb/in. <sup>2</sup>
TPYLN226	Tail pylon stress No. 226, lb/in. <sup>2</sup>
TPYLN227	Tail pylon stress No. 227, lb/in. <sup>2</sup>
TPYLN228	Tail pylon stress No. 228, lb/in. <sup>2</sup>
TPYLN229	Tail pylon stress No. 229, lb/in. <sup>2</sup>
TPYLN230	Tail pylon stress No. 230, lb/in. <sup>2</sup>
TRFLAP	Tail-rotor flapping angle, deg
TRIMPIT	Tail-rotor impressed pitch, deg
TRPBEAM5	Tail-rotor pitch beam load No. 5, lb
TRP2	Tail-rotor blade stress P2, lb/in. <sup>2</sup>
TRQ2	Tail-rotor torque, lb-lb
TRSPEDI	Tail-rotor spindle edgewise, in.-lb
TRSCONT	Tail-rotor stationary control load, lb
TRTHRN	Tail-rotor antitorque cell, lb
TWACC	Tail-wheel acceleration, g
UHZSTB1	Upper horizontal stabilizer fitting No. 1, lb/in. <sup>2</sup>
UHZSTB2	Upper horizontal stabilizer fitting No. 2, lb/in. <sup>2</sup>
UHZSTB4	Upper horizontal stabilizer fitting No. 2, lb/in. <sup>2</sup>
USAXLD	Upper horizontal stabilizer fitting axial load, lb
USLATLD	Upper horizontal stabilizer fitting bending load, lb
USROLLMO	Upper horizontal stabilizer fitting rolling moment, lb.-lb
VCOPF	Vertical acceleration copilot floor, g
VIPBOOM	Indicated airspeed, boom - PSID, knots
VPF	Vertical acceleration pilot floor, g
VSTTULT	Vertical acceleration left upper horizontal stabilizer tip, g
VSTTURT	Vertical acceleration right upper horizontal stabilizer tip, g
VTGB	Vertical acceleration tail gearbox, g
VWGTPLT	Vertical acceleration left wing tip, g
VWGTPRT	Vertical acceleration right wing tip, g
WINGFORFL	Wing force fail (force delta) indicator
WINGH	Left-wing pitch actuator load cell, lb
WINGI	Right-wing pitch actuator load cell, lb
WINGJ	Left-wing pivot point vertical load cell, lb
WINGK	Right-wing pivot point vertical load cell, lb
WINGL	Left-wing pivot point drag load cell, lb
WINGM	Right-wing pivot point drag load cell, lb
WIACLTLO	Wing-tilt-actuator left lower cylinder pressure, lb/in. <sup>2</sup>
WIACLTUP	Wing-tilt-actuator left upper cylinder pressure, lb/in. <sup>2</sup>

WIACRLO	Wing-tilt-actuator right lower cylinder pressure, lb/in. <sup>2</sup>
WIACRUP	Wing-tilt-actuator right upper cylinder pressure, lb/in. <sup>2</sup>
YAWACC	Aircraft yaw acceleration, deg/sec <sup>2</sup>
YAWRAT	Aircraft yaw rate, deg/sec
RUNTONE	Run tone

APPENDIX C

ROTOR SYSTEMS RESEARCH AIRCRAFT

FLIGHT ENVELOPE

OFS(MWK)/84-108

August 9, 1984

TO: FHI/RSRA Test Director

FROM: OFS and FHX/Aerospace Engineers

SUBJECT: Rotor Systems Research Aircraft Flight Envelope

The flight flutter envelope of the Rotor Systems Research Aircraft (RSRA) was expanded to 218 KEAS from May 8, 1984 to June 20, 1984 at the Ames Dryden Flight Research Facility. Two configurations were tested. The first configuration consisted of:

1. Main rotor off
2. Tail rotor on
3. Wing incidence angle set at five degrees
4. Full flaps with the gear down.

This configuration was flown to verify that the left landing gear door was free of aeroelastic instabilities to airspeeds of 168 KEAS.

The second configuration was:

1. Main rotor off
2. Tail rotor on
3. Wing incidence angle set at five degrees
4. Five degree flaps with the gear up.

This configuration was flown to expand the flight envelope of the vehicle.

#### AIRSPEED CALIBRATION

The method that was used to determine the calibrated airspeed was to add ten knots to the indicated airspeed values. Because of the low airspeeds involved, equivalent airspeed was assumed to be equal to calibrated airspeed. Additional airspeed

calibration work is being accomplished during the remainder of the flight test program. This new data may change the calibration of the airspeed system.

#### LANDING GEAR DOOR

The left landing gear door was modified by adding layers of fiber glass in the area of the gear/door strut attachment. The door was also stiffened by adding a bar to connect the top and bottom of the door at the aft end.

The expansion involved a ground vibration test (GVT) and a flight test. The GVT was conducted on April 20, 1984. The door, which was mounted on the aircraft, was excited using impact (calibrated hammer) excitation. The response of the door was measured in the x,y, and z directions at location 1 in figure C1. Figure C1 illustrates the points at which the door was excited with the hammer. Structural modes up to 60 Hz were measured and recorded. Table C1 lists the modal frequency and damping values for each mode identified. The mode shapes for the modes identified are shown in Figures C2 through C6.

Flight tests were conducted with the aircraft gear extended (door open). The wing flaps were fully extended for this test. The door was excited by random atmospheric turbulence at speeds of 154 and 168 KEAS at 10,000 feet density altitude. The door was instrumented with an accelerometer at the forward and aft end. The accelerometers were mounted normal to the skin of the door. Three modes were tracked at each speed. The frequency and damping versus airspeed plots for each mode are presented in figures C7, C8 and C9. The 19.58 Hz bending mode was not excited during flight test. The 55.47 Hz second bending mode was excited but the frequency and damping were not estimated. This was due to the 50 Hz analysis bandwidth. Satisfactory damping and damping trends were exhibited for the landing gear door.

#### FIXED WING AND TAIL ROTOR ENVELOPE EXPANSION

The flutter envelope for the RSRA was expanded to 218 KEAS at 10,000 feet density altitude. The test points flown were at 166, 175, 186, 202 and 218 KEAS. The frequency and damping versus airspeed plots are presented in Figures C10 through C20. Ten structural modes and one tail rotor mode were tracked. These modes were identified by frequency comparison with Sikorsky ground vibration test data. Good correlation existed between the flight data and the ground vibration data. Two lightly damped modes are exhibited in figures C13 and C19. These were the antisymmetric wing edgewise (fore and aft) bending and tail rotor edgewise bending modes, respectively. Although these modes are lightly damped, the damping trends remained flat over the airspeed range tested.

The wing flaps were set at five degrees to reduce the buffet on the lower horizontal stabilizer. Setting the flaps at angles greater than five degrees did not significantly reduce the buffet while retracting the flaps significantly increased the buffet. Wing incidence angle was changed from five degrees to seven and one half degrees during flight 5A-6 at 165 KEAS. There was no noticeable effect on the lower horizontal stabilizer buffet.

The buffet excited the lower horizontal stabilizer yaw (8.2 Hz) and vertical bending modes (19.0 Hz) and the fuselage lateral bending mode (9.2 Hz). Although the magnitude of these modes increased with increasing airspeed, the damping remained greater than seven percent for these three modes.

The aircraft is normally flown with the stability augmentation system (SAS) on. Test points at 164 and 202 KEAS were flown to determine if there were any adverse effects on structural damping with the SAS off. It was determined that there were no adverse effects with the SAS off.

### CONCLUSIONS

The RSRA was flown to a maximum speed of 218 KEAS. A total of 14 modes were tracked during the envelope expansion flights. These modes consisted of three landing gear door modes, ten fixed wing structural modes and one tail rotor mode. The damping levels and trends were satisfactory.

The SAS was turned off at 164 and 202 KEAS. The SAS off test points did not reveal any significant changes in structural damping, although the damping values were generally lower than the SAS on test point values.

The flutter envelope of the RSRA, with the main rotor off and the tail rotor on, has been cleared to 218 KEAS or 255 KTAS, whichever is less with the wing incidence angle set at five degrees leading edge up. The RSRA may be flown at any wing incidence angle to a speed of 164 KEAS or 190 KTAS, whichever is less. The RSRA may be flown to 202 KEAS or 234 KTAS, whichever is less with the SAS turned off. These do not include any upset margins of safety on airspeed. The flight envelopes are presented in figure C21.

Michael W. Kehoe

John F. Madden III

### Enclosures

cc:

OFS/A. Carter	FHI/W. Synder
OFS/R. Knight	FH/D. Few
OFS/L. Felt	OAS/G. Hall
OP/W. Painter	OA/F. Drinkwater III
ODO/J. Groen	

TABLE C1

## LEFT LANDING GEAR DOOR

## GROUND VIBRATION TEST RESULTS

<u>Freq (Hz)</u>	<u>Damp (g)</u>	<u>Mode</u>
10.23	0.021	Pitch/Yaw
19.58	0.038	1st Bending
26.63	0.036	Pitch
31.23	0.035	Torsion
55.47	0.019	2nd Bending



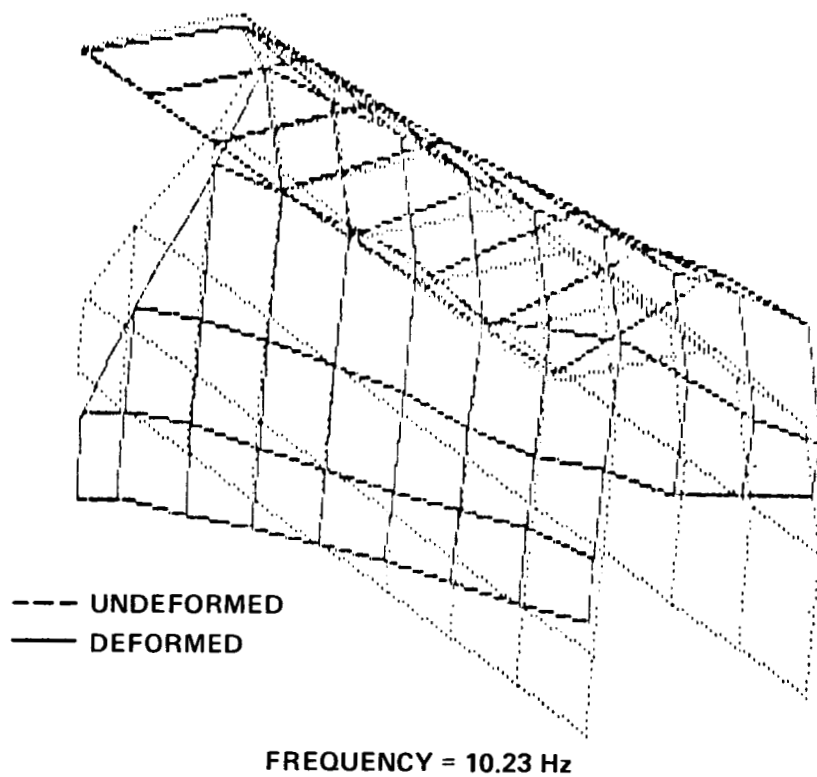


Figure C2.- Left Landing Gear Door Pitch/Yaw Mode Shape

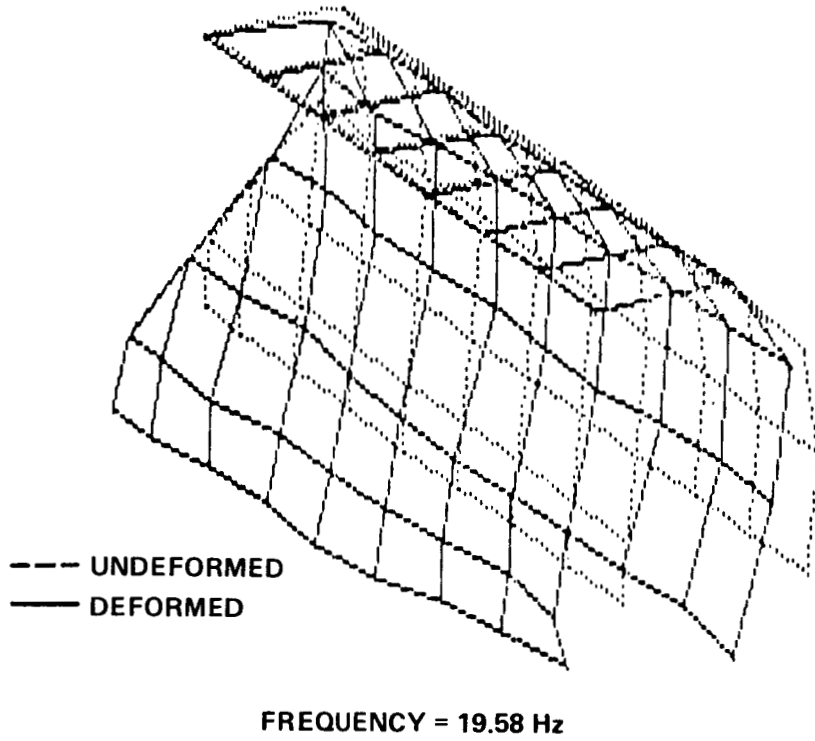


Figure C3.- Left Landing Gear Door Bending Mode Shape

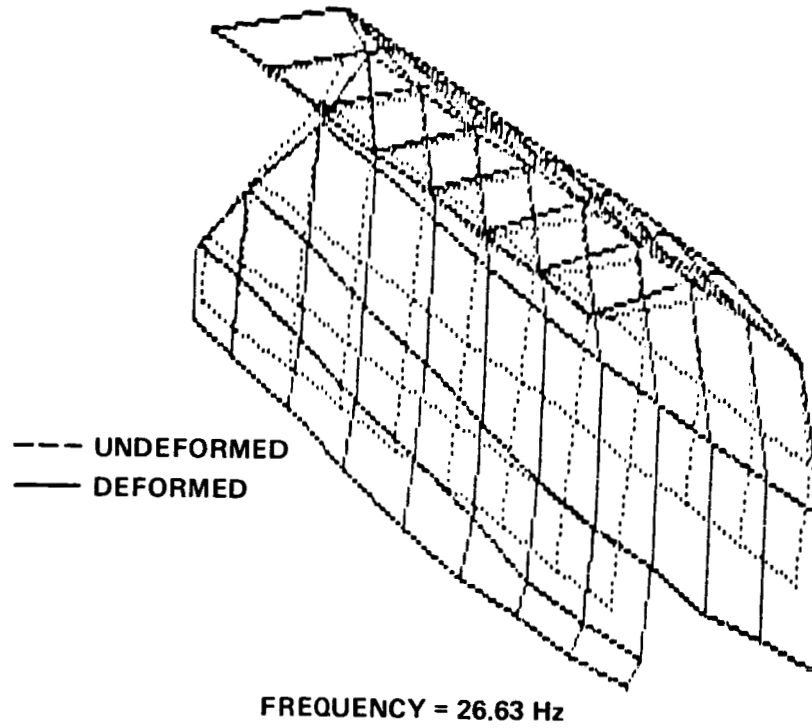


Figure C4.- Left Landing Gear Door Pitch Mode Shape

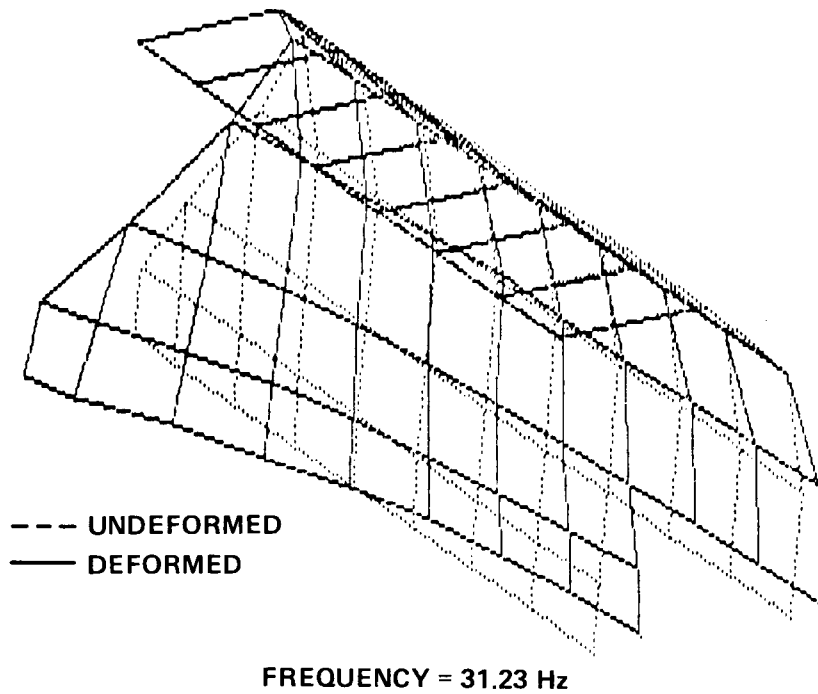


Figure C5.- Left Landing Gear Door Torsion Mode Shape

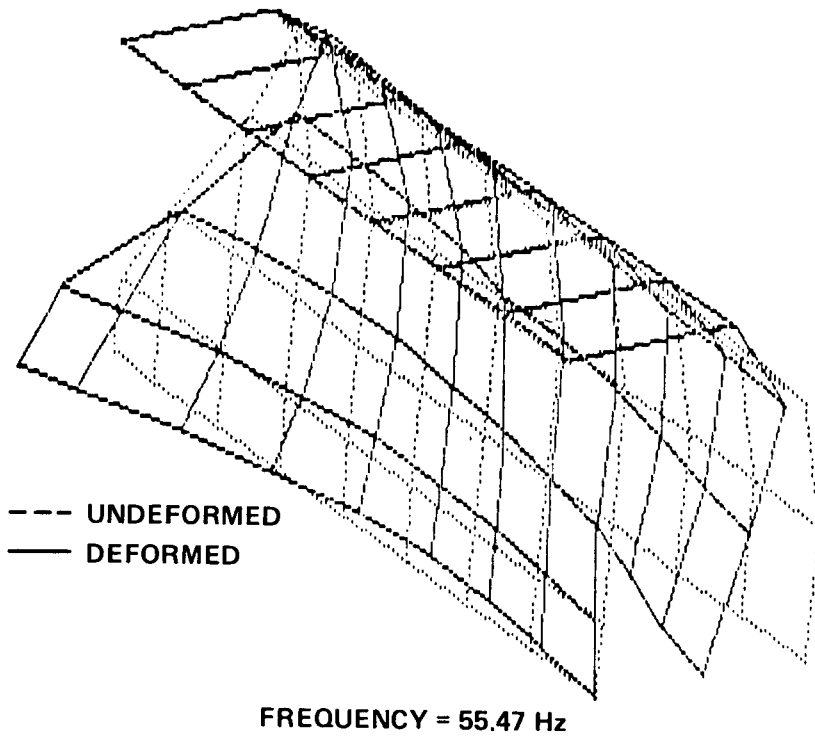


Figure C6.- Left Landing Gear Door Second Bending Mode Shape

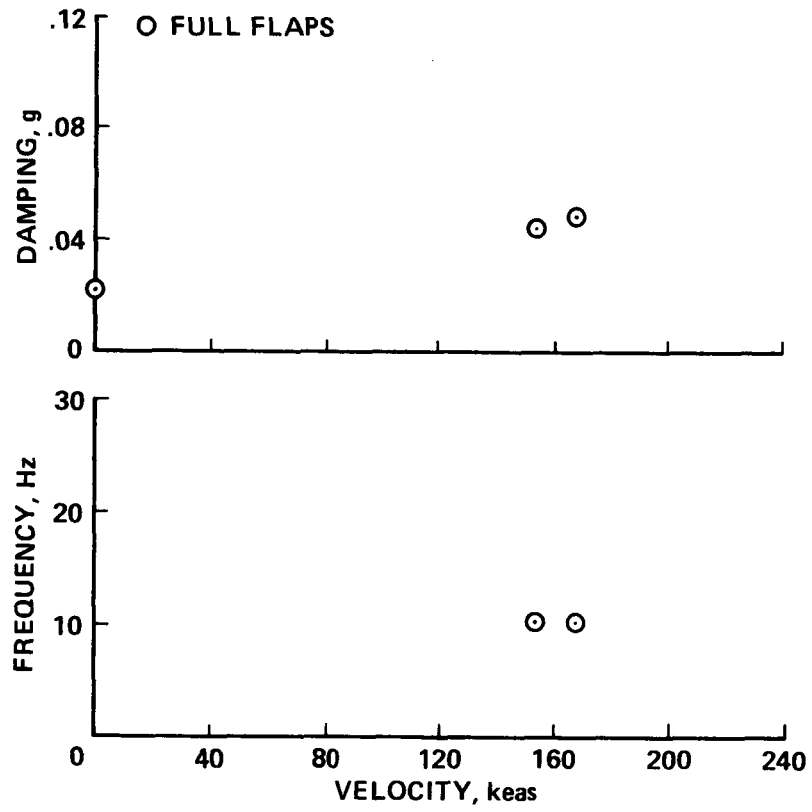


Figure C7.- Left Landing Gear Door Pitch/Yaw Modal Data

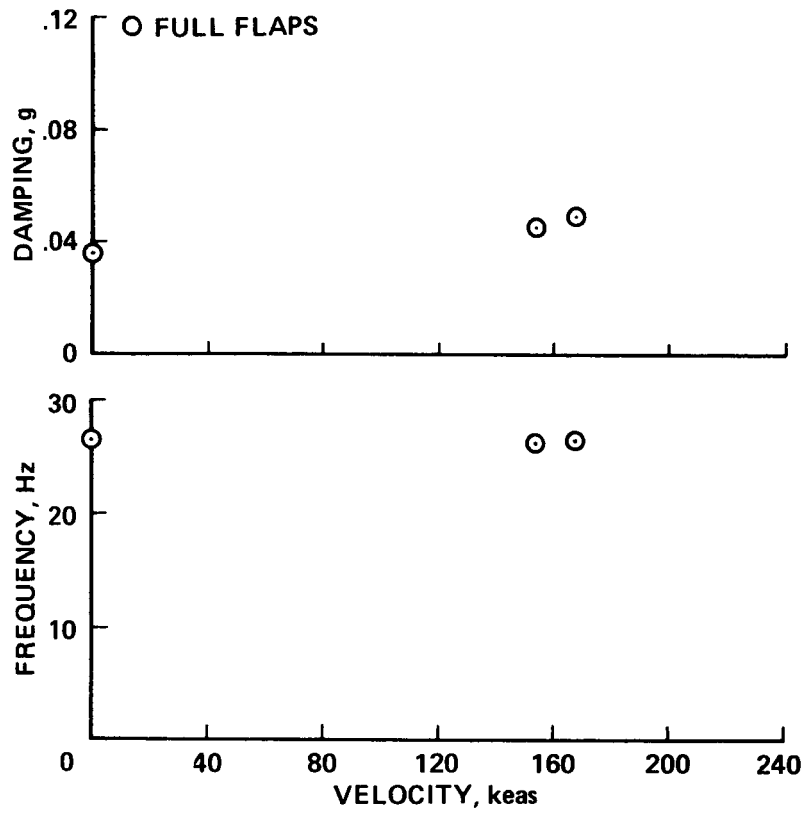


Figure C8.- Left Landing Gear Door Pitch Modal Data

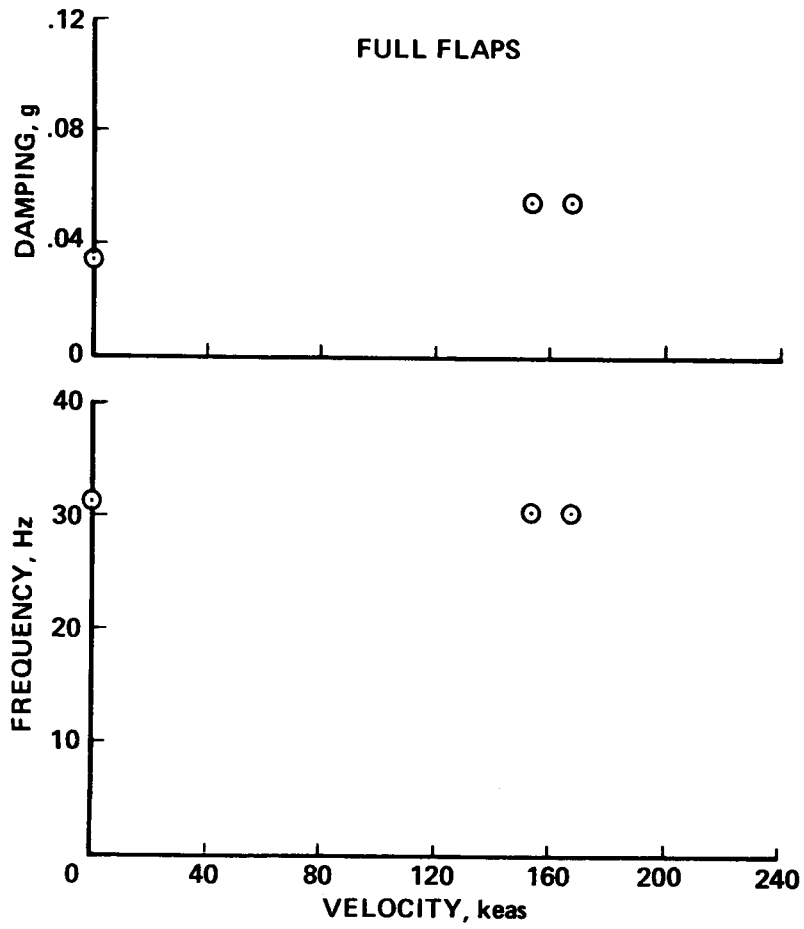


Figure C9.- Left Landing Gear Door Torsion Modal Data

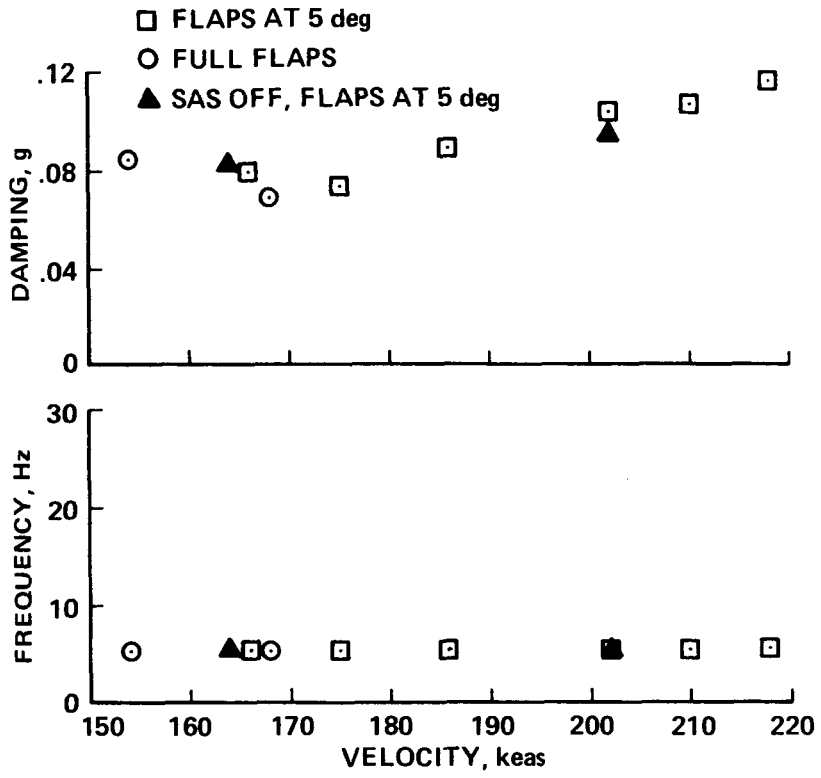


Figure C10.- Pylon Bending Modal Data

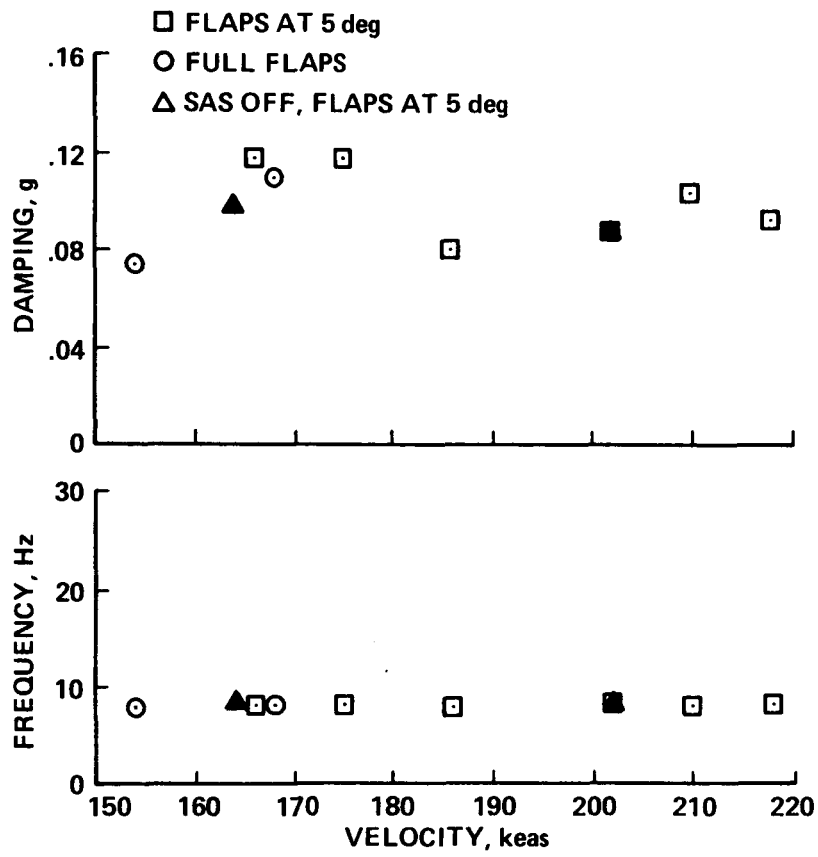


Figure C11.- Lower Stabilizer Yaw Modal Data

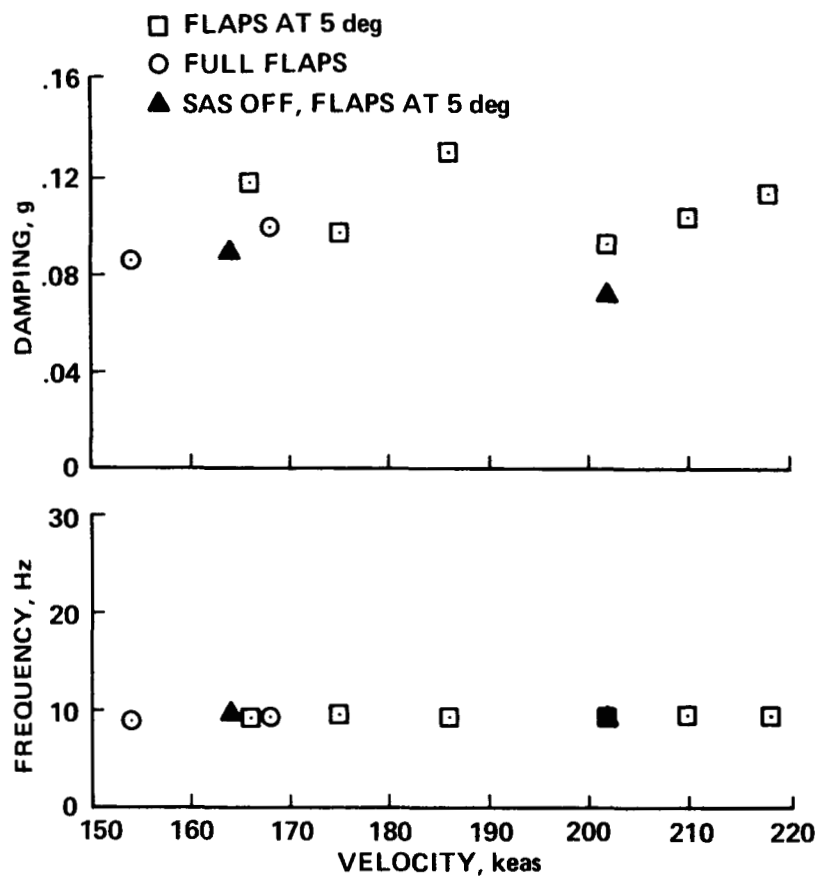


Figure C12.- Fuselage Lateral Bending Modal Data

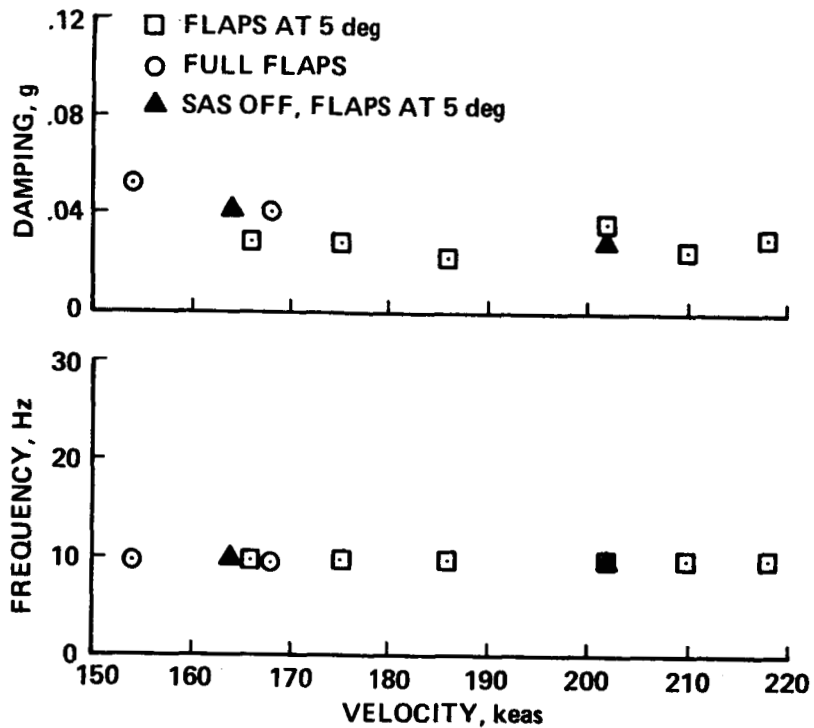


Figure C13.- Antisymmetric Wing Edgewise Bending Modal Data

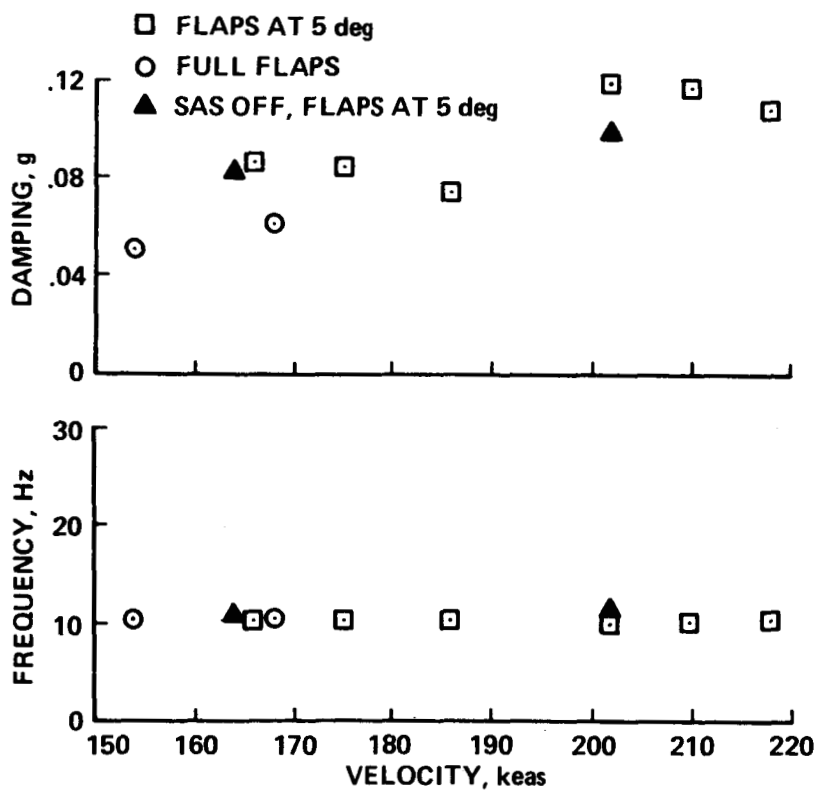


Figure C14.- Symmetric Wing Bending Modal Data

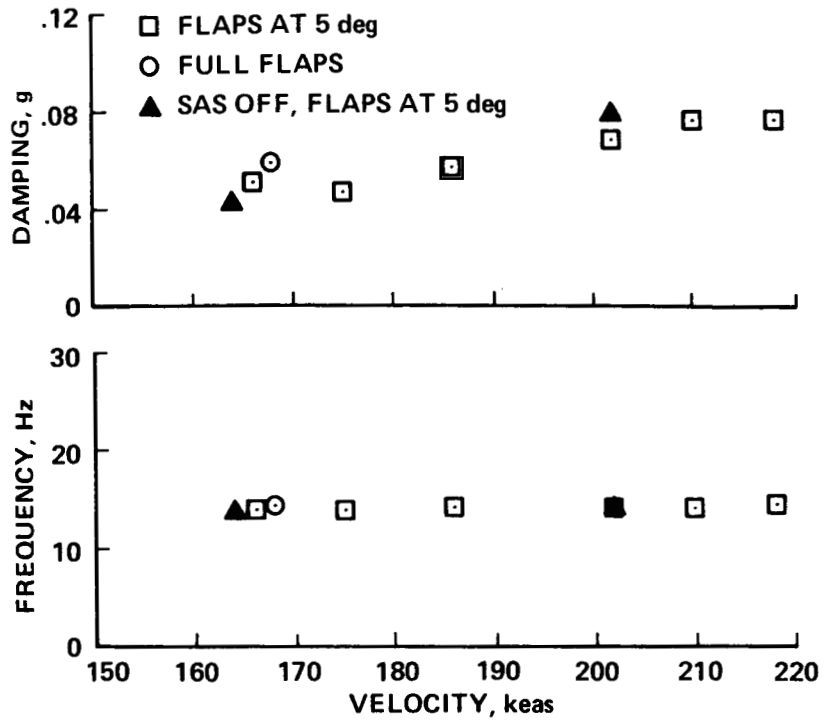


Figure C15.- TF-34 Engine Vertical Modal Data

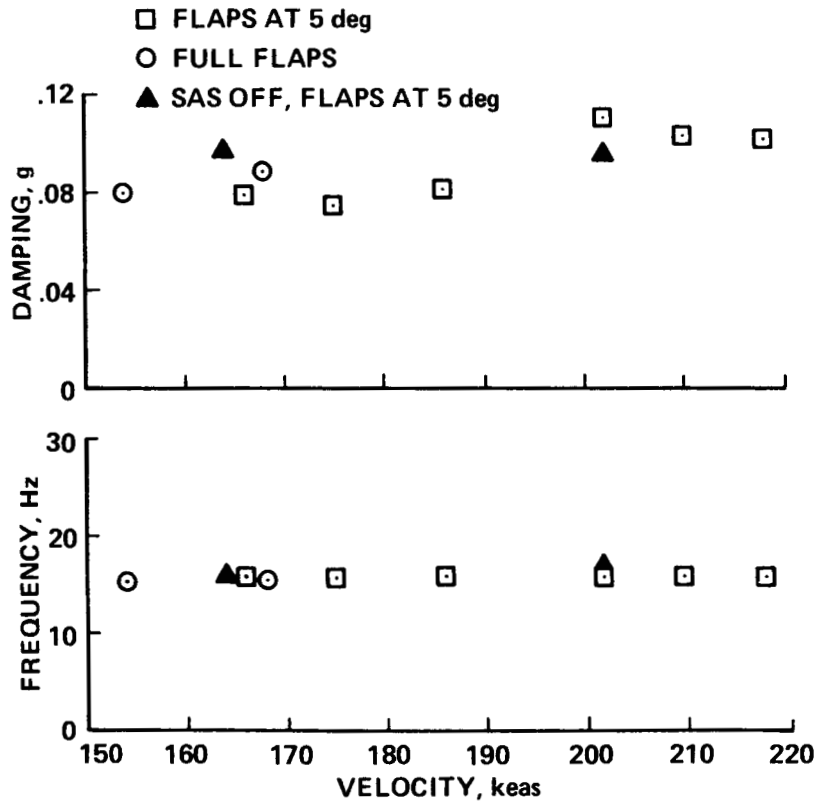


Figure C16.- Pylon Torsion Modal Data

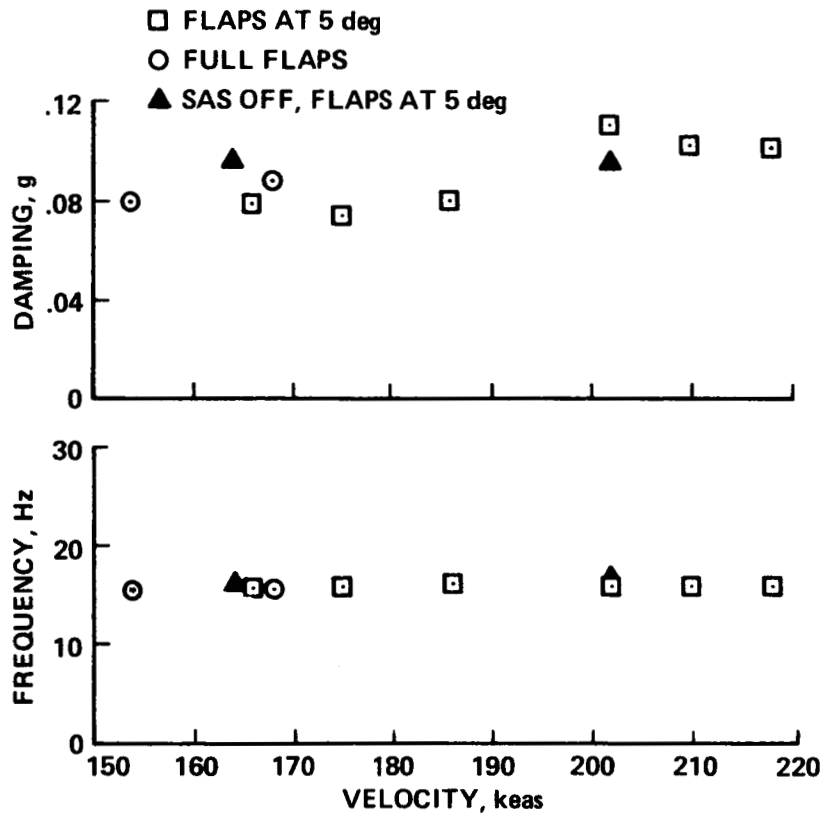


Figure C17.- Lower Stabilizer Symmetric Bending Model Data

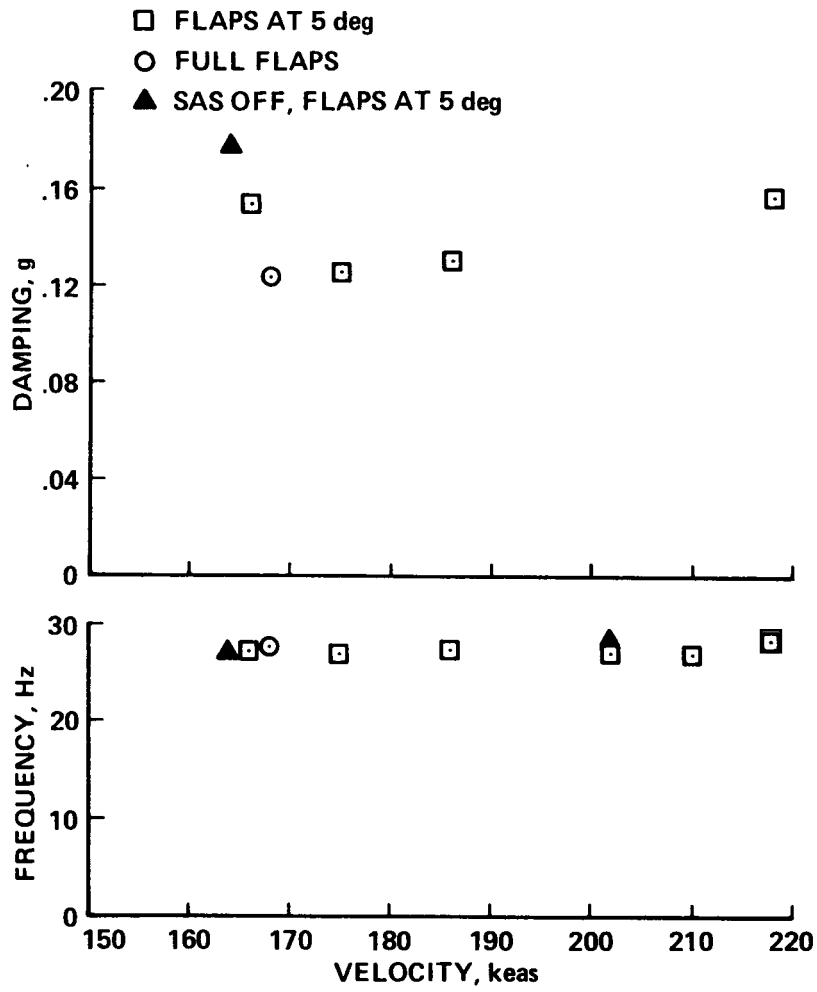


Figure C18.- Aileron Rotation Modal Data

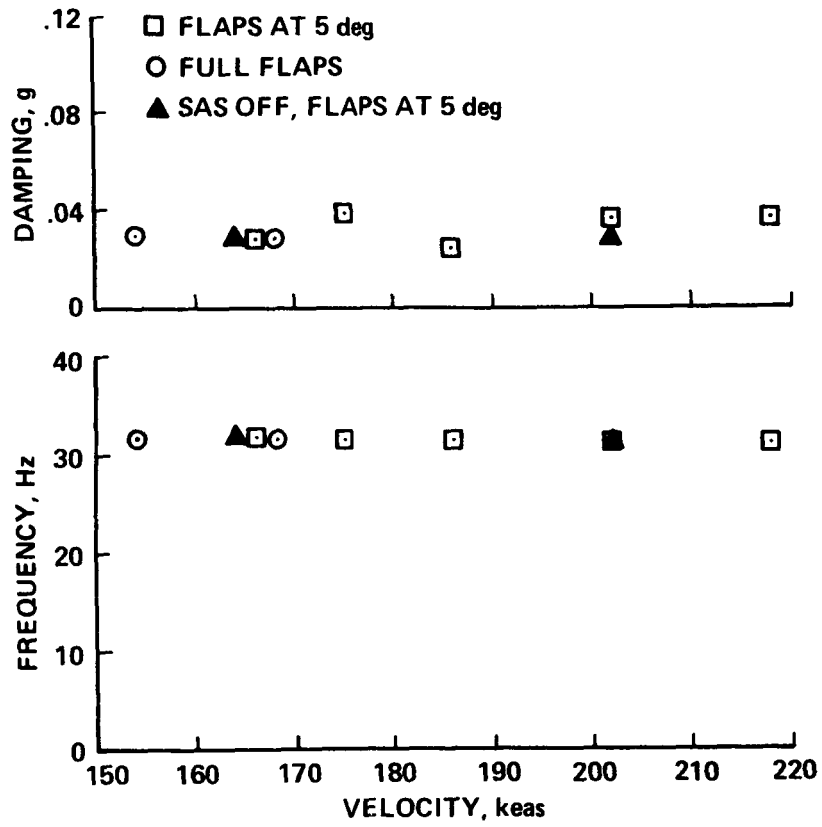


Figure C19.- Tail Rotor Edgewise Bending Modal Data

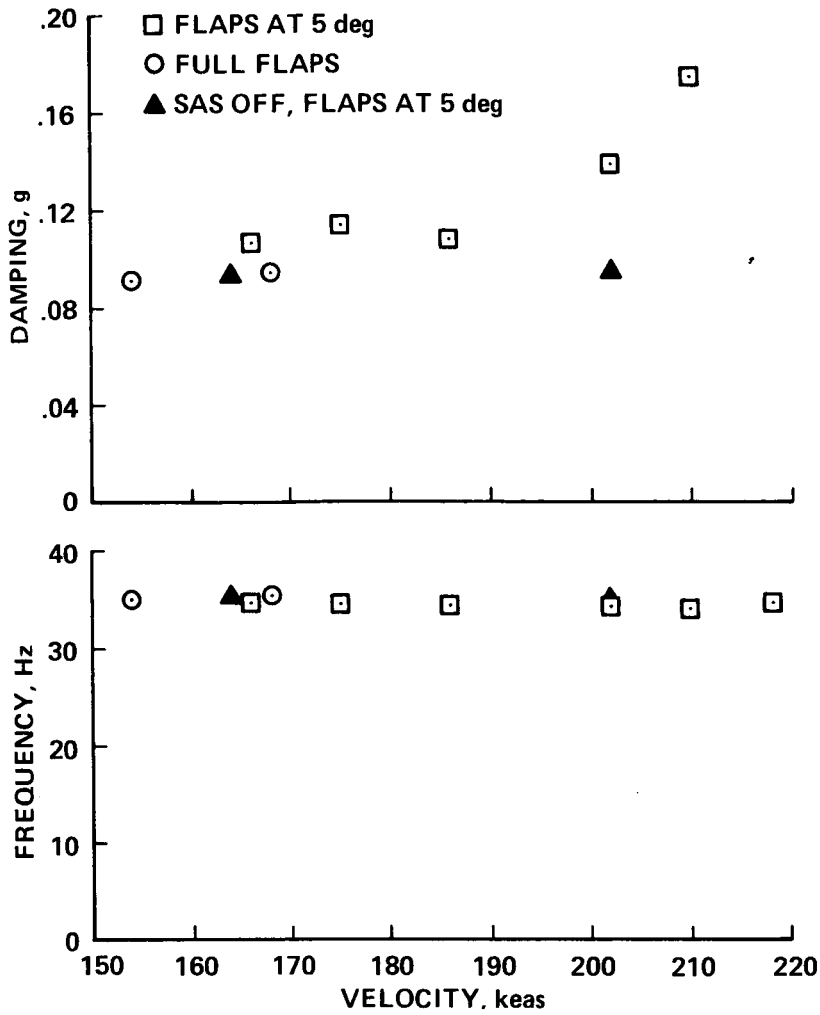


Figure C20.- Antisymmetric Third Wing Bending Modal Data

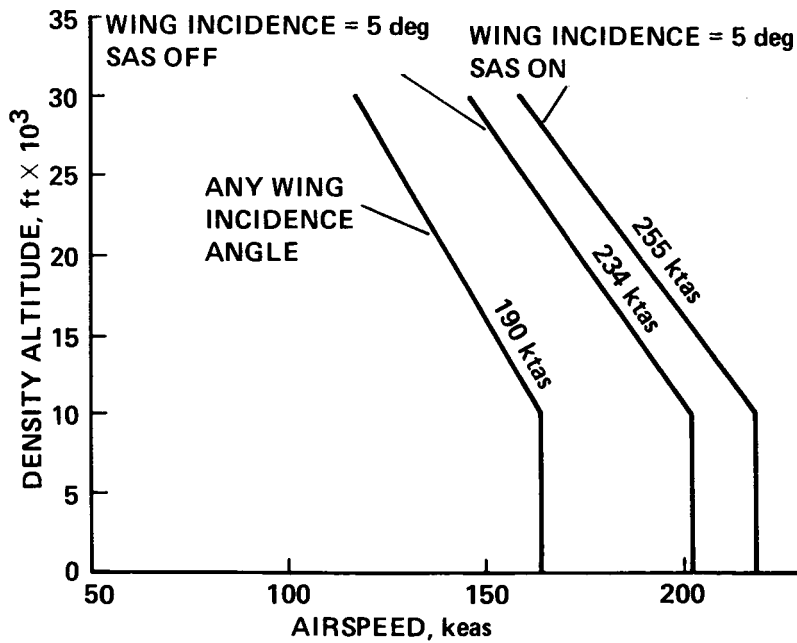


Figure C21.- Cleared RSRA Flight Envelope

## REFERENCES

1. Houck, J. A.; Moore, F. L.; Howlett, J. J.; Rellock, K. S.; and Browne, M. M.: Rotor Systems Research Aircraft Simulation Mathematical Model. NASA TM-78629, 1977.
2. Kufeld, R. M.: Rotor Systems Research Aircraft: Fixed-Wing Simulation Results. NASA TM-85863, 1983.
3. Skow, A. M.; and Erickson, G. E.: Modern Fighter Aircraft Design for High Angle-of-Attack Maneuvering. AGARD-LS-121, Dec. 1982.
4. Burks, J. S.: Rotor Systems Research Aircraft (RSRA) Rotor Force and Measurement System. AIAA Paper 81-2516, Nov. 1981.
5. Erickson, R. E. et al: NASA Rotor Systems Research Aircraft Flight Test Data Report: Helicopter and Compound Configuration. NASA TM-85843, 1984.
6. Monteleone, Robert A.: Systems Requirements for Rotor Systems Research Aircraft. SER-72039, prepared under contract NAS1-13000 by Sikorsky Aircraft, Mar. 15, 1977.
7. Acree, C. W., Jr.: Preliminary Report on In-Flight Measurement of Rotor Hub Drag and Lift Using the RSRA. NASA TM-86764, 1985.

1. Report No. NASA TM-86789		2. Government Accession No.		3. Recipient's Catalog No.	
4. Title and Subtitle NASA ROTOR SYSTEMS RESEARCH AIRCRAFT: FIXED-WING CONFIGURATION FLIGHT-TEST RESULTS				5. Report Date February 1986	
				6. Performing Organization Code	
7. Author(s) R. E. Erickson, J. L. Cross, R. M. Kufeld, C. W. Acree, Jr., D. Nguyen, and R. W. Hodge (Sikorsky Aircraft Co., Stratford, CT)				8. Performing Organization Report No. A-85363	
				10. Work Unit No.	
9. Performing Organization Name and Address Ames Research Center Moffett Field, CA 94035				11. Contract or Grant No.	
				13. Type of Report and Period Covered Technical Memorandum	
12. Sponsoring Agency Name and Address National Aeronautics and Space Administration Washington, DC 20546				14. Sponsoring Agency Code 505-42-51	
				15. Supplementary Notes Point of contact: R. M. Kufeld, Ames Research Center, MS237-5, Moffett Field, CA 94035 (415) 694-6571 or FTS 464-6571	
16. Abstract This report documents the fixed-wing, airplane configuration flight-test results of the Rotor Systems Research Aircraft (RSRA), NASA 740, at Ames/Dryden Flight Research Center. Fourteen taxi and flight tests were performed from December 1983 to October 1984. This was the first time the RSRA was flown with the main rotor removed; the tail rotor was installed. These tests confirmed that the RSRA is operable as a fixed-wing aircraft. Data were obtained for various takeoff and landing distances, control sensitivity, trim and dynamics stability characteristics, performance rotor-hub drag, and acoustics signature. Stability data were obtained with the rotor hub both installed and removed. The speed envelope was developed to 261 knots true airspeed (KTAS), 226 knots calibrated airspeed (KCAS) at 10,000 ft density altitude. The airplane was configured at 5° wing incidence with 5° wing flaps as a "normal" configuration. Level-flight data were acquired at 167 KCAS for wing incidence from 0° to 10°. Step inputs and doublet inputs of various magnitudes were utilized to acquire dynamic stability and control sensitivity data. Sine-wave inputs of constantly increasing frequency were used to generate parameter identification data. The maximum load factor attained was 2.34 g at 206 KCAS.					
17. Key Words (Suggested by Author(s)) Rotor Systems Research Aircraft Fixed wing Flight testing Rotor-hub drag Tail rotor acoustics				18. Distribution Statement  Unlimited  Subject Category - 05	
19. Security Classif. (of this report) Unclassified		20. Security Classif. (of this page) Unclassified		21. No. of Pages 123	22. Price* A04